How polymers shape the physicochemical environment of the gut

Thesis by

Asher Preska Steinberg

In Partial Fulfillment of the Requirements

for the degree of

Doctor of Philosophy

CALIFORNIA INSTITUTE OF TECHNOLOGY

Pasadena, California

2019

(Defended April 12, 2019)

Asher Preska Steinberg
ORCID: 0000-0002-8694-7224

ACKNOWLEDGEMENTS

There are so many people I have to thank for shaping me into the scientist and person I am today. First and foremost, I would like to thank my adviser, Rustem Ismagilov. Thank you for taking me into your lab and showing me the power of the scientific method. When I reflect on my experiences, Brandeis (my undergraduate institution) was the place where I discovered the joy of curiosity-driven science. Yet, I really had no clue how to answer the questions I asked. Here, in your lab at Caltech, I learned how to answer these questions using the scientific method. This is not to say that we are not curiosity-driven in the Ismagilov lab (because we certainly are), it is simply to say that you have stretched me beyond this; I am now not only curious but also crave meaningful questions. To that end, I would like to thank you for reminding me to be curious when I struggled and had lost my way.

I would like to thank my wonderful thesis committee (Zhen-Gang Wang, David Tirrell, Julie Kornfield) as a whole for pushing me to seek clean and unambiguous answers in the inherently messy problems I chose to take on during my PhD. My brother once told me that the first time he put on glasses the world was crisp, warm, and vibrant with color. This, for me, serves as a metaphorical description of a meeting with Zhen-Gang (my thesis chair) to discuss polymer physics. Zhen-Gang, thank you for showing me the wonders of polymer physics, for always having your door open to me, and for your warm words of wisdom. Dave, thank you for not only deeply probing the science that I conduct, but also asking if I am asking the right question. You are able to do this with a level of grace and precision I can only hope to one day emulate. Julie, thank you for always pushing me to think more deeply about my polymers. Your unabashed curiosity is contagious, and thank you for sharing some of that with me.

Caltech is a special place. The graduate experience here is a crucible; it shapes and changes the way you think and gives you the tools you need to solve any problem. In this way, it stretches the fabric of your being. Yet, simultaneously, the Caltech community is a place of support and kinship. I have been lucky to have made so many wonderful friends here and benefited from the many support systems that the institute provides. Jon Kindem and Ottman Tertuliano; many have viewed us as an inseparable trio over the past years (hence the alternate names of “the bike mafia”, “the three musketeers”, and possibly some others that should not be written here). Thank you for being the best partners in crime I could have asked for, and for becoming my family out here in California. To Sam Ho, thank you for our countless coffee dates; I am grateful that together we are able to simultaneously laugh and cry at the craziness of life. I would be completely remiss if I did not mention Sujit Datta; Sujit, thank you for being one of the goofiest, most brilliant, and strong-willed people I know. Your mentorship and friendship here at Caltech and beyond has been a gift. To Michael Porter, thank you for being such a wonderful partner in crime in the lab and beyond. I look forward to hearing about your future adventures at Caltech and participating

in our future adventures together. To Tasha Shelby, thank you for your curiosity, your wonderful writing, and your friendship. I would also like to thank all of my wonderful labmates; each and every one of you has given me scientific and/or emotional support as well as friendship over the years.

I have been lucky to have benefited from many wonderful support systems at Caltech. Thank you to both the Health Center and Counseling Center for keeping me healthy throughout my journey here. Thank you to Barb Catlin and the Caltech Jazz Band for everything! You have provided me with a "home away from home" here at Caltech. Thank you to Lee Coleman and the Caltech Meditation Mob for keeping me balanced every Tuesday. Of course, my life would have been a mess if there were not so many wonderful administrators at Caltech. Special thanks to Sohee Lee, Irina Meininger, Abigail McCann; without the three of you, I may have never been able to convene a committee meeting. Also, thanks to the wonderful staff of the animal facility and the present and past chemistry grad program administrators — Alison Ross and Agnes Tong.

Lastly, there are many beyond Caltech who constantly breathe life into me. I would like to thank Jeremie Palacci. I often blame you for getting me into this nasty business in the first place, and I would like to thank you for that. In particular, thank you for showing me the joy and virtue of following my curiosity to wherever it takes me. To my extended family: Nick Monath and the Boyd-Zieglers. You are all gifts. Nick, thank you for always being there for me through everything; you are the best friend everyone must wish they had. Boyd-Zieglers, thank you for also always being there for me and even flying across the country to help me when I was down and out. To my family: Merrill, Mom, and Dad. Thank you all for your unconditional love. Merrill, thank you for continually helping me have perspective, your silliness, and for being another one of my best friends. Mom and Dad: thank you for letting me complain just enough to get it out of my system, but then quickly reminding me what a gift my life is. Thank you for your constant patience as I work and dance through life. Mom, thank you for your careful listening, love, and always reminding to enjoy my life. Dad, thank you for your listening, your eccentricity, love, and your steadfast faith in me.

A poet, I believe, once said, “The whole universe is in a glass of wine.” We shall never know in what sense he meant it for poets do not write to be understood, but it *is* true that if you look at a glass of wine closely enough you will see the entire universe … And if our small minds for some convenience divide this glass of wine, this universe, into parts – to physics, biology, geology, astronomy, psychology – remember Nature doesn’t know it, so we should put it back together and not forget, at last, what it is for. Let it give one final pleasure more; drink it up and forget about it all.

-Richard P. Feynman, “The Relation of Physics to the Other Sciences,” 1961

ABSTRACT

The gut is where food is digested and nutrients are absorbed, therapeutics are often delivered, and many infections take hold. The gut microbiota is in symbiosis with its host, and can influence host health and behavior. Though the gut holds these central roles, little is understood about the physics of how soft materials interact with and shape the physicochemical environment of the gut. Soft materials abound in the gut in the form of particulates (e.g., microbes, viruses, therapeutic particles, food granules) and polymers (e.g., dietary fibers, therapeutics, food additives). This thesis explores the soft matter physics of the gut and how physicochemical interactions can influence gut structure and function. This is studied through a combination of mouse experiments and numerical calculations. In the first part of this thesis, we investigate how particulates interact with polymers in the small intestine. We find that polymers from dietary fiber can aggregate particulates by a mechanism that is qualitatively consistent with depletion interactions. This mechanism is distinct from agglutination via specific chemical interactions. In the second part of this thesis, we investigate how polymers interact with the colonic mucus hydrogel. Colonic mucus is the nexus of host-microbe interactions. It is a barrier which protects against microbial infiltration, and alterations to its physical structure have been linked to changes in host health. Here, we find that polymers compress the colonic mucus hydrogel. For uncharged polymers, this mechanism can be described by a simple, mean-field model based on Flory-Huggins solution theory. Further, we find that microbes can modulate the extent of mucus compression by degrading polymers in the gut. In the last part of this thesis, we find that charged polymers (polyelectrolytes) compress mucus by a Donnan mechanism.

PUBLISHED CONTENT AND CONTRIBUTIONS

1. A. Preska Steinberg, S. S. Datta, T. Naragon, J. C. Rolando, S. R. Bogatyrev, R. F. Ismagilov. 2018. "High-molecular-weight polymers from dietary fiber drive aggregation of particulates in the murine small intestine." eLife. 8:e40387. DOI: 10.7554/eLife.40387

   This article investigates the interactions between polymers and particulates in the murine small intestine. My role was as follows (text reproduced from page 85 of this thesis):

   Co-designed all experiments and co-analyzed all experimental results; developed theoretical tools and performed all calculations; co-developed imaging analysis pipeline in ImageJ; developed computational tools for bootstrapping procedure; co-developed microscopy assay for examining luminal contents from mice gavaged particles used in Figure 2.1C and 1D; Co-performed, designed, and analyzed data from experiments involving oral administration of particles in Figure 2.1; performed, designed, and analyzed data from all *ex vivo* aggregation experiments in SI fluid in Figures 2.2, 2.3, 2.5-7, 2.S2, and 2.S5; performed, designed, and analyzed data from all GPC measurements in Figures 2.3, 2.5-7, and Tables 2.S1-7; performed, designed, and analyzed data from all *in vitro* aggregation experiments with PEG solutions in Figure 2.4D, Figure 2.4 – figure supplements 1-2, and with dietary fiber in Figure 2.7A; developed a computational approach for theoretical calculations in 2.4H and 2.4I and performed all calculations; performed, designed, and analyzed data from Western blots in Figures 2.5E, 2.6E, 2.S3, and 2.S4; helped supervise animal husbandry of MUC2KO colony; performed animal husbandry for WT mice on autoclaved diets in Figure 2.6 and 2.S5; performed animal husbandry for mice on pectin and Fibersol-2 diets in Figure 2.7; performed, designed, and analyzed all zeta potential measurements in Table 2.S8; performed pH measurements on luminal fluid in Figure 2.S2; co-interpreted results; co-wrote the paper.

2. S. S. Datta, A. Preska Steinberg, and R. F. Ismagilov. 2016 "Polymers in the gut compress the colonic mucus hydrogel." PNAS 113(26):7041-7046. doi: 10.1073/pnas.1602789113

   This article investigates the interactions between polymers and the colonic mucus hydrogel. We find that polymers compress the colonic mucus hydrogel. My role was as follows (text reproduced from page 128 of this thesis):

   Co-designed all experiments and coanalyzed all experimental results; codeveloped theoretical tools and coperformed the experiments and calculations; performed some of the FC oil measurements and analyzed some of the results in Figures 3.1

and 3.S1; performed some of the ex vivo experiments and analyzed some of the results in Figures 3.2–4 and 3.S3–S7; codeveloped the theoretical model; cooptimized and coperformed calculations for the theoretical model and coanalyzed results in Figure 3.3; performed a sensitivity analysis for the theoretical model shown in Figure 3.S9; performed dynamic light scattering measurements of polymers and probes; designed and performed GPC measurements in Figure 3.S10; cowrote the paper.

3. A. Preska Steinberg, Z.-G. Wang, R. F. Ismagilov. 2019 “Food polyelectrolytes compress the colonic mucus hydrogel by a Donnan Mechanism”. Submitted.

   This article investigates the interactions between charged polymers (polyelectrolytes) and the colonic mucus hydrogel. My role was as follows:

   Designed research; performed research; analyzed data; co-wrote the paper.

TABLE OF CONTENTS

LIST OF ILLUSTRATIONS AND/OR TABLES

Number *Page*

Chapter 1

INTRODUCTION[1]

The physicochemical environment of the gut

Polymers are ubiquitous in nature. DNA and RNA are the polymers which encode life. These are far from the only polymers found in organisms, as they are secreted as mucus, glycoproteins, proteoglycans, and extracellular matrices (to name a few examples). Polymers are regularly ingested by many animals for sustenance in the form of dietary fibers. In addition to the examples given above, humans also ingest polymers in the form of food additives and therapeutic polymers. Polymers are macromolecules (i.e., very large molecules). These macromolecules are chains of repeating molecular units, or monomers. Depending on the stiffness of the polymer and its interactions with the solvent, these macromolecules can take on different conformations in space, ranging from a jumble of monomers to a random walk (depicted in Figure 1.1) to almost rod-like (1).

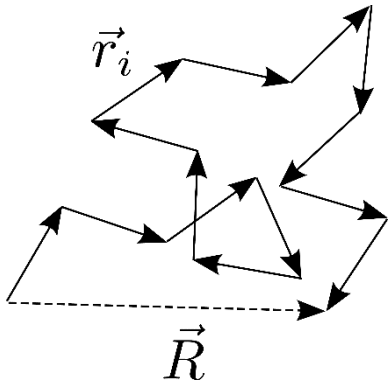

Figure 1.1. Schematic depicting an "ideal" polymer chain in which the polymer takes on a random walk configuration. Each individual arrow ($\vec{r_i}$) is a vector corresponding to a monomer. $\vec{R}$ is the end-to-end vector of the chain (i.e., the sum of all the individual vectors, $\vec{r_i}$) .

The motivation of this thesis is to understand how polymers in the human diet influence the physical structure of the gut through physicochemical interactions. By the "physical structure of the gut", we mean this in the most literal sense; the physical constituents of the gut environment and their spatial distribution. This is illustrated in Figure 1.2. The physical constituents of the gut include particulates (e.g., microbes, food granules, and therapeutic

[1] Sections of this chapter are adapted from a manuscript in preparation.

particles), dietary and secreted polymers (examples given in the preceding paragraph), the mucus layer, and the epithelium (2–6). By "physicochemical interactions", we refer specifically to forces that arise and can be predicted from polymer thermodynamics. In the subsequent work, we focus on how polymers interact with two aspects of the physical structure of the gut: particulates and the colonic mucus hydrogel.

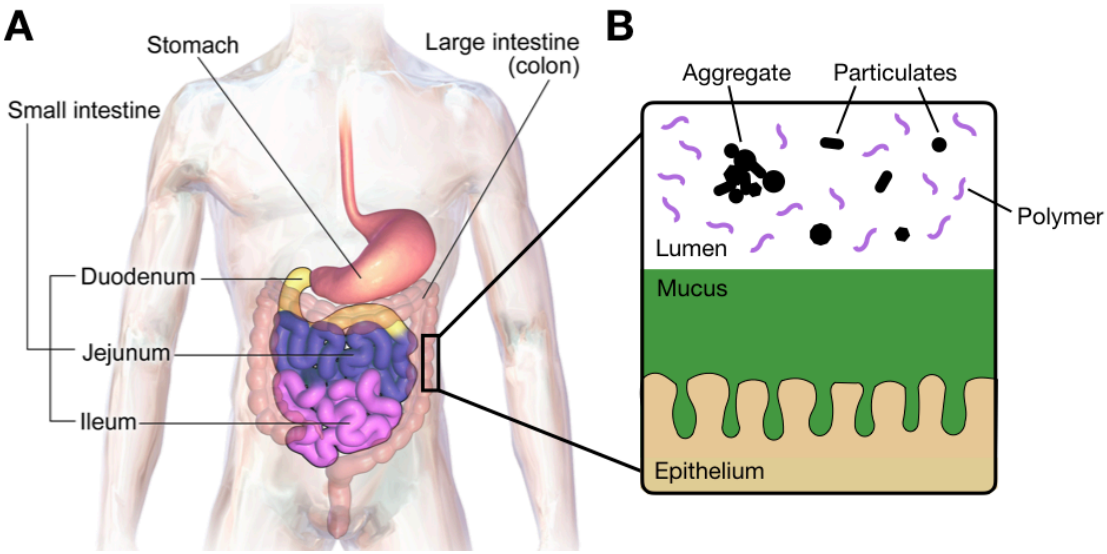

Figure 1.2: (A) Schematic of the human gastrointestinal tract adapted from ref. (29). (B) Schematic depicting the "physical constituents" of the gastrointestinal tract.

Particulates abound in the gut in the form of microbes, viruses, cell debris, particles which carry drugs, and food granules (2,4,7–9). It has been shown that the way in which these particulates are spatially structured is important to their function. In the case of therapeutic particles, it is thought that the aggregation or clumping of particles hinders their uptake at mucosal surfaces, impeding effective delivery (8,10) (see Figure 1.2 for an illustrated example of an "aggregate" of particulates). For microbes, aggregation is linked to their function in the gut. How aggregation influences microbial function appears to vary on a case by case basis. It has been shown that the aggregation of the pathogen *Salmonella Typhimurium* via a form of chemical agglutination promotes its clearance and protects against infection (11). Additional experimental evidence suggests that aggregation may promote clearance of other bacteria (11,12) and keeps microbes separated from the

epithelium (13). In contrast, recent experiments have suggested that in some instances bacterial aggregation can promote colonization (14). These are just a few examples which demonstrate how the spatial distribution of particulates can affect their function in the gut.

Mucus in the colon has a two-layer structure (15,16) (see Figure 1.3 for illustration). The inner layer is a polymer network (i.e., hydrogel) which is held together by chemical cross-links, physical entanglements, and electrostatic interactions (17–19). The outer layer is a polymer solution, in which the polymers are mucins, and is where the microbiota resides (15,16). The primary mucin in both layers is MUC2, and the prevailing hypothesis in the literature is that this outer layer is formed due to proteolytic cleavages of MUC2 (15). This two layer structure is also found in germ-free mice (mice without microbes), suggesting that these proteases are endogenous (15). Why the transition between the outer and the inner mucus layers appears to be so sharp in micrographs of colonic mucus remains unclear. Moreover, this two-layer structure is conserved across both rodents and humans (5).

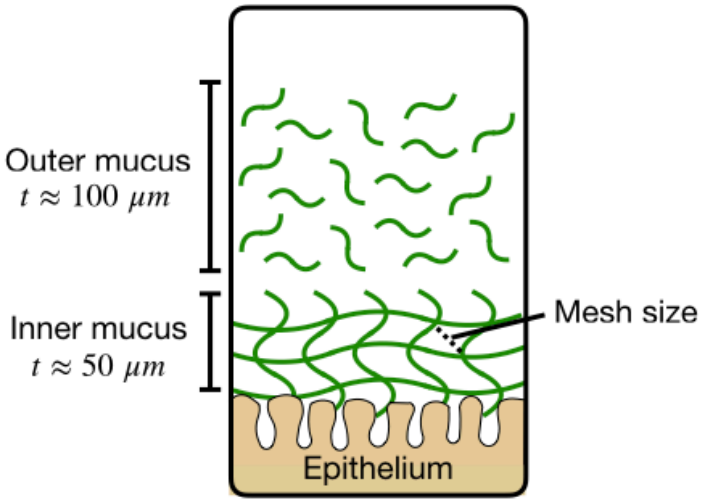

Figure 1.3: Schematic depicting the two layer structure of colonic mucus. The inner mucus layer (labeled "Inner mucus") is a cross-linked hydrogel, whereas the outer mucus layer (labeled "Outer mucus") is a loose layer of mucus (a solution of mucin polymers), which extends into the lumen of the colon. Approximate thicknesses (t) of both layers are those reported for mice in ref. (15).

The inner mucus layer in the colon (which will also be referred to in this thesis as the "colonic mucus hydrogel") has been shown to play several key roles in shaping the gut environment. It mediates host-microbe interactions by acting as the physical barrier which separates microbes from the host (15,16). It has been demonstrated experimentally that

changes in the physical properties of this barrier, such as its mesh size and thickness, are correlated to changes in host health (20–22). Recent work has demonstrated that a thin mucus hydrogel is correlated with both microbial encroachment upon the epithelium and increased gut inflammation (22). In mouse models of colitis, the colonic mucus hydrogel has been shown to be more penetrable to bacteria, and humans with ulcerative colitis have mucus which is more penetrable to particles (20). Muc2-deficient mice, which do not secrete colonic mucus, have been shown to develop colitis and colon cancer (21,23).

Using polymer physics to understand gut physiology

Upon examination of the works we have referenced up to this point, it may lead the reader to conclude that investigations of the gut are all conducted using techniques from microbiology, molecular biology, genetics, and biochemistry. Without question, these have proven to be powerful tools for understanding the gut microbiome, deciphering complex interactions between microbes and their host, and understanding gut physiology. In this work, however, we will leverage approaches from polymer physics to understand the interactions between polymers and the physical structure of the gut. As (we hope) the reader will see, this will yield a mechanistic understanding of gut physiology that both builds upon and complements our current understanding of the gut from the perspectives of these different disciplines. In this approach, we will focus on how the physical properties of dietary polymers (e.g., size, concentration, charge) can influence gut physiology. Furthermore, it will be reductionist and coarse-grained in nature; instead of keeping track of every individual atom that composes this system (the system being that which is described in Figure 1.2), we will seek the minimal set of parameters needed to explain and predict the interactions between dietary polymers and the other physical constituents of the gut. Two theoretical approaches will be used to describe these interactions. One will be to write down the total free energy of the system and solve for the chemical potentials of its components at equilibrium. This approach will be leveraged in Chapter III. The other approach will be to predict the behavior of the system in terms of forces which stem from the polymer osmotic pressure. This approach will be leveraged in Chapters II and IV. These two approaches both find their roots in the statistical thermodynamics of polymers, and

one could re-write any section of this thesis in the language of either approach and should reach the same conclusions.

Continuing in the same vein, one way to contextualize this work is to think of the phenomena described in this work as forms of polymer-driven osmotic effects. In Chapter II, we find small intestinal polymers aggregate particles in a manner that is qualitatively consistent with polymer-induced depletion interactions. Polymer-induced depletion interactions arise when large polymers are excluded from the space between particles, leading to a difference in the osmotic pressure between the polymer solution and the space between particles (24–26). This acts as a driving force bringing particles together. In Chapters III and IV, we study the interactions between polymers and the colonic mucus hydrogel. One can think of the colonic mucus hydrogel as acting as a semi-permeable membrane for polymers where exclusion is on the basis of physical size, electrostatic interactions, and chemical interactions (27). This leads to an osmotic pressure difference between the polymer solution and mucus, resulting in compression. Overall, the described phenomena support the idea that polymers can influence gut physiology through simple, osmotic forces that stem from their physicochemical properties.

Thesis outline

This thesis will move longitudinally through the intestines, starting with the small intestine then moving to the large intestine.[2] In all sections, we will combine *in vivo* and *ex vivo* mouse experiments with numerical calculations grounded in the statistical physics of polymers to understand the problems at hand. In Chapter II, we investigate the aggregation of particulates in the small intestine. We find that particulates aggregate spontaneously in luminal fluid from the small intestine. Our results suggest that mucins and immunoglobulins are not necessary for this aggregation to occur. Instead, we find that by feeding mice dietary fibers of different molecular weights, we can control aggregation. Our

[2] The reader may notice that we are skipping over the cecum. Interestingly, the anatomy of the mouse cecum is very different than that of humans (28). In mice, it is much larger (relative to other sections of the gut) and more of a "sack", while in humans it is more of a small protrusion or a "cul-de-sac". It has been relatively understudied in mice for this reason. In humans the function of the cecum is not entirely clear.

results are qualitatively consistent with polymer-induced depletion interactions, which is distinct from aggregation via chemical agglutination (in which polymers bind or stick to particles to clump them). In Chapters III and IV, we investigate the interactions between polymers and the colonic mucus hydrogel. In Chapter III, we find that polymers can compress mucus. We find that the extent of compression can be modulated by tuning the molecular weight and concentration of the polymer. This mechanism can be described using a simple, mean-field model based on Flory-Huggins solution theory. Furthermore, we find that gut microbes can indirectly modulate mucus compression by degrading polymers in the gut. In Chapter IV, we add in the additional complexity of polymer charge, and find that charged polymers (polyelectrolytes) compress mucus by a Donnan mechanism.

References

1. Rubinstein M, Colby RH. Polymer Physics. New York: OUP Oxford; 2003.

2. Donaldson GP, Lee SM, Mazmanian SK. Gut biogeography of the bacterial microbiota. Nat Rev Microbiol [Internet]. 2015;14(1):20–32. Available from: http://www.nature.com/doifinder/10.1038/nrmicro3552

3. Hasler WL. Integrative Responses of the Gastrointestinal Tract and Liver to a Meal. In: Textbook of Gastroenterology, Fifth Edition. 2009. p. 1–14.

4. Goldberg M, Gomez-Orellana I. Challenges for the oral delivery of macromolecules. Nat Rev Drug Discov [Internet]. 2003;2(4):289–95. Available from: http://www.nature.com/doifinder/10.1038/nrd1067

5. Johansson MEV, Sjövall H, Hansson GC. The gastrointestinal mucus system in health and disease. Nat Rev Gastroenterol Hepatol. 2013;10(6):352–61.

6. Turner JR. Intestinal mucosal barrier function in health and disease. Nat Rev Immunol [Internet]. 2009;9(11):799–809. Available from: http://dx.doi.org/10.1038/nri2653

7. McGuckin MA, Lindén SK, Sutton P, Florin TH. Mucin dynamics and enteric pathogens. Nat Rev Microbiol [Internet]. 2011;9(4):265–78. Available from: http://dx.doi.org/10.1038/nrmicro2538

8. Maisel K, Ensign L, Reddy M, Cone R, Hanes J. Effect of surface chemistry on nanoparticle interaction with gastrointestinal mucus and distribution in the gastrointestinal tract following oral and rectal administration in the mouse. J Control Release. 2015;40(6):1301–15.

9. Faisant N, Gallant DJ, Bouchet B, Champ M. Banana starch breakdown in the human small intestine studied by electron microscopy. Eur J Clin Nutr [Internet].

1995;49(2):98–104. Available from: http://europepmc.org/abstract/MED/7743990

10. Maisel K, Chattopadhyay S, Moench T, Hendrix C, Cone R, Ensign LM, et al. Enema ion compositions for enhancing colorectal drug delivery. J Control Release [Internet]. 2015;209:280–7. Available from: http://dx.doi.org/10.1016/j.jconrel.2015.04.040

11. Moor K, Diard M, Sellin ME, Felmy B, Wotzka SY, Toska A, et al. High-avidity IgA protects the intestine by enchaining growing bacteria. Nature [Internet]. 2017;544(7651):498–502. Available from: http://www.nature.com/doifinder/10.1038/nature22058

12. Lukic J, Strahinic I, Milenkovic M, Nikolic M, Tolinacki M, Kojic M, et al. Aggregation factor as an inhibitor of bacterial binding to gut mucosa. Microb Ecol. 2014;68(3):633–44.

13. Bergström JH, Birchenough GMH, Katona G, Schroeder BO, Schütte A, Ermund A, et al. Gram-positive bacteria are held at a distance in the colon mucus by the lectin-like protein ZG16. Proc Natl Acad Sci [Internet]. 2016;113(48):13833–8. Available from: http://www.pnas.org/lookup/doi/10.1073/pnas.1611400113

14. Donaldson GP, Ladinsky MS, Yu KB, Sanders JG, Yoo BB, Chou WC, et al. Gut microbiota utilize immunoglobulin A for mucosal colonization. Science (80-) [Internet]. 2018;800(May):eaaq0926. Available from: http://www.sciencemag.org/lookup/doi/10.1126/science.aaq0926

15. Johansson ME V, Phillipson M, Petersson J, Velcich A, Holm L, Hansson GC. The inner of the two Muc2 mucin-dependent mucus layers in colon is devoid of bacteria. Proc Natl Acad Sci U S A. 2008;105(39):15064–9.

16. Johansson ME V, Larsson JMH, Hansson GC. The two mucus layers of colon are

organized by the MUC2 mucin, whereas the outer layer is a legislator of host-microbial interactions. Proc Natl Acad Sci U S A. 2011;108:4659–65.

17. Ambort D, Johansson ME V., Gustafsson JK, Nilsson HE, Ermund a., Johansson BR, et al. Calcium and pH-dependent packing and release of the gel-forming MUC2 mucin. Proc Natl Acad Sci. 2012;109(15):5645–50.

18. Verdugo P. Supramolecular dynamics of mucus. Cold Spring Harb Perspect Med. 2012;2(11).

19. Ambort D, Johansson ME V, Gustafsson JK, Ermund A, Hansson GC. Perspectives on mucus properties and formation- lessons from the biochemical world. Cold Spring Harb Perspect Med. 2012;2(11).

20. Johansson ME V, Gustafsson JK, Holmen-Larsson J, Jabbar KS, Xia L, Xu H, et al. Bacteria penetrate the normally impenetrable inner colon mucus layer in both murine colitis models and patients with ulcerative colitis. Gut. 2014;63(2):281–91.

21. Bergstrom KSB, Kissoon-Singh V, Gibson DL, Ma C, Montero M, Sham HP, et al. Muc2 protects against lethal infectious colitis by disassociating pathogenic and commensal bacteria from the colonic mucosa. PLoS Pathog. 2010;6(5).

22. Chassaing B, Koren O, Goodrich JK, Poole AC, Srinivasan S, Ley RE, et al. Dietary emulsifiers impact the mouse gut microbiota promoting colitis and metabolic syndrome. Nature [Internet]. 2015;519(7541):92–6. Available from: http://www.ncbi.nlm.nih.gov/pubmed/25731162

23. Velcich A, Yang W, Heyer J, Fragale A, Nicholas C, Viani S, et al. Colorectal Cancer in Mice Genetically Deficient in the Mucin Muc2. Science (80-) [Internet]. 2002;295(5560):1726–9. Available from: http://www.sciencemag.org/cgi/doi/10.1126/science.1069094

24. Asakura S, Oosawa F. On interaction between two bodies immersed in a solution of macromolecules. J Chem Phys. 1954;22(1954):1255–6.

25. Asakura S, Oosawa F. Interaction between particles suspended in solutions of macromolecules. J Polym Sci. 1958;33:183–92.

26. Vrij A. Polymers at interfaces and the interactions in colloidal dispersions. Pure Appl Chem. 1976;48:471–83.

27. Lieleg O, Vladescu I, Ribbeck K. Characterization of particle translocation through mucin hydrogels. Biophys J [Internet]. 2010;98(9):1782–9. Available from: http://dx.doi.org/10.1016/j.bpj.2010.01.012

28. Nguyen TLA, Vieira-Silva S, Liston A, Raes J. How informative is the mouse for human gut microbiota research? Dis Model Mech. 2015;8(1):1–16.

29. Blausen.com staff. Medical gallery of Blausen Medical 2014. WikiJournal Med. 2014;1(2). DOI:10.15347/wjm/2014.010

Chapter 2

HIGH-MOLECULAR-WEIGHT POLYMERS FROM DIETARY FIBER DRIVE AGGREGATION OF PARTICULATES IN THE MURINE SMALL INTESTINE

1. A. Preska Steinberg, S. S. Datta, T. Naragon, J. C. Rolando, S. R. Bogatyrev, R. F. Ismagilov. 2018. "High-molecular-weight polymers from dietary fiber drive aggregation of particulates in the murine small intestine." eLife. 8:e40387. DOI: 10.7554/eLife.40387

Abstract

The lumen of the small intestine (SI) is filled with particulates: microbes, therapeutic particles, and food granules. The structure of this particulate suspension could impact uptake of drugs and nutrients and the function of microorganisms; however, little is understood about how this suspension is re-structured as it transits the gut. Here, we demonstrate that particles spontaneously aggregate in SI luminal fluid ex vivo. We find that mucins and immunoglobulins are not required for aggregation. Instead, aggregation can be controlled using polymers from dietary fiber in a manner that is qualitatively consistent with polymer-induced depletion interactions, which do not require specific chemical interactions. Furthermore, we find that aggregation is tunable; by feeding mice dietary fibers of different molecular weights, we can control aggregation in SI luminal fluid. This work suggests that the molecular weight and concentration of dietary polymers play an underappreciated role in shaping the physicochemical environment of the gut.

Introduction

The small intestine (SI) contains numerous types of solid particles. Some of these particles include microbes, viruses, cell debris, particles for drug delivery, and food granules (1–5).

Little is understood about the state of these particles in the small intestine; do these particles exist as a disperse solution or as aggregates? An understanding of how particulate matter is structured as it moves through the SI would contribute to fundamental knowledge on a host of topics, such as how microbes, including probiotics and pathogens, function in the SI (6–10). Knowledge of how particle suspensions change during transit would also provide insight into how the uptake of drugs and nutrients is affected by the physiochemical properties of the SI environment (3,4). It would also give us better comprehension of how the SI acts to clear potential invaders and harmful debris (2,11).

Polymers abound in the gut in the form of secretions (e.g., mucins and immunoglobulins) and dietary polymers (e.g., dietary fibers and synthetic polymers). It is well known that host-secreted polymers can cause aggregation of particles via chemical interactions; for example, mucins (12–16), immunoglobulins (17–25), and proteins (26) can cause bacteria to aggregate via an agglutination mechanism. However, non-adsorbing polymers can also cause aggregation via purely physical interactions that are dependent on the physical properties of the polymers, such as their molecular weight (MW) and concentration (27–33). Here, we investigate whether these physical interactions play a role in structuring particles in the SI. For this work, we study the interactions between polystyrene particles densely coated with polyethylene glycol (PEG) and the luminal contents of the SI. It has been demonstrated previously that PEG-coated particles have little or no chemical interactions with biopolymers (34,35), so using PEG-coated particles allows us to isolate and investigate only the interactions dominated by physical effects.

Results

PEG-coated particles aggregate in fluid from the murine small intestine

It has been observed that both bacteria (19–21,23,25,26) and particles (3,36–38) aggregate in the gut. Experiments have been performed in which mice are orally co-administered carboxylate-coated nanoparticles, which are mucoadhesive, and PEG-coated nanoparticles, which are mucus-penetrating (3). The carboxylate-coated particles formed large aggregates

in the center of the gut lumen. In contrast, PEG-coated particles were sometimes found co-localized with carboxylate-coated particles and also penetrated mucus, distributing across the underlying epithelium of the SI as aggregates and single particles.

To evaluate the distribution of particulate suspensions in the SI, we suspended 1-µm-diameter fluorescent PEG-coated particles (see *Materials and Methods* for synthesis) in buffers isotonic to the SI and orally administered them to mice. We chose 1 µm-diameter particles because of their similarity in size to bacteria. We collected luminal contents after 3 h and confirmed using confocal fluorescence and reflectance microscopy that these particles aggregated with each other and co-aggregated with what appeared to be digesta (Figure 2.1*C* and *D*; *Materials and Methods*). On separate mice, fluorescent scanning was used to verify that particles do transit the SI after 3 h (Figure 2.1*A* and *B*; *Materials and Methods*).

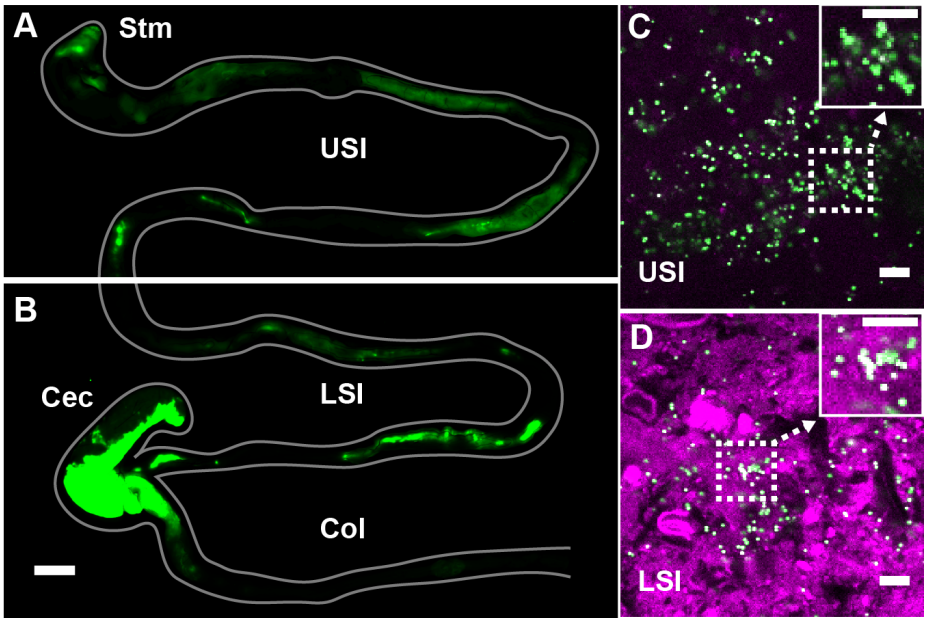

Figure 2.1: PEG-coated particles aggregate in the murine small intestine (SI). (A and B) Fluorescent scanner image of gastrointestinal tract (GIT) from a mouse orally administered a suspension of 1-µm diameter PEG-coated particles (green). Scale bar is 0.5 cm. (see Figure 2-S1 for image processing steps and how contours of gut were outlined). (C and D) Confocal micrographs of luminal contents from the upper (C) and lower (D) SI of a mouse orally gavaged with PEG-coated particles (green) showing scattering from luminal contents (purple). Scale bars are 10 µm. Stm = Stomach; USI = upper SI; LSI = lower SI; Col = colon.

Given the rich complexity of the SI, wherein particles co-aggregate with digesta and bacteria, and are subjected to the mechanical forces of digestion and transit (39), and other phenomena, we developed an *ex vivo* assay to characterize the structure of particles in luminal fluid from the SI of mice. As a simple starting point, we sought to understand interactions among particles of known chemistry and the luminal fluid of the SI. To minimize chemical interactions with the biopolymers of the SI, we again chose PEG-coated polystyrene particles. PEG coatings have been shown to minimize biochemical interactions between polystyrene particles and biopolymers in a variety of contexts (34,35), and thus PEG-coated particles are commonly used in drug delivery (3,38,40).

To create PEG-coated polystyrene particles for the *ex vivo* experiments, we took 1-μm-diameter carboxylate-coated polystyrene particles and conjugated PEG to the surface (*Materials and Methods*). We used NMR to verify that PEG coated the surface of the particles (see *Materials and Methods* and Table 2.S8). We found that by coating with PEG 5 kDa and then coating again with PEG 1 kDa to backfill the remaining surface sites on the particle allowed us to achieve a lower zeta potential than applying a single coat of PEG 5 kDa (Table 2.S8). We chose these particles for use in our assay. It has been suggested in the literature that a near-zero zeta potential minimizes the interactions particles have in biological environments (35).

To collect luminal fluid from the SI of mice, we excised the SI of adult mice (8-16 weeks old), divided it into an upper and lower section, and gently collected the luminal contents on ice. To separate the liquid and solid phase, we centrifuged the contents and collected the supernatant. To further ensure that any remaining solid material was removed from the fluid phase, we filtered the supernatant through a 30-μm pore size spin column and collected the filtrate (see *Materials and Methods* for more details). We then placed the PEG-coated particles in the SI luminal fluid at a volume fraction of ≈0.001. A low-volume fraction was chosen because bacteria in the healthy SI are found at similarly low-volume fractions (41–43). We found that, despite the PEG coating and low-volume fraction, aggregates of particles formed in 5-10 min (Figure 2.2*A-D*), a timescale much shorter than

the transit time for food through the SI, which can be as short as ~80 min in healthy humans (39) and ~60 min in mice (44). On longer timescales, peristaltic mixing could also play a role (39); during fasting, the migrating motor complex (MMC) cycle first consists of a period of quiescence for ~30-70 min, followed by a period of random contractions, then by 5 to 10 minutes in which contractions occur at 11-12 counts per minute (cpm) in the duodenum and 7-8 cpm in the ileum. After eating, MMC is substituted with intermittent contractions in the SI and waves can occur at a frequency of 19-24 cpm in the distal ileum 1-4 h later. We therefore chose to focus on aggregation at short timescales (~10 min) because we sought to understand the initial formation of aggregates before aggregation is influenced by mechanical forces such as shear due to peristaltic mixing and the transit of food.

To quantify the amount of aggregation in samples of luminal fluid, we developed a method to measure the sizes of all aggregates in solution using confocal microscopy (see *Materials and Methods*). From these datasets, we created volume-weighted empirical cumulative distribution functions (ECDFs) of all the aggregate sizes in a given solution. We used these volume-weighted ECDFs to compare the extent of aggregation in a given sample (Figure 2.2*F* and *H*). To test the variability of aggregation in samples collected from groups of mice treated under the same conditions, we compared the extent of aggregation in pooled samples taken from three groups, each consisting of three male mice on a standard chow diet. We plotted the volume-weighted ECDFs of each sample (Figure 2.2*F* and *H*) and observed that the variation among the groups under the same conditions appeared to be small compared with the differences between the samples and the control.

To quantify the variability of aggregation among groups using an additional method, we bootstrapped our datasets to create 95% bootstrap confidence intervals (CI) of the volume-weighted average aggregate size of each of the three groups and the control in Hank's balanced salt solution (HBSS) (Figure 2.2*G* and *I*; see *Materials and Methods* for complete details of the bootstrapping procedure). All 95% bootstrap CI either overlapped or came

close to overlapping, again suggesting there was little variability among pooled samples treated under the same conditions (male mice on a standard chow diet).

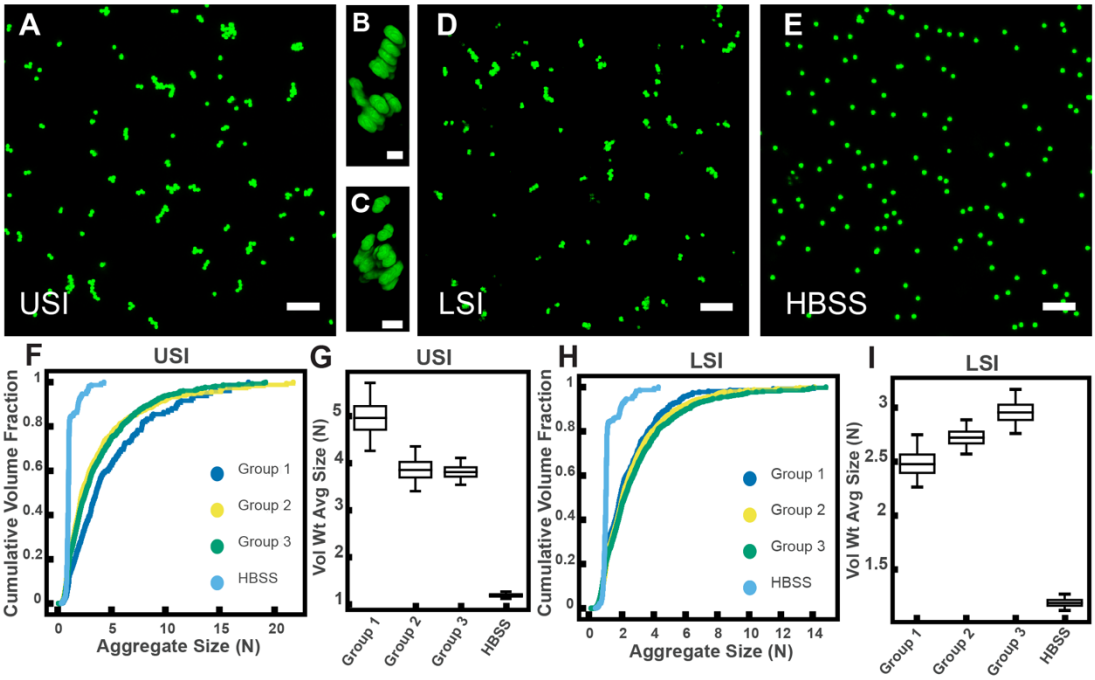

Figure 2.2: PEG-coated particles aggregate in fluid from the murine small intestine (SI) *ex vivo*. The 1-µm-diameter PEG-coated particles form aggregates in fluid collected from the upper (A-C) and lower (D) SI in ~10 min. (A and D) Maximum z-projections of 10 optical slices taken on a confocal microscope. (B and C) 3D renderings of aggregates found in panel A. (E) Maximum z-projection of the same particles in HBSS. Scale bars are 10 µm in 2D images and 2 µm in 3D images. (F and H) Volume-weighted empirical cumulative distribution functions (ECDFs) comparing aggregation of the particles in pooled samples from the upper (F) and lower (H) SI of three separate groups of male chow-fed mice (each group consisted of three mice) and a control (particles suspended in HBSS). The vertical axis is the cumulative volume fraction of the total number of particles in solution in an aggregate of a given size. The horizontal axis (aggregate size) is given as the number of particles per aggregate (N). (G and I) Box plots depicting the 95% empirical bootstrap CI of the volume-weighted average aggregate size (given in number of particles per aggregate, N) in samples from the upper (G) and lower (I) SI (the samples are the same as those from panels F and H). The line bisecting the box is the 50th percentile, the upper and lower edges of the box are the 25th and 75th percentile respectively, and the whiskers are the 2.5th and 97.5th percentiles. USI = upper SI; LSI = lower SI. See *Materials and Methods* for bootstrapping procedure.

Fractionation of SI fluids suggests polymers play a role in aggregation of PEG-coated particles

Given that polymers can aggregate particles and bacteria via several mechanisms (12–33), we hypothesized that biopolymers in SI luminal fluid are involved in the aggregation of our PEG-coated particles. We therefore sought to first quantify the physical properties of the polymers in the luminal fluid of the SI. To do this, we used a 0.45-μm filter to remove additional debris and ran samples from a group of three chow-fed mice on a gel permeation chromatography (GPC) instrument coupled to a refractometer, a dual-angle light scattering (LS) detector, and a viscometer (details in *Materials and Methods*). Chromatography confirmed that polymers were indeed present in the SI fluid (Figure 2.3*A* and *D*). Because we do not know the refractive index increment (dn/dc) of the polymers present in these samples and the polymers are extremely polydisperse, we cannot make exact calculations of the physical parameters of these polymers. We can, however, calculate estimated values by assuming the range of the dn/dc values to be about 0.147 for polysaccharides and about 0.185 for proteins and then dividing the sample into different fractions based on retention volume (estimates of concentration and MW of polymers are displayed on Figure 2.3*A* and *D*). The estimates suggest that the SI is abundant in polymers with a range of MWs.

To qualitatively test our hypothesis that biopolymers in the SI were involved in the aggregation of our PEG-coated particles, we collected SI luminal fluid from a different group of three male, chow-fed mice. We performed an additional filtration step (0.45-μm) to further ensure the removal of any solid materials. This filtrate was then separated into aliquots and each aliquot was run through a different MW cut-off (MWCO) filter (see *Materials and Methods*). We then collected the eluent of each aliquot and compared the aggregation of our PEG-coated particles in each (Figure 2.3*B, C, E,* and *F*). We generally found less aggregation in the fractionated samples compared with the 30- and 0.45-μm filtered samples. When the MWCO was decreased to 3 kDa, the observed aggregation in the eluent matched the extent of aggregation observed for particles in HBSS. Overall, these

data supported our hypothesis that polymers were involved in the aggregation of these particles.

Interestingly, in the lower SI, we observed more aggregation in the 0.45-µm filtered sample compared with the 30-µm filtered sample. From handling the samples, we observed that the 30-µm filtered samples appeared to be more viscous than the 0.45-µm filtered samples. We postulate that this increase in viscosity was due to the formation of self-associating polymeric structures, although we did not test this assumption. We attribute this decrease in aggregation in the 30-µm filtered samples to slower aggregation kinetics due to decreased diffusivity of particles in this viscous medium. This decrease in aggregation at high polymer concentrations or viscosities is also observed in solutions of model polymers, as discussed in the next section.

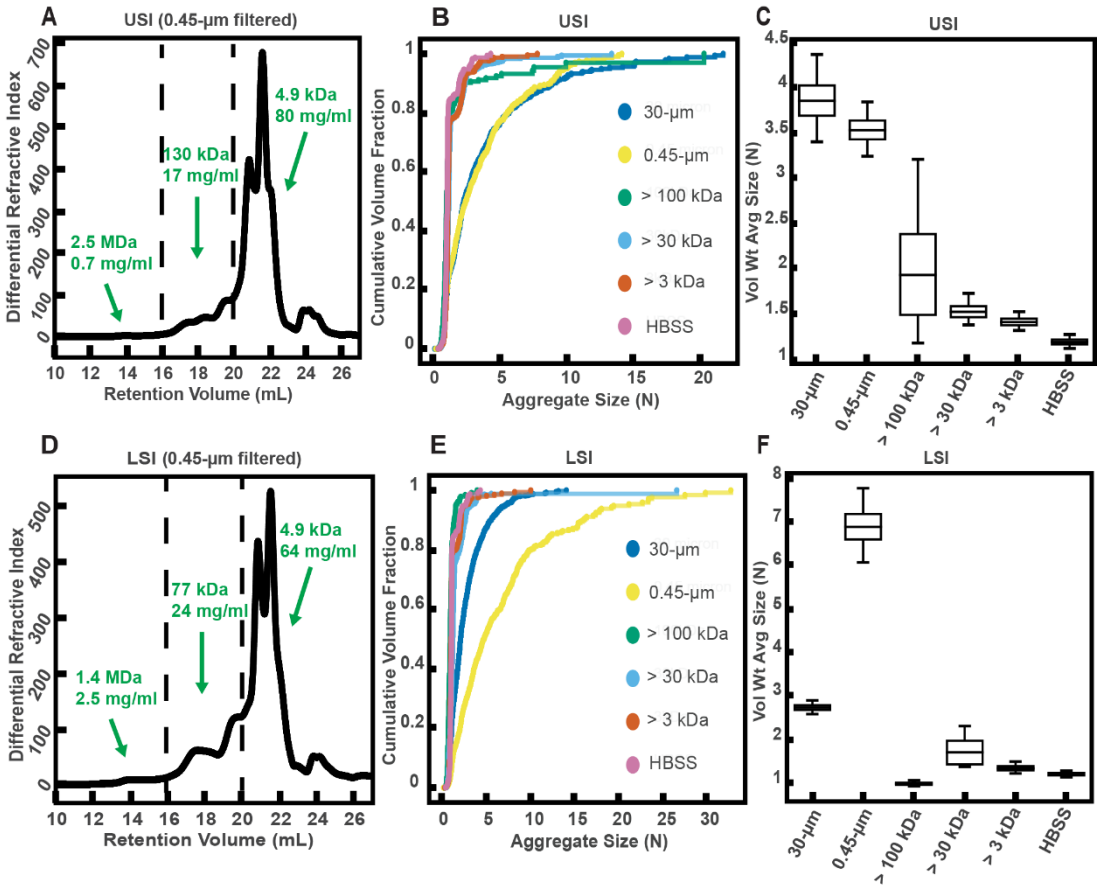

Figure 2.3: Gel permeation chromatography (GPC) of fluid from the small intestine (SI) and aggregation of PEG-coated particles in fractionated fluid from SI. (A and D) Chromatograms of samples from the upper (A) and lower (D) SI from a group of three chow-fed mice. Dashed lines indicate the three retention volumes the chromatograms were divided into for analysis: 11-16 mL, 16-20 mL, and >20 mL. Estimated concentrations and molecular weight (MW) are reported in green on the chromatograms for each retention volume. (B and E) Volume-weighted empirical cumulative distribution functions (ECDFs) of aggregate sizes in the upper (B) and lower (E) SI liquid fractions of chow-fed mice which have been run through MW cut-off (MWCO) filters with different MWCOs. As a control, aggregate sizes were also measured for particles placed in HBSS. The vertical axis is the cumulative volume fraction of the total number of particles in solution in an aggregate of a given size. The horizontal axis is aggregate size (number of particles per aggregate, N). (C and F) Box plots depict the 95% empirical bootstrap CI of the volume-weighted average aggregate size (given in number of particles per aggregate, N) in the samples from panels B and E, respectively (see *Materials and Methods* for bootstrapping procedure). The line bisecting the box is the 50th percentile, the upper and lower edges of the box are the 25th and 75th percentile respectively, and the whiskers are the 2.5th and 97.5th percentiles.

Aggregation of PEG-coated particles in model polymer solutions shows complex dependence on the concentration and MW of polymers.

Before exploring the complex environment of the SI further, we sought to first understand how our PEG-coated particles behaved in simple, well-characterized polymer solutions with similar MW and concentrations to those polymers we found in the SI in the previous experiments (Figure 2.3*A* and *D*). It has been demonstrated that the aggregation of colloids and bacteria can be controlled by altering the concentration and size of the non-adsorbing polymers to which particles are exposed (27–33). In these controlled settings, particles aggregate due to what are known as depletion interactions (27–29). Many groups have focused on depletion interactions with hard-sphere-like colloids; they often use polymethylmethacrylate particles sterically stabilized with polyhydroxystearic acid, because these particles closely approximate hard-sphere-like behavior (45,46). In these scenarios, depletion interactions are often described as forces that arise when particles get close enough to exclude polymers from the space between them, resulting in a difference in osmotic pressure between the solution and the exclusion region, leading to a net attractive force (27–31). Others have instead chosen to describe the phase behavior of the colloid/polymer mixture in terms of the free energy of the entire system (33,47). Short-range attractions (polymer radius is ten-fold less than particle radius) between hard-sphere colloids induced by polymers have been described successfully in the language of equilibrium liquid–gas phase separation (48,49).

Some groups have explicitly accounted for the effects of the grafted polymer layer used to sterically stabilize colloids when studying interactions between polymer solutions and colloids (50–58); this includes groups studying mixtures of polystyrene particles sterically stabilized with grafted layers of PEG (MWs of 750 Da and 2 kDa) and aqueous solutions of free PEG polymer (MW from 200 Da to 300 kDa) (51,52). It has been found experimentally that in mixtures of polymers and sterically stabilized colloids, the colloids form aggregates above a threshold polymer concentration. At even higher concentrations,

as the characteristic polymer size shrinks, the colloids cease to aggregate, a phenomenon referred to as "depletion stabilization."

To test whether our PEG-coated particles behave similarly to what has been previously found in mixtures of polymers and sterically stabilized particles, we created polymer solutions with PEG at a range of polymer concentrations and MWs and measured the extent of aggregation in these polymer/particle mixtures (Figure 2.4*A-D*). We chose PEGs that have MWs similar to the MW of polymers we found naturally occurring in the SI (Figure 2.3*A, D*): 1 MDa, 100 kDa, and 3350 Da. Using PEGs with similar physical properties (i.e., MW, concentration) as a simple model of polymers found in the SI allows us to focus solely on physical interactions between the particles and polymers. We created PEG solutions in HBSS at mass concentrations similar to those measured for polymers in the SI (Figure 2.3*A* and *D*) and imaged the polymer/particle mixtures after ~10 min. HBSS was chosen because it has a similar pH and ionic strength to that of the SI (59,60). At the high ionic strengths of these buffered aqueous solutions (~170 mM), any electrostatic repulsions that can occur between particles should be screened to length scales of order the Debye screening length ~0.7 nm (61,62), nearly an order of magnitude smaller than the estimated length of the surface PEG brush (~6.4 nm; see *Materials and Methods* for more details). We again chose to look at aggregation on short timescales (after ~10 min) because we sought to understand the initial formation of aggregates; in the SI, on longer timescales, aggregation will likely also be influenced by mechanical forces such as shear due to peristaltic mixing and the transit of food.

For PEG 1 MDa and 100 kDa solutions we found aggregates of similar sizes to those observed in the SI luminal fluid (Figure 2.4*A-D*). We did not detect any aggregation for the PEG 3350 Da solutions (Figure 2.4*D*). Because the pH is known to vary across different sections of the gastrointestinal tract and this could affect the observed aggregation behavior, we measured the pH in luminal fluid from the upper and lower small intestine (see *Figure 2-S2* and *Materials and Methods*). We found that the upper small intestine (USI) luminal fluid was $pH = 6.0 \pm 0.1$ and for the lower small intestine (LSI) $pH =$

7.5 ± 0.3. For the HBSS used, $pH = 7.6 \pm 0.1$ (See *Materials and Methods*), which matches that of the LSI but not the USI. We therefore conducted the same *in vitro* experiment for PEG 1 MDa in phosphate buffered saline with $pH = 6.0 \pm 0.1$ (*Materials and Methods* and Figure 2.4 – figure supplement 1). We found some differences in the aggregation, but the overall trends were similar to before.

Overall, though our system is not at equilibrium at these short timescales, we found trends consistent with what has been observed in the literature for depletion interactions with sterically stabilized particles (50–58). At dilute polymer concentrations, the extent of aggregation increased with concentration. At higher polymer concentrations, the extent of aggregation began to decrease as the solutions begin to "re-stabilize." Additionally, the extent of aggregation was greater for longer polymers. Interestingly, we found that the curves for the long polymers in Figure 2.4D could be collapsed by normalizing the polymer concentration by the overlap concentration (which denotes the transition between the dilute to semi-dilute polymer concentration regimes) for each respective polymer solution (Figure 2.4 – figure supplement 2). We next sought to describe the inter-particle potential using theory that combines depletion interactions with steric interactions.

We applied previously established theoretical frameworks that combine depletion interactions with steric interactions to better understand our system (50,54,58). To account for the depletion attractions between colloids we used the Asakura–Oosawa (AO) potential (U_{dep}) (27–29):

$$U_{dep}(r) = \begin{cases} +\infty \; for \; r \leq 0 \\ -2\pi\Pi_P a\left(R_P - \frac{r}{2}\right)^2 \; for \; 0 < r < 2R_P \\ 0 \; for \; r > 2R_P \end{cases} \qquad (Eq. 2.1)$$

where U_{dep} is given in joules, Π_P is the polymer osmotic pressure (in Pa), a is the radius of the colloid (in m), R_P is the characteristic polymer size (in m), and r is the separation distance between bare particle surfaces (in m). This form of the depletion potential equation assumes that $a >> R_P$, a condition satisfied for 1 μm particles we used. For the polymer

osmotic pressure, we used the following crossover equation for a polymer in a good solvent (63,64):

$$\Pi_P = \frac{N_{Avo}kT}{MW} c_P \left(1 + \left(\frac{c_P}{c_P^*}\right)^{1.3}\right) \qquad (Eq.\,2.2)$$

where Π_P is given in pascals, N_{Avo} is Avogadro's number, k is the Boltzmann constant, T is the temperature (in kelvins), MW is the molecular weight of the polymer (in Da), c_P is the polymer mass concentration (in kg/m^3), and c_P^* is the polymer overlap concentration (in kg/m^3). This equation describes the polymer osmotic pressure well in both the dilute and semi-dilute regime.

For the characteristic polymer size, we used the concentration-dependent radius of gyration (31,65). This can be written as:

$$R_P(c_P) = R_g(0)\left(\frac{Mw}{N_{Avo}kT}\frac{d\Pi_P}{dc_P}\right)^{-\frac{1}{2}} \qquad (Eq.\,2.3)$$

where $R_P(c_P)$ is the concentration-dependent radius of gyration or the characteristic polymer size given in meters, $R_g(0)$ is the radius of gyration (in m) at dilute concentrations and Π_P is given by equation 2.2. The characteristic polymer size is given by the dilute radius of gyration at low concentration and is close to the correlation length of the polymer solution, or the average distance between monomers, in the semi-dilute regime. Therefore, using equations 2.2 and 2.3, we acquire the correct limits for the depletion potential; the Asakura–Oosawa potential in the dilute regime and the depletion potential described by Joanny, Liebler, and de Gennes in the semi-dilute regime (66). Similar crossover equations have been found to adequately describe experimentally observed depletion aggregation in polymer-colloid mixtures where the polymer concentration spans the dilute and semi-dilute regimes (67). Using literature values for the hydrodynamic radii of the PEGs (68) and the Kirkwood-Riseman relation, which relates the hydrodynamic radius to the radius of gyration (68–70), we estimated $R_g(0)$ for each polymer. We estimated $R_g(0) \approx 62.6$, 16.7,

2.9 nm for PEG 1 MDa, 100 kDa, and 3350 Da, respectively. Using both the estimates of $R_g(0)$ and the MW of each polymer, we then estimated c_p^* for each polymer (63,71). We estimated c_p^* = 1.6, 8.6, and 52.6 mg/mL for PEG 1 MDa, 100 kDa, and 3350 Da, respectively.

To account for steric interactions between the two grafted layers upon close inter-particle separations, we used equation 2.4 (50,52). For inter-particle separation distances between L and $2L$, where L is the length of the grafted layer, the steric interactions between the two grafted layers can be described using the Flory–Huggins free energy of mixing:

$$U_{s,mix}(r) = \frac{4\pi akT}{\upsilon_1}\left(\overline{\phi_2^a}\right)^2\left(\frac{1}{2}-\chi\right)\left(L-\frac{r}{2}\right)^2 \qquad (Eq.\,2.4)$$

where $U_{s,mix}$ is the steric interaction energy due to mixing (given in joules), a is the particle radius (in m), υ_1 is the volume of a water molecule (in m^3), $\overline{\phi_2^a}$ is the average volume fraction of the grafted polymer (unitless), χ is the Flory–Huggins interaction parameter for the grafted polymer and the solvent (unitless), and L is the length of the grafted layer (in m). For PEG in aqueous solvents, $\chi = 0.45$ (72). Our NMR measurements (see *Materials and Methods* for details) suggest that the grafting density of PEG is within the brush regime. We therefore use the Alexander–de Gennes approximation (63) and our NMR measurements to estimate the length of the grafted layer (L) as $L \sim 6.4$ nm and the average volume fraction to be $\overline{\phi_2^a} \sim 0.43$.

For inter-particle separations closer than L, one needs to account for elastic deformations of the grafted layers (50,57). This is far greater in magnitude than U_{dep}, so one can simply assume that at this point the potential is extremely repulsive. For inter-particle separations greater than L:

$$U(r) = \begin{cases} U_{s,mix} + U_{dep}\ for\ L < r < 2L \\ U_{dep}\ for\ r \geq 2L \end{cases} \qquad (Eq.\,2.5)$$

Using this theoretical framework, we can build a physical intuition for the system **(**Figure 2.4*E*-*G***)**. Long polymers have depletion layers that extend out past the brush layer and overlap, inducing attractions between the particles (Figure 2.4*E*). For short polymers ($R_P < L$), the depletion attractions are buried within the steric repulsions induced by the brush and there are effectively no attractions among the particles (Figure 2.4*F*). We can use this crossover to estimate the magnitudes of the minima in the inter-particle potentials for the three PEG solutions **(**Figure 2.4*H***)**. It should be noted that we have made several simplifications; for example, we do not consider interactions between free polymers and the grafted layer, which could lead to partial penetration of free polymers into the grafted layer or possible compression of the grafted layer by the free polymers (50,56,57). Despite such simplifications, we find that the calculated minima display similar concentration trends to the trends seen in the average aggregate sizes **(**Figure 2.4*D***).** These calculations offer an explanation for why there is no aggregation of PEG-coated particles in solutions of PEG 3350.

Another factor that needs to be considered at the short timescales and low-volume fractions we are working at is aggregation kinetics (73–75). The probability that particles collide in solution is directly related to the diffusion coefficient and the volume fraction of the particles. As we increase the polymer concentration we increase the viscosity of the solution and decrease the diffusivity of the particles. In Figure 2.4*I*, we plot theoretical estimates of the diffusion coefficients of the particles against the concentrations of the PEG solutions. These diffusion coefficients were estimated using literature measurements, the Stokes–Einstein–Sutherland equation, and the Huggins equation for viscosity (63,68).

Because our system has not reached equilibrium, in this case the non-monotonic dependence of aggregation on polymer concentration for long polymers is due to a complex interplay between thermodynamics and kinetics (which we have not untangled). However, both the dependence of diffusivity (Figure 2.4*I***)** and the equilibrium prediction of inter-particle minima **(**Figure 2.4*H***)** on polymer concentration suggest that we should expect a decrease in aggregation at high polymer concentrations. The inter-particle minima also

suggests that we should not expect short polymers to induce aggregation. Both trends are consistent with what we observe. Understanding how our PEG-coated particles behave in these so-called "simple" polymer solutions with similar physical properties to the intestinal polymers we detected (Figure 2.3*A* and *D*) informs the interpretation of the results of the next sections.

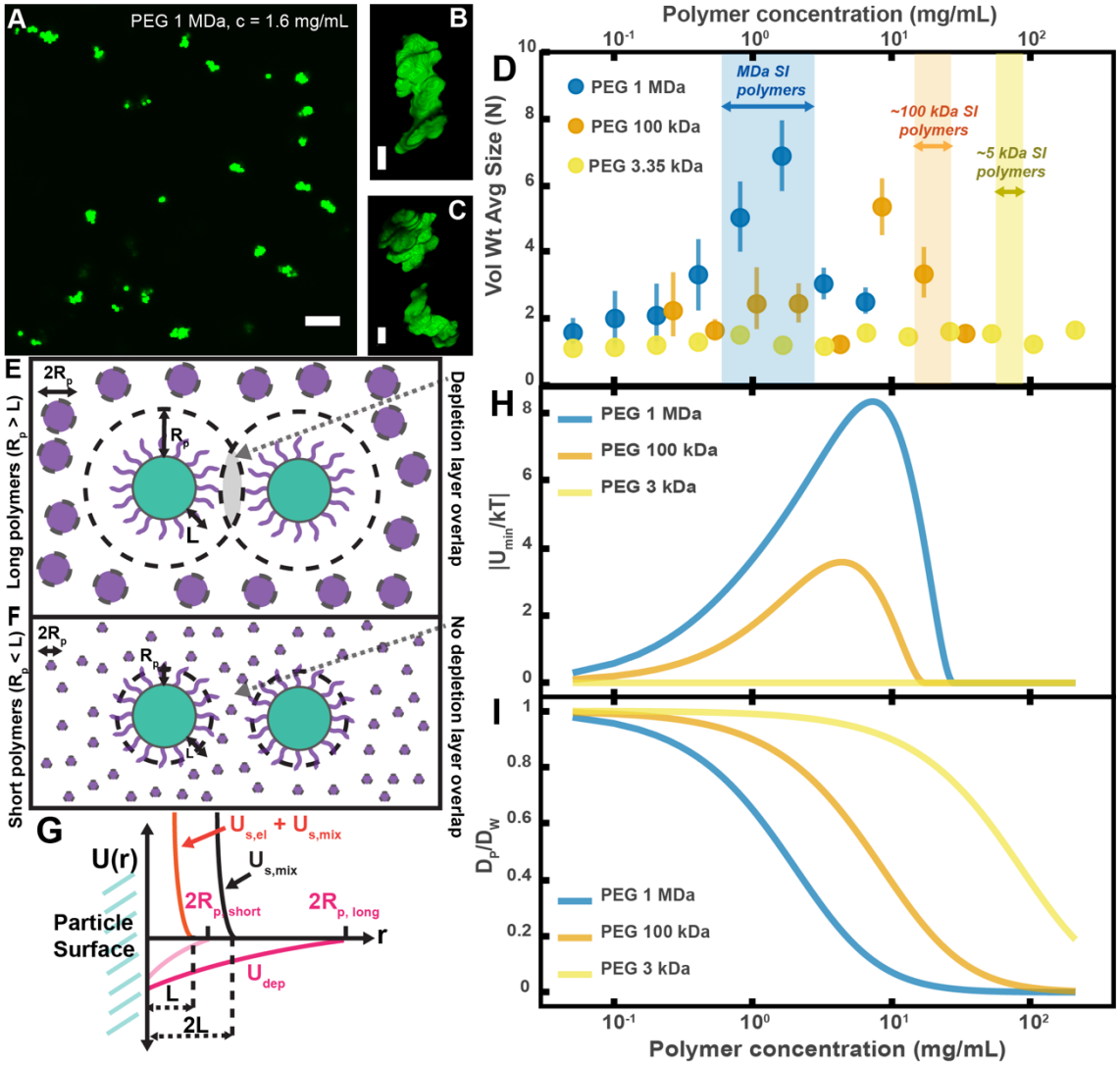

Figure 2.4: Aggregation of PEG-coated particles in model polymer solutions shows complex dependence on molecular weight (MW) and concentration of PEG. **(A)** Aggregates of 1 µm diameter PEG-coated particles in a 1 MDa PEG solution with a polymer concentration (c) of 1.6 mg/mL. Image is a maximum z-projection of 10 optical slices taken on a confocal microscope. Scale bar is 10 µm. **(B** and **C**) 3D renders of

aggregates found in panel A. Scale bars are 2 μm. **(D)** Volume-weighted average sizes for serial dilutions of PEG solutions of three MW (1 MDa, 100 kDa, and 3350 Da). Volume-weighted average sizes are plotted on the vertical axis in terms of number of particles per aggregate (N) against polymer mass concentration (c_P) in mg/mL. The vertical error bars are 95% empirical bootstrap CI (see *Materials and Methods* for bootstrapping procedure). Shaded regions indicate the concentration ranges of detected intestinal polymers of similar MW. **(E)** Schematic depicting depletion interactions induced by "long polymers" (polymer radius (R_P) > length of the brush, L). Free polymers are depicted as purple spheres. Colloids are depicted in green with the grafted brush layer in purple. The depletion layer around each colloid is depicted by dotted lines. The overlap region between the two depletion layers is indicated in grey. **(F)** Schematic depicting depletion interactions induced by "short polymers" (R_p < L). The depletion zone does not extend past the length of the brush and there is effectively no overlap in the depletion layers; the depletion attractions are "buried" within the steric layer. (**G**) Schematic depicting the different contributions to the inter-particle potential (U(r)) against inter-particle separation distance (r). The hard surfaces of the particles are in contact at r = 0. U_{dep} depicts the depletion potential for a short polymer ($R_{P,short}$) and a long polymer ($R_{P,long}$). $U_{s,mix}$ shows the contribution to the steric potential due to mixing. $U_{s,el} + U_{s,mix}$ shows the contribution due to elastic deformations and mixing at close inter-particle separations. **(H)** The magnitude of the minima of the inter-particle potential (U_{min}/kT) plotted against polymer concentration for the three PEG solutions in (D). **(I)** Diffusion coefficients estimated from the Stokes–Einstein–Sutherland equation for 1 μm particles in the PEG solutions used in (D). Diffusion coefficients of particles in polymer solutions (D_P) are normalized by the diffusion coefficients in water (D_W) and plotted against polymer concentration. **Figure supplement 1** shows the dilution series for PEG 1 MDa at pH = 6.0 compared to pH = 7.6. **Figure supplement 2** shows the dilution series displayed in Figure 2.4D where the polymer concentration has been normalized by the overlap concentration of each polymer solution.

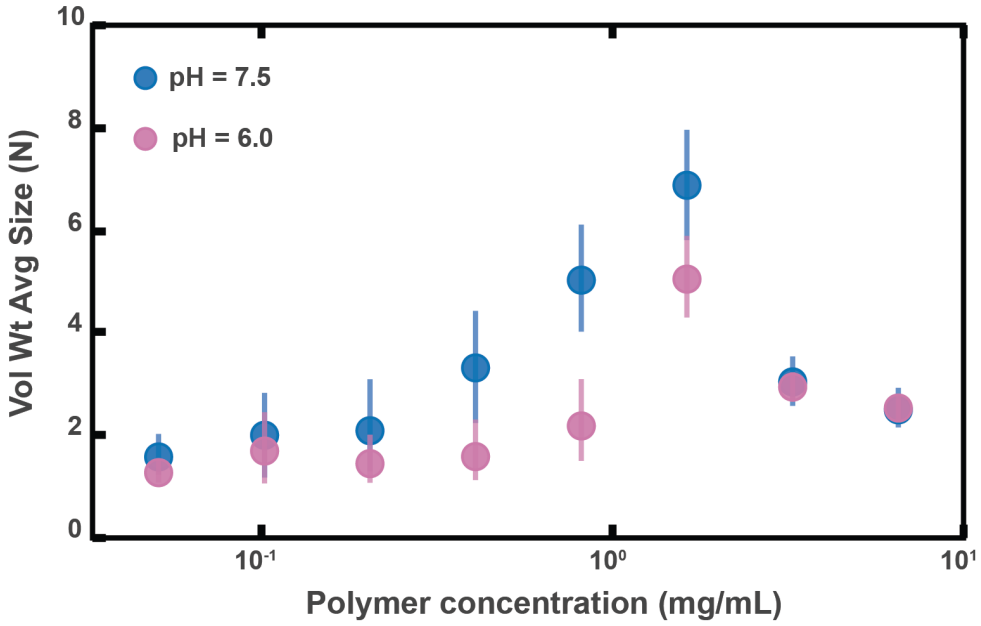

Figure 2.4 – figure supplement 1: Aggregation of PEG-coated particles in model polymer solutions with different pH**. (A)** Volume-weighted average sizes for serial dilutions of 1 MDa PEG solutions in a phosphate buffered saline solution with $pH = 6.0 \pm 0.1$ (labeled pH = 6.0) and in Hank's balanced salt solution (HBSS) with $pH = 7.6 \pm 0.1$ (same data from Figure 2.4D). Volume-weighted average sizes are plotted on the vertical axis in terms of number of particles per aggregate (N) against polymer mass concentration (c_p) in mg/mL. The vertical error bars are 95% empirical bootstrap CI (see *Materials and Methods* for bootstrapping procedure).

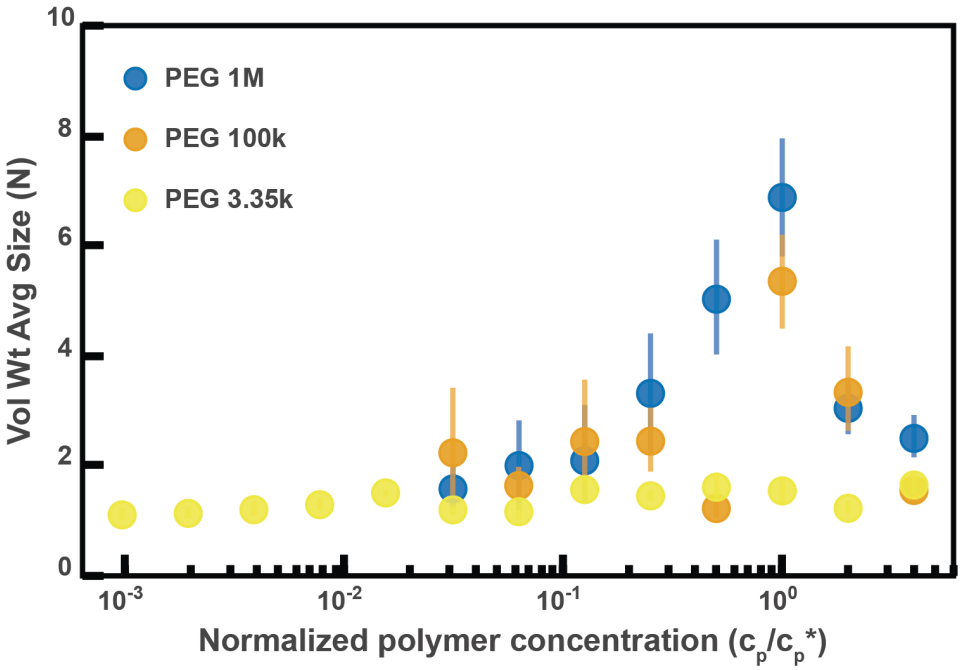

Figure 2.4 – figure supplement 2: Aggregation of PEG-coated particles in model polymer solutions from Figure 4D normalized by polymer overlap concentration. Volume-weighted average sizes for serial dilutions of 1 MDa PEG solutions in Hank's balanced salt solution (HBSS). Volume-weighted average sizes are plotted on the vertical axis in units of number of particles per aggregate (N) against the "normalized polymer concentration." The normalized polymer concentration is the polymer mass concentration (c_p) in mg/mL divided by the overlap concentration of each polymer solution (c_p^*) in mg/mL. The overlap concentrations for PEG 1 MDa, 100 kDa, and 3350 Da are c_p^* = 1.6, 8.6, and 52.6 mg/mL, respectively. The vertical error bars are 95% empirical bootstrap CI (see *Materials and Methods* for bootstrapping procedure).

MUC2 may play a role in the aggregation of PEG-coated particles, but is not required for aggregation to occur

It has been demonstrated that mucins can aggregate and bind to bacteria *in vitro* (12–16); thus, we wanted to test whether mucins, such as Mucin 2 (MUC2), which is the primary mucin secreted in the SI (76,77), drive the aggregation of PEG-coated particles in SI fluid. It is known that in the presence of Ca^{2+} and at $pH \leq 6.2$, MUC2 can form aggregates or precipitate out, but it is soluble without Ca^{2+} or at higher pH (78). Our measurements of the pH throughout the SI suggest that it is possible that MUC2 precipitates out in the upper

small intestine; however, because it is unclear how much Ca^{2+} is in the lumen of the upper small intestine, there could be soluble MUC2 in the upper small intestine. Additionally, the literature suggests that, based on the pH, there should be soluble MUC2 in the lower small intestine. We therefore tested if MUC2 drives aggregation in both the upper and lower small intestine. To do this, we compared the aggregation of our PEG-coated particles in samples from MUC2 knockout (MUC2KO) mice to samples from wild-type (WT) mice. To carefully preserve the native composition of the SI fluid, we used a protease-inhibitor cocktail when collecting the samples (see *Materials and Methods*). We confirmed mouse MUC2KO status via genotyping and Western blot (Figure 2.5*E*; *Materials and Methods*). The Western blot detected MUC2 in the colons of WT mice and not MUC2KO mice, as expected, however it did not detect a signal for MUC2 in the SI of either the WT or MUC2KO mice. We speculate that the lack of MUC2 signal in the SI of WT mice may be due to low levels of MUC2 present in the luminal contents of the SI.

We observed aggregation in samples from both the MUC2KO and WT mice (Figure 2.5*A-B*). To test the strength of the aggregation effect in the different samples, we serially diluted the samples and measured the average aggregate size to see when the effect disappeared (Figure 2.5*C-D*). As explained in the previous section, we do not necessarily expect to see a linear decrease in aggregation with dilution. For simplicity, we will refer to the dilution factor at which aggregation begins to disappear as the "aggregation threshold." We found differences in the aggregation threshold in the samples from MUC2KO and WT mice **(**Figure 2.5*C-D*), suggesting that although MUC2 is not required for aggregation to occur, it could play a role in the aggregation of PEG-coated particles.

We wanted to test differences in the MW distribution of the polymers found in these samples, so we 0.45-μm-filtered our samples and analyzed them by GPC (see *Materials and Methods*). The chromatograms from the refractometer (Figure 2.5*F-G*) suggest that the polymer composition of MUC2KO and WT samples were qualitatively similar. Following the same methods in Figure 2.3, we made estimates of the physical parameters of the detected polymers. These estimates are summarized in Tables 2.S1–S2 for both the upper

and lower SI of MUC2KO and WT mice. We find that these estimates suggest there are some differences in the polymeric composition of the SI of these two groups.

To test whether these measured differences in polymeric composition are reflected in differences in aggregation, we looked at aggregation in the 0.45-μm-filtered samples. We found that the undiluted samples from both groups displayed aggregation (Figure 2.S3*A-B*). We then created serial dilutions of the samples and found different aggregation thresholds for the samples (Figure 2.S3*C-D*). These results further confirm our conclusion that although MUC2 may play a role in particle aggregation, it is not required for aggregation to occur.

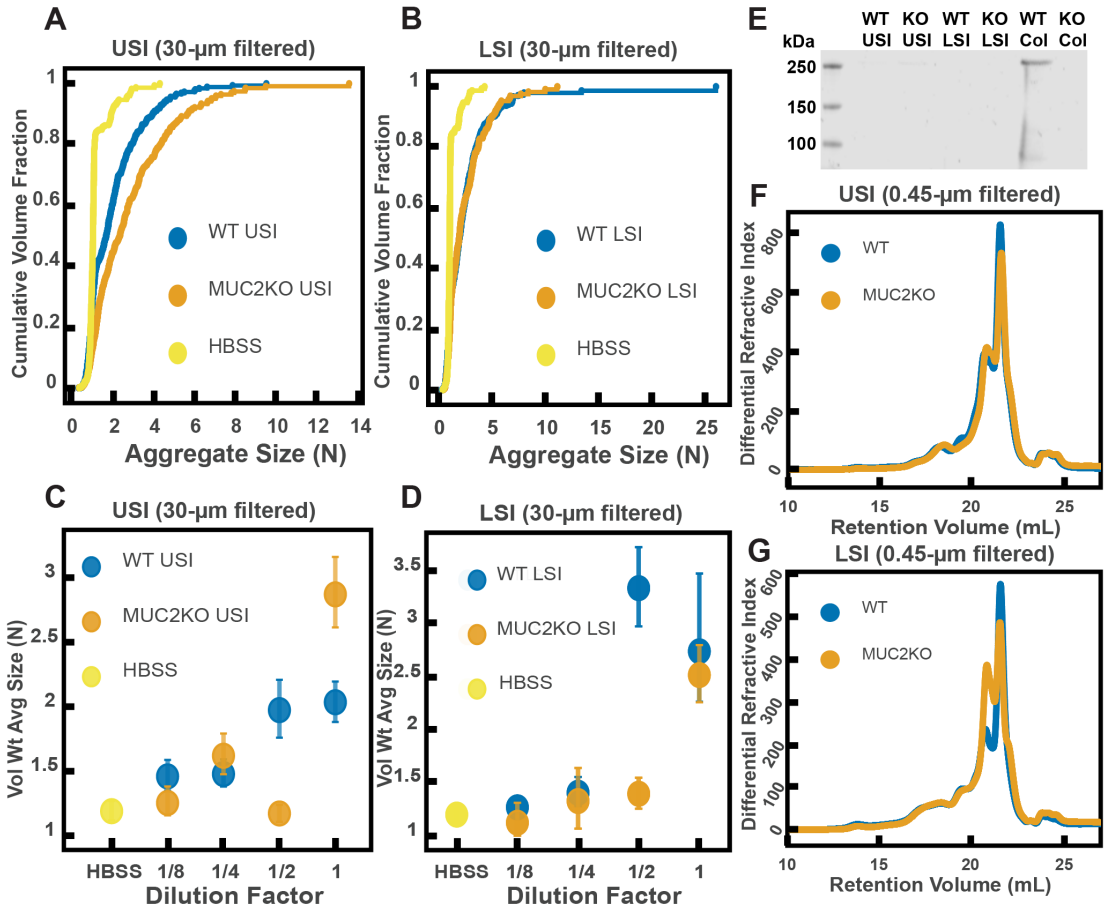

Figure 2.5: Quantification of the aggregation of particles in the small intestine (SI) in MUC2 knockout (MUC2KO) and wild-type (WT) mice. (A and B) Volume-weighted empirical cumulative distribution functions (ECDFs) comparing aggregation of the particles in undiluted, 30-µm filtered samples from the upper (A) and lower (B) SI of two separate groups of wild-type (WT) and MUC2-knockout (MUC2KO) mice to the control (particles suspended in HBSS). The vertical axis is the cumulative volume fraction of the total number of particles in solution in an aggregate of a given size; the horizontal axis is aggregate size in number of particles per aggregate (N). (C and D). Volume-weighted average aggregate sizes (Vol Wt Avg Size) for serial dilutions of 30-µm-filtered samples from the upper (C) and lower (D) SI of two separate groups of WT and MUC2KO mice. The dilution factor is plotted on the horizontal axis; a dilution factor of 1 is undiluted, ½ is a two-fold dilution. The vertical error bars are 95% empirical bootstrap CI (see *Materials and Methods*). (E) Western blots of 30-µm filtered samples from the SI and the colon of WT and MUC2KO mice. WT USI = WT upper SI; KO USI = KO lower SI; WT LSI = WT lower SI; KO USI = KO upper SI; WT Col = WT colon; KO Col = KO colon (F and G). Chromatograms of samples from the upper (F) and lower (G) SI of groups of WT and MUC2KO mice.

Immunoglobulins may play a role in aggregation, but are not required for aggregation to occur

It has also been demonstrated that immunoglobulins can bind to bacteria and induce them to aggregate (17–25). We therefore wanted to test the hypothesis that immunoglobulins drive the aggregation of PEG-coated particles in the SI. To do this, we compared the aggregation of our PEG-coated particles in samples from groups of mutant mice that do not produce immunoglobulins (Rag1KO), to samples from groups of WT mice. Again, to carefully preserve the native composition of the SI fluid, we used a protease-inhibitor cocktail when collecting the samples (see *Materials and Methods*). Because Rag1KO mice are immunocompromised, they need be fed an autoclaved chow diet. To control any potential differences in diet, both the Rag1KO and WT mice were fed an autoclaved chow diet for 48 h before samples were collected.

The mice were confirmed to be Rag1KO via genotyping and Western blot (Figure 2.6*E*). According to the literature, IgA is abundant in the SI (79). As expected, we saw a signal for IgA in the upper and lower SI of WT mice. We also tested for less abundant immunoglobulins such as IgG and IgM (Figure 2.S4 and Figure 2.S5, respectively), but did not detect their presence in the luminal contents of either WT or KO mice.

We observed aggregation in 30-μm-filtered samples from Rag1KO and WT mice (Figure 2.6*A* and *B*). To test the strength of the aggregation effect in the different samples, we serially diluted the samples and compared the volume-weighted average aggregate sizes at each dilution (Figure 2.6*C* and *D*). We found differences in the amount of aggregation between the Rag1KO and WT samples at different dilutions, suggesting that although immunoglobulins are not required for aggregation to occur, they could play a role in the aggregation of PEG-coated particles.

We wanted to test differences in the MW distribution of the polymers found in these samples, so we 0.45-μm-filtered our samples and analyzed them by GPC (see *Materials*

and Methods). The chromatograms from the refractometer (Figure 2.6*F* and *G*) suggested that the Rag1KO and WT samples were visually similar. We again made estimates of the physical parameters of the polymers in these samples (summarized in Tables 2.S3–S4). These estimates suggest that there are some differences in the polymeric composition of the SI of these two groups of mice.

To test whether these measured differences in polymeric composition correspond with differences in aggregation, we quantified aggregation in the 0.45-μm-filtered samples. We found that the undiluted samples for both groups displayed aggregation (Figure 2.S6*A* and *B*). When we created serial dilutions of the samples we found that the levels of aggregation were similar (Figure 2.S6*C* and *D*). Taken together, the results suggest that immunoglobulins may play some role in aggregation, but the presence of immunoglobulins are not required for aggregation to occur.

Interestingly, there are some differences in the levels of aggregation in WT mice fed the autoclaved diet compared with the standard chow diet. The two diets are nutritionally the same, only the processing is different. When samples from the WT mice in the MUC2KO experiments are compared with samples from the WT mice in the Rag1KO experiments are compared, it is apparent that, compared with WT mice fed the normal chow diet, samples from WT mice fed the autoclaved diet had (i) a lower average concentration of polymers and (ii) polymers of lower overall MW (see “WT” samples in Tables 2.S1–S4). These observations suggested two hypotheses: (1) dietary polymers may play a role in aggregation and (2) aggregation may be controlled by changing the polymer composition of the diet. We tested these hypotheses next.

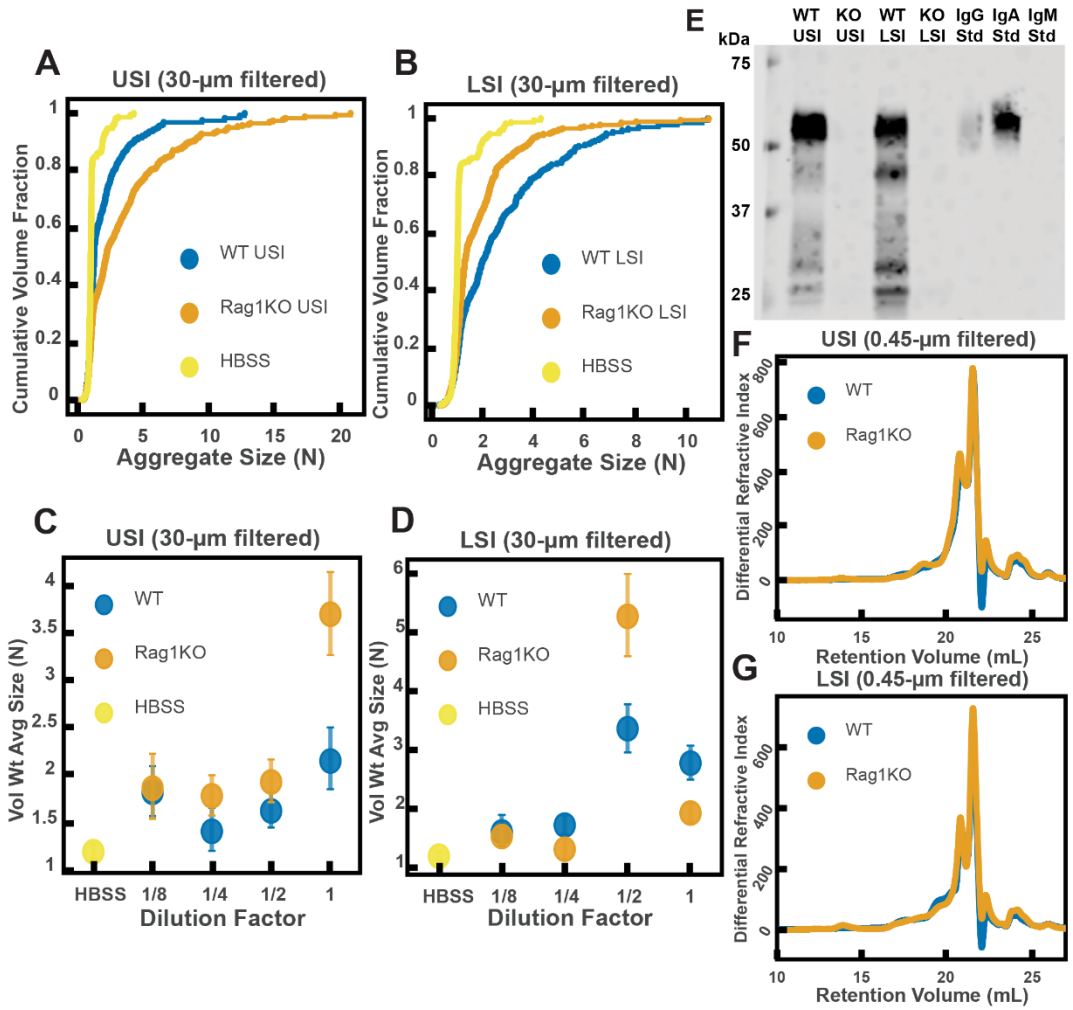

Figure 2.6: Quantification of the aggregation of particles in the small intestine (SI) in Immunoglobulin-deficient (Rag1KO) and wild-type (WT) mice. (A and B) Volume-weighted empirical cumulative distribution functions (ECDFs) comparing aggregation of the particles in undiluted, 30-µm filtered samples from the upper (A) and lower (B) SI of two separate groups of wild-type (WT) and immunoglobulin-deficient (Rag1KO) mice to the control (particles suspended in HBSS). Plotted on the vertical axis is the cumulative volume fraction of the total number of particles in solution in an aggregate of a given size. Plotted on the horizontal axis are aggregate sizes in number of particles. (C and D). Volume-weighted average aggregate sizes (Vol Wt Avg Size) for serial dilutions of 30-µm filtered samples from the upper (C) and lower (D) SI of two separate groups of WT and Rag1KO mice. The dilution factor is plotted on the horizontal axis, where a dilution factor of 1 is undiluted, ½ is a two-fold dilution, and so on. The vertical error bars are 95% empirical bootstrap CI using the bootstrapping procedure described in *Materials and Methods*. (E) Western blots of 30-µm filtered samples from the SI of WT and Rag1KO mice. WT USI = WT upper SI; KO USI = KO lower SI; WT LSI = WT lower SI; KO USI = KO upper SI. (F and G) Chromatograms of samples from the upper (F) and lower (G) SI of groups of WT and Rag1KO mice.

Polymers in the diet control aggregation of PEG-coated particles in a manner consistent with depletion-type interactions

As described in Figure 2.4, the extent of aggregation can be controlled by altering the polymer size and concentration of the polymer solution. Furthermore, as pointed out above, SI fluid from mice fed autoclaved and non-autoclaved diets induced different levels of aggregation. We hypothesized that aggregation behavior would differ between mice fed polymers of different sizes—even if the polymers were composed of similar chemical monomers and were present at the same polymer mass concentration. We hypothesized that mice fed short polymers would exhibit less aggregation in the SI (i.e., short polymers reduce the strength of the effect because depletion attractions are reduced). We predicted that the converse would be true for long polymers (i.e., long polymers increase the strength of the effect because depletion attractions are increased).

We first identified two candidate dietary carbohydrate polymers; Fibersol-2, a "resistant maltodextrin" composed of D-glucose monomers (80,81), with a MW of ~3500 Da (see Table 2.S5) and apple pectin, composed of D-galacturonic acid and D-galacturonic acid methyl ester monomers (82,83), with a MW of ~230 kDa (Table 2.S5). Before feeding mice these polymers, we first tested their effects on aggregation *in vitro* at various concentrations in buffer (Figure 2.7*A*). We found similar trends to the PEG solutions in Figure 2.4. Pectin at low (~0.05 to ~1 mg/mL) and very high mass concentrations showed little aggregation (~7 mg/mL) and showed the most aggregation at an intermediate concentration (~1.5 to ~3 mg/mL). Fibersol-2 did not induce much aggregation up to a mass concentration of ~240 mg/mL.

To test our hypothesis that we could use polymer size to control aggregation, we devised a simple experiment. One group of mice was fed a solution of Fibersol-2 and a second group was fed a solution of apple pectin for 24 h. The mass concentrations of the fibers in the two solutions were matched at 2% w/v and 5% w/v sucrose was added to each to ensure the mice consumed the solutions. Mesh-bottom cages were used to ensure that the mice did

not re-ingest polymers from fecal matter via coprophagy. According to the literature, neither of these two polymers should be broken down in the SI (81,84,85). As before, all samples were collected with a protease-inhibitor cocktail.

As before, we created serial dilutions of the small intestinal luminal fluid and looked at the extent of aggregation in each sample. In the 30-µm-filtered samples from the upper SI we observed more aggregation in the pectin-fed mice compared with the Fibersol-2 fed mice (Figure 2.7*E*). For the undiluted 30-µm-filtered lower SI sample, the pectin-fed mice samples formed a gel-like material which we were unable to pipette and therefore could not use for aggregation experiments. This gelation is not too surprising considering that pectin can form a gel in certain contexts (83,86). We were able to dilute this gel four-fold and then compare the aggregation in serial dilutions of the pectin-fed LSI to the Fibersol-2-fed LSI. We found, again, more aggregation in the pectin-fed mice than the Fibersol-2-fed mice (Figure 2.7*G*).

We again 0.45-µm-filtered these samples and ran them on GPC to test differences in the MW and size distributions of the polymers in these samples. The chromatograms from the refractometer (Figure 2.7*C* and *D*) suggest that there are differences in the polymeric distribution in the two groups of mice. Figure 7*B* shows chromatograms of just Fibersol-2 and pectin in buffer. We see that pectin elutes between 14-18 min, which is where we see an enhancement of the concentration of high-MW polymers in the samples from the SIs of the group fed pectin. We also see that Fibersol-2 elutes between 18-22 min, which is where we see an enhancement in the concentration of low-MW polymers in the samples from the SI of the group fed Fibersol-2. We again made estimates of the physical parameters of the polymers in these samples which are summarized in Tables 2.S6 and 2.S7**.** The estimates also suggest that there are differences in the polymeric composition of the SI of the two groups. Overall, the data from GPC suggests that the pectin-fed mice have more high-MW polymers than the Fibersol-2-fed mice. Low-MW polymers appear to be more abundant in Fibersol-2 fed mice compared with pectin-fed mice. We observed visually that the SI contents of the pectin-fed mice formed a gel and pectin is also known to self-associate to

form a gel or aggregates in solution (83,86). We note, therefore, that by 0.45-μm-filtering these samples we may be removing these structures and decreasing the concentration of pectin in our samples.

To test that these measured differences in polymeric composition are reflected in differences in aggregation, we tested aggregation in the 0.45-μm-filtered samples. We found that in both the upper and lower SI samples, the samples from the pectin-fed group showed more aggregation than the samples from the group fed Fibersol-2 (Figure 2.7*F* and *H*). When we created serial dilutions of these samples, we found that the samples from the mice fed Fibersol-2 showed almost no aggregation at any concentration whereas the samples from pectin-fed mice showed aggregation. We also observed that we needed to dilute the 30-μm-filtered samples more to achieve the greatest extent of aggregation (Figure 2.7*E* and *G*). We speculate that this shift in the aggregation behavior between the 30-μm-filtered and 0.45-μm-filtered samples is due to some of the polymers being lost when 0.45-μm-filtering the samples as a result of the aforementioned self-association of pectin.

These data taken together lead us to conclude that polymers in the diet can be used to control the aggregation of PEG-coated particles. This data further suggests that feeding higher MW polymers at the same mass concentration as lower MW polymers leads to an enhancement in aggregation. Due to the high polydispersity and complex chemical composition of SI luminal fluid as measured by GPC, it is unfeasible to apply the same theoretical analysis as was done in Figure 2.4 to these data. We can, however, note that visually the behavior is qualitatively consistent with the depletion-type interactions found in simple PEG solutions in Figure 2.4.

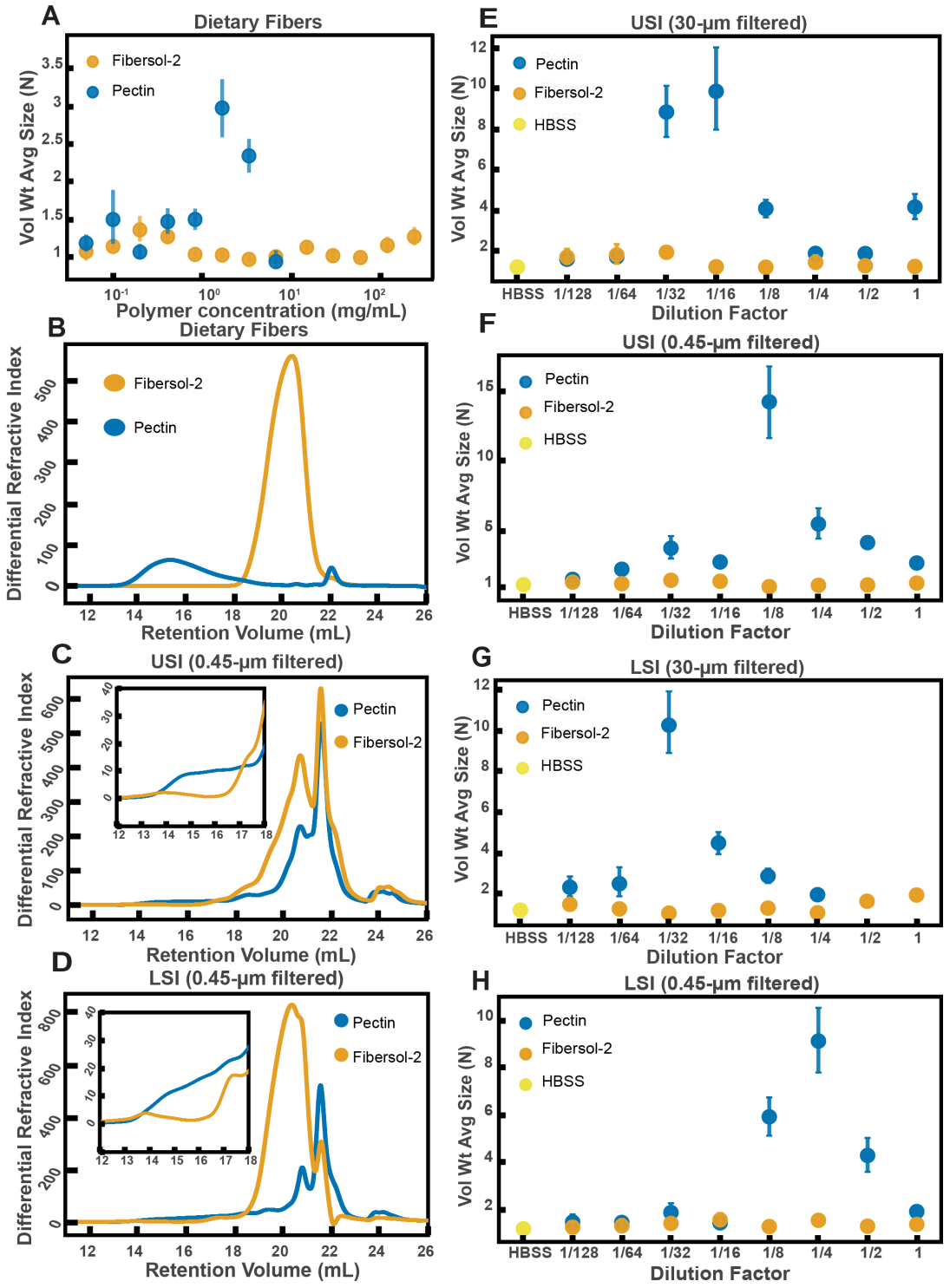

Figure 2.7: Quantification of aggregation of PEG-coated particles in the small intestine (SI) of mice fed different polymers from dietary fiber. **(A)** Volume-weighted average aggregate sizes (Vol Wt Avg Size) for serial dilutions of apple pectin and Fibersol-2. Volume-weighted average sizes are plotted on the vertical axis in terms of number of particles per

aggregate (N) against polymer concentration (mg/mL). The vertical error bars are 95% empirical bootstrap CI using the bootstrapping procedure described in *Materials and Methods.* **(B)** Chromatograms of apple pectin and Fibersol-2 in buffer. (**C and D)** Chromatograms of samples from the upper (E) and lower (F) SI of two separate groups of mice (fed pectin or Fibersol-2). **(E-H)** Volume-weighted average aggregate sizes (Vol Wt Avg Size) for serial dilutions of 30-μm-filtered samples from the upper (E) and lower (G) SI of two separate groups of mice (fed pectin or Fibersol-2) to the control (particles suspended in HBSS). (**F and H**) Serial dilutions of 0.45-μm-filtered samples from the same groups. The dilution factor is plotted on the horizontal axis, where a dilution factor of 1 is undiluted, and ½ is a two-fold dilution. The vertical error bars are 95% empirical bootstrap CI using the bootstrapping procedure described in *Materials and Methods*.

Discussion

This work shows that even PEG-coated particles, which have minimal biochemical interactions, form aggregates in the luminal fluid of the SI. It reveals a previously unknown way in which dietary polymers can impact, and be used to control, the structure of particles in the SI. We speculate that this phenomenon may play a role in the aggregation of other particles in the SI such as microbes, viruses, nanoparticles for drug delivery, and food granules. In these systems, other factors will also inevitably affect the formation of these aggregates (e.g. interactions with mucins and immunoglobulins); thus, it will be important to explore the interplay among all these factors. Another important next step is to investigate how mixing in the SI and the co-aggregation of different types of particles may affect aggregation. We speculate that the aggregation of particles in the SI could also have functional consequences, such as promoting colonization by microbes, affecting infection by pathogens, and altering clearance of microbes (2,6–8,10,11). Aggregation will also need to be considered when designing nanoparticles for drug delivery (3,4).

We found that MUC2 and immunoglobulins, which have been found to aggregate microbes both *in vivo* and *in vitro* (12–25), are not required for the aggregation of PEG-coated particles. Instead, we found that by feeding mice dietary polymers with similar chemistry but very different sizes we could tune the extent of aggregation in the SI. These polymers (pectin and Fibersol-2) are forms of fiber commonly found in the human diet. We found that feeding long polymers induced aggregation, whereas short polymers did not. More

work needs to be done to understand the underlying mechanism, but surprisingly the observed aggregation behavior in the SI luminal fluid from mice fed dietary polymers of different sizes is qualitatively consistent with the aggregation behavior in simple PEG solutions, where aggregation is driven by depletion interactions. Overall, this suggests a simple dietary method for controlling aggregation in the gut. It will be important to extend this work to microbes and other particles commonly found in the gut and to measure the relative contributions of polymer-driven aggregation and chemical-driven aggregation. We note that mucins and immunoglobulins are polymers that can also self-associate into structures of very high MW (78,87,88), suggesting that they could cause aggregation via both physical and chemical mechanisms. Interestingly, during the review of this manuscript, a study was published with *in vitro* work done using model buffer solutions of mucins, DNA, and other biopolymers further implying that aggregation of bacteria by host-polymers can be depletion-mediated (89). *In vivo*, it will also be important to consider the effects of flow, as it has been shown that flow in non-Newtonian fluids can induce particle aggregation (90–92). In particular, studies have suggested that the combination of flow and polymer elasticity can lead to aggregation (93) and that shear thinning viscosity can influence aggregation as well (94). In our work, we neglected flow effects for simplicity and thus our findings are most applicable to the initial formation of aggregates before aggregation is influenced by mechanical forces due to peristaltic mixing and the transit of food. A rudimentary estimate of the Weissenberg number (see *Materials and Methods)*, which weighs the contributions of elastic and viscous forces, yields $\mathrm{Wi} \sim 0.3 \text{ to } 10$, suggesting that elasticity-induced effects may play a role in the SI and will be an important direction to pursue in follow-up studies. If flow-induced clustering does occur *in vivo*, the literature suggests it would aid in the process, perhaps enhancing particle aggregation.

We note that current dietary guidelines do not differentiate between fibers of low and high MW (95,96). Our work implies that the MW of fiber, and the subsequent degradation of a high-MW fiber into a low-MW component (97), which we have discussed previously in the context of mucus compression, is important in defining the physicochemical environment of the gut. Further studies will be required to understand the effects of

industrial food processing on MW of the dietary polymers present in foods, and which processing methods preserve or produce high-MW polymers that impact mucus compression (97) and particle aggregation in the gut.

Materials and Methods

Table 2.1: Key Resources Table

Reagent type (species) or resource	Designation	Source or reference	Identifiers	Additional information
MUC2KO, C57BL/6 mice (female)	MUC2KO	Eugene Chang Lab provided initial breeding pairs which were provided to them from Leonard H. Augenlicht at the Department of Oncology of Albert Einstein Cancer Center		Genotyping was performed by Transnetyx Inc.; Western blot was done to confirm lack of MUC2 (See Fig. 2.5E)
Rag1KO, C57BL/6 mice (male)	Rag1KO	Provided by Mazmanian Lab at Caltech		Western blot was done to confirm lack of IgA as explained in the text (See Fig. 2.6E)
C57BL/6 mice (all male except for WT controls in MUC2KO experiments in Figure 5 and S3)	WT	The Jackson Laboratory		
antibody	MUC2 polyclonal antibody	Biomatik	Cat No: CAU27315	

	(rabbit host)			
antibody	Li-Cor IRDye 800CW Goat Anti-Rabbit IgG	Li-Cor	P/N 925-32211	
antibody	Li-Cor IRDye 800 CW Goat Anti-Mouse IgG	Li-Cor	P/N 925-32210	
antibody	Li-Cor IRDye 800 CW Goat Anti-Mouse IgM	Li-Cor	P/N 925-32280	
antibody	Goat Anti-Mouse IgA-unlabeled	SouthernBiotech	Cat No: 1040-01	
antibody	Li-Cor IRDye 800 CW Donkey Anti-Goat IgG	Li-Cor	P/N 925-32214	
chemical compound, drug	apple pectin	Solgar Inc.	"Apple pectin powder"; SOLGB7012000B	
chemical compound, drug	Fibersol-2	Archer Daniels Midland/Matsutani LLC	Product code: 013100, Lot #: CY4P28540	
chemical compound, drug	USP grade sucrose	Sigma-Aldrich		
chemical compound, drug	Protease inhibitor cocktail	Roche cOmplete, Mini, EDTA-free Protease-Inhibitor cocktail, Roche		
chemical compound, drug	PEG 100kDa	Dow	POLYOX WSR N-10	

chemical compound, drug	PEG 1 MDa	Dow	POLYOX WSR N-12K	
chemical compound, drug	PEG 3350	Bayer	MiraLAX	
chemical compound, drug	Hanks' Balanced Salt Solution (without calcium, magnesium, phenol red)	GE Healthcare Life Sciences	Product code: SH30588.02	
software, algorithm	3D aggregate analysis pipeline	This paper; source code available through Dryad		Description in Materials and Methods; source code provided on Dryad
other	mesh-bottom (or wire-bottom) floors	Lab Products, Inc.	P/N: 75016	
other	1-µm diameter PEG 5kDa-coated polysytrene beads	This paper		Description of synthesis in Materials and Methods
other	1-µm diameter PEG 5kDa-coated polysytrene beads with PEG 1 kDa "back-filling"	This paper		Description of synthesis in Materials and Methods
other	standard chow diet	PicoLab	PicoLab Rodent Diet 20; Product #5053	

other	autoclaved chow diet	PicoLab	Laboratory Autoclavable Rodent Diet 5010	

Details of animals used

All mice were male or female specific pathogen free (SPF) C57BL/6 mice between 8-16 weeks old. Mice on a standard, solid chow diet were given food and water *ad libitum.* Immunoglobulin-deficient (Rag1KO) mice were maintained on an autoclaved chow diet due to their immunocompromised status. The control group of WT mice used as a comparison to this group was maintained on the same autoclaved chow diet for 48 h before euthanasia. Genotyping of MUC2 deficient (MUC2KO) and Rag1KO mice was done by Transnetyx (Transnetyx, Inc., Cordova, TN, USA). Mice given only apple pectin (Solgar, Inc., Leonia, NJ, USA) with sucrose (USP grade, Sigma-Aldrich, St. Louis, MO, USA) or Fibersol-2 (Archer Daniels Midland/Matsutani LLC, Chicago, IL, USA) with sucrose were first raised on a standard chow diet and given water *ad libitum,* then were maintained on a restricted diet consisting of only 2% apple pectin + 5% sucrose or 2% Fibersol-2 + 5% sucrose for 24 h. For those 24 h, these mice were kept on mesh-bottom cages to prevent the re-ingestion of polymers from the standard chow diet via coprophagy. The MUC2KO colony was raised and maintained by the Ismagilov Lab. The Rag1KO mice were provided by the Mazmanian lab (Caltech). All other mice were from Jackson Labs (The Jackson Laboratory, Bar Harbor, ME, USA). All animal experiments were approved by the California Institute of Technology (Caltech) Institutional Animal Care and Use Committee (IACUC) and the U.S. Army's Animal Care and Use Review Office (ACURO). Mice were euthanized via CO_2 inhalation as approved by the Caltech IACUC in accordance with the American Veterinary Medical Association Guidelines on Euthanasia (98).

Oral administration of particles

Particles were gavaged at a concentration of 0.1–2% w/v in either 1x HBSS or 1x PBS. We used small fluid volumes (50 μL) to minimize volume-related artifacts (3). We chose

buffers isotonic to the SI because it has been shown that the isotonicity of the delivery medium can greatly affect the *in vivo* particle distribution (38). In some experiments, animals were food-restricted for 4 h prior to administration of particles. It has been previously demonstrated though that food-restriction has minimal effects on the *in vivo* distribution of PEG-coated particles (3). In all experiments animals were euthanized 3 h after administration of particles.

Fluorescent scanner experiments

Gastrointestinal tracts (GIT) were excised and laid out flat on petri dishes on ice. Drops of saline were then placed around the GIT and the petri dishes were sealed with parafilm. Samples were then immediately brought to the fluorescent laser scanner (Typhoon FLA 9000) for imaging. Samples were scanned with an excitation wavelength of 473 nm and a 530 nm bandpass filter.

Imaging of luminal contents from mice orally administered particles

Immediately after euthanization the small intestines of the mice were excised and divided into an upper and lower section. The luminal contents were collected by gently squeezing the intestines with tweezers. They were placed directly onto a glass slide and encircled by a ring of vacuum grease that did not touch the contents. A coverslip was then immediately placed on top to create an air-tight chamber. Samples were kept on ice during the collection process. The samples were then immediately taken for imaging. All imaging was performed using a Zeiss LSM 800 or a Leica DMI6000, using either bright-field microscopy, epifluorescence microscopy (GFP, L5 Nomarski prism), confocal fluorescence microscopy (488 nm excitation and 490-540 nm detection), or confocal reflectance microscopy (561 nm excitation and 540-700 nm detection).

Collection of intestinal luminal fluid

Immediately after euthanasia, the SI of each mouse was excised and divided into an upper and lower section. If luminal fluid was collected from the colon, then the colon was also

excised. The luminal contents were then collected from each section in separate tubes and kept on ice. The luminal contents from an individual mouse was insufficient in volume to perform all the required analyses (i.e. *ex vivo* aggregation, GPC, and sometimes Western blot), so contents were pooled from a group of three mice of the same age that were co-housed. These pooled samples, kept divided by section, were then spun down at 17 kG at 4 °C for 1 h to separate the liquid and solid portions of the contents. The supernatant of each sample was collected and then placed on 30 μm filters (Pierce Spin Columns – Snap Cap, Thermo Fisher Scientific, Waltham, MA, USA) and spun down at 17 kG at 4 °C for 1 h. Part of the filtrates of each sample were then collected, divided into aliquots, and frozen at -20 °C for future experiments. The remaining portion of the filtrates was then taken and placed on 0.45 μm centrifugal filters (Corning Costar Spin-X centrifuge tube filters; cellulose acetate membrane, pore size 0.45 μm, sterile) and spun down at 5 kG at 4 °C for 1 h. For experiments in which a protease-inhibitor cocktail (Roche cOmplete, Mini, EDTA-free Protease-Inhibitor Cocktail, Roche, Indianapolis, IN, USA) was used, a 100x concentrated stock solution was prepared in HBSS (without calcium, magnesium, and phenol red; GE Healthcare Life Sciences, Marlborough, MA, USA). The same procedure as detailed above were followed for the collection of luminal fluid, except immediately after the luminal contents were brought back from the animal facility on ice, 10 μL of the 100x protease-inhibitor cocktail was added to each tube. The mixtures were then vortexed briefly to mix. The contents were then spun down at 17kG at 4 °C as described above to separate the solid from liquid contents. The liquid fraction collected from each group before 30 and 0.45 μm filtration was usually ~200–300 mL, so the additional 10 μL of protease-inhibitor cocktail only diluted the samples by ~5% at most.

Ex vivo and in vitro aggregation assays

We took 1-μm diameter PEG 5 kDa-coated polystyrene beads (with PEG 1 kDa "back-filling") and suspended them at 10 mg/mL in deionized water. Before use, they were vortexed to re-suspend in solution and then sonicated for 1 min. The particle solution was then added to the polymer solution or small intestinal luminal fluid at a ratio of 1:10. After

addition of particles, the mixture was vortexed for 10 seconds. Then, 2 µL of the mixture was then immediately pipetted into an imaging chamber created with a SecureSeal imaging spacer (0.12 mm depth and 9 mm diameter, Electron Microscopy Sciences, Hatfield, PA, USA) and a glass slide. The top of the imaging chamber was immediately sealed with a #1.5 coverslip. The samples were then imaged approximately 10 min later. In PEG solution experiments and serial dilution experiments, HBSS (without calcium, magnesium, phenol red; GE Healthcare Life Sciences) was used to dilute.

In the 1 MDa PEG experiments conducted in phosphate buffered saline (PBS) with pH = 6 (Figure 4 – figure supplement 1) the PBS solution was initially prepared with 138 mM sodium chloride, 7.5 mM monosodium phosphate dihydrate, 1.1 mM disodium phosphate heptahydrate, and deionized (DI) water (Milli-Q). The sodium chloride was added to ensure that the ionic strength matched that of Hank's balanced salt solution. The pH was then measured using an Orion 2-Star Benchtop pH Meter (Thermo Scientific) with an Orion 9110DJWP Double Junction pH electrode (Thermo Fisher Scientific) after first calibrating the instrument using the following reference standard buffers: pH = 10 (VWR BDH5078-500 mL), pH = 7 (VWR BDH5046-500 mL), and pH = 4 (VWR BDH5024-500 mL). The pH of the solution was then adjusted to pH = 6 using 1 M NaOH in DI water.

Microscopy for ex vitro and in vitro aggregation assays

All imaging was performed using a Zeiss LSM 800, using confocal fluorescence microscopy (488 nm excitation, detection at 490-540 nm). We collected 3D stacks which were 200 x 200 x 40 µm in volume. 3D renders of aggregates were created using Imaris software from Bitplane, an Oxford Instruments Company.

Imaging analysis

All image analysis was done in FIJI (ImageJ 2.0.0) using an ImageJ macro written using the ImageJ macro scripting language. These macros are available in Dryad. Z-stacks were saved as 16 bit .czi files and were subsequently loaded into FIJI. Each z-stack extended

~40 μm deep into each sample in the z-direction and was composed of 113 slices. As a result of the depth of the stacks in the z-direction, we observed a significant drop-off in measured aggregate fluorescence between the first slice and the last slice, likely due to scattering from the intestinal fluid and the particles themselves. To ensure that aggregates throughout a given stack had a similar brightness, which is important for the 3D Object Counter plugin, the median pixel intensity for aggregates in every slice was set as the maximum pixel intensity value for every slice. To achieve this, first the 10^{th} slice and the 10^{th} to last slice of the z-stack were selected and thresholded using the Otsu method (99), creating a binary image of the aggregates in the two slices. The binary images were used as masks to measure the median pixel intensity of each aggregate in the two slices as well as the mean and max pixel intensity values for the background of both images. The drop-off in intensity was assumed to be approximately linear, so the median pixel intensity for aggregates in each slice was determined by interpolating between the median aggregate pixel intensity values from the 10^{th} slice and 10^{th} to last slice. The minimum pixel intensity value for each slice was determined by adding 1/3 of the mean background pixel intensity to 2/3 of the maximum background pixel intensity for the 10^{th} and 10^{th} to last slices (this was necessary to deal with the challenge determining background pixel intensities) and then interpolating to calculate the minimum for all other slices. The process of intentionally introducing image clipping in the z-stacks was justified by the manner in which aggregates were identified; aggregates were first measured by total volume instead of by particle count, thus being able to discern individual particles inside of each aggregate was unnecessary.

The 3D Objects Counter plugin in FIJI was used to measure various parameters, including the volume of each aggregate. The plugin initially thresholds all slices in a stack using a single thresholding value, which requires objects in every slice of a stack to be roughly the same intensity (hence, the thresholding procedure described previously). The plugin takes the resulting now-binary z-stack and determines the number of voxels occupied by each aggregate and converts voxel volume to metric volume using metadata in each .czi file. A second macro was used to determine the average size of a singlet (single particle) for each

z-stack. In this macro, we identified 10 singlets by visually inspecting the sample to determine the average size of a singlet. This was then used to normalize differences in measured aggregate volume between samples by converting to a particle count per aggregate. This normalization step was necessary due to variations in the average measured singlet size between samples. It also helped account for any differences in the thresholding procedure from sample to sample.

The accuracy of this method for determining aggregate sizes was validated by comparing empirical cumulative distribution functions (ECDFs) of the cross-sectional area of the aggregates in a given z-stack determined by the ImageJ macro to ECDFs generated by visually inspecting the samples to measure the cross-sectional areas of aggregates. This comparison was done for at least three separate z-stacks. ImageJ macros will be made available upon request.

Quantification of aggregate sizes

The sizes of aggregates in solution were quantified in two ways. One was by comparing the volume-weighted empirical cumulative distribution functions (ECDFs) of the aggregate sizes of each sample to each other. The volume-weighted ECDF, $\hat{F}$, as follows (100):

$$\hat{F}(N) = \frac{1}{\sum N_i} \sum_{i=1}^{n} I(N_i \leq N) \qquad (Eq. 2.6)$$

$$I(N_i \leq N) = \begin{cases} N_i \; if \; N_i \leq N \\ 0 \; if \; N_i > N \end{cases} \qquad (Eq. 2.7)$$

where N_i is the number of particles per aggregate and n is the total number of aggregates in solutions (where single particles also count as aggregates).

The other way in which the extent of aggregation was quantified was by creating bootstrap replicates of the ECDFs of the aggregate distributions of each sample and computing the

volume-weighted average aggregate size ($\langle N \rangle$; given in number of particles per aggregate) for each bootstrap replicate. The volume-weighted average aggregate size is given by the following equation in units of "number of particles per aggregate":

$$\langle N \rangle = \frac{\sum_{i=1}^{n} N_i^2}{\sum_{i=1}^{n} N_i} \qquad (Eq. 2.8)$$

This allowed us to calculate 95% empirical bootstrap CI on the volume-weighted average aggregate size. We generated 10,000 bootstrap replicates from the original ECDF of each sample to generate these. The advantage of this approach is that we do not need to assume anything about the underlying probability distribution; it is non-parametric (100). The original ECDFs, from which the replicates were generated, each contained at least 300 aggregates, in many cases containing ~1000 or more aggregates. The codes used for the analyses (volume-weighted ECDFs and 95% empirical bootstrap CIs) were written in Python 3.6.4 and are available on Dryad.

Filtration with MW cut-off filters

Small intestinal luminal fluid was collected and 0.45 μm-filtered as described in "Collection of Luminal Fluid". It was then divided up and placed on MWCO filters (Pierce Protein Concentrators, Thermo Fisher Scientific) of with the following MWCOs: 100 kDa, 30 kDa, and 3 kDa. The samples were then centrifuged at 15 kG at 4 °C for 2 h, checking every 15 min for the first hour if additional volume had flowed through. After the eluent from each was collected, they were diluted back to their original volumes with HBSS.

pH measurements of luminal fluid

Pooled samples of luminal fluid were collected from each section (stomach, upper small intestine, lower small intestine, cecum, and colon) and 30 μm-filtered as described in "Collection of Luminal fluid" (with use of the same protease inhibitor cocktail). Samples were collected from two separate groups of 2-month old B6 male mice on a standard chow diet. Each group had three mice. Because there was only ~25 μL of luminal fluid from the

colons of each group we did not 30 μm-filter the colonic fluid as there was concern all the fluid would be retained by the filter. The colonic contents were simply spun down at 17 kG at 4 °C for 1 h to separate the liquid and solid portions of the contents. Then the supernatant (luminal fluid) was collected. Measurements were done using an Orion 2-Star Benchtop pH Meter. The instrument was first calibrated with three reference standard buffers: pH = 10 (VWR BDH5078-500 mL), pH = 7 (VWR BDH5046-500 mL), and pH = 4 (VWR BDH5024-500 mL). Measurements were conducted at T = 25 °C. There was at least 100 μL of sample from each section except for the stomach sample from one group of mice and from colon samples from both groups. Measurements were conducted with both a standard pH electrode (Orion 9110DJWP Double Junction pH Electrode) and a micro pH electrode (Orion 9810BN Micro pH Electrode, Thermo Fisher Scientific). This was done because the standard electrode is only accurate for samples with volumes of 200 μL whereas the micro electrode is accurate for samples as small as 0.5 μL in volume. The results are consistent with other results for rodents (101,102) with the exception of a study conducted with mice of a different gender, strain, and fed an 18% protein diet (103).

For the pH measurement of HBSS, the pH was measured with both the standard and micro pH electrodes, and three technical replicates were done with each probe. The value for the pH reported in the main text is the average of all six measurements.

Estimation of coverage and length of grafted PEG layer

Based on our NMR measurements (see section NMR of PEG-coated particles with "backfill") the grafting density (Γ) of the PEG polymer on our PEG 5 kDa-coated particles with PEG 1 kDa backfill should be approximately: $\Gamma = 0.48\ \text{chains/nm}^2$ (to estimate this we assume that all of the PEG on the surface is PEG 5 kDa). One can estimate the grafting density at which the grafted chains transition from separate coils to overlapping coils or the brush regime by calculating the grafting density at which coils would just begin to overlap (104). This can be estimated as:

$$\Gamma^* \sim \frac{1}{\pi R_g^2} \qquad (Eq. 2.9)$$

where R_g is the radius of gyration of the grafted polymer. Using literature measurements of the hydrodynamic radius of PEG 5 kDa and the Kirkwood-Riseman relation, this can be estimated as $R_g \sim 3.45$ nm. We therefore estimate that $\frac{\Gamma}{\Gamma^*} \sim 5$, meaning that the grafting density is such that the polymer coils on the surface should be overlapping and within the brush regime. To estimate the length and average volume fraction of the layer, we therefore made the assumption that the grafted polymer layer behaved as a brush and used the Alexander-deGennes brush approximation (63,105). This theory was originally developed for high-MW polymer coils, but has also been found, surprisingly, to quantitatively capture forces for grafted layers only a few segments long (105). We estimated the length (L) of the brush as (63):(62,95). This theory was originally developed for high-MW polymer coils, but has also been found, surprisingly, to quantitatively capture forces for grafted layers only a few segments long . We estimated the length (L) of the brush as:

$$L \sim N\Gamma^{\frac{1-\nu}{2\nu}} b^{\frac{1}{\nu}} \qquad (Eq. 2.10)$$

where *N* is the number of monomers per grafted chain, ν is the Flory exponent, and *b* is the Kuhn length of the grafted polymer. We used b = 0.76 nm based on literature measurements (106) and took $\nu \cong 0.588$, because aqueous salt solutions are good solvents for PEG (107). Lastly, we estimated the number of monomers per chain by assuming the number of monomers is approximately equation to the number of Kuhn segments and the relationship between the radius of gyration, the Kuhn length and the number of Kuhn segments (63): $N \sim \left(\frac{R_g}{b}\right)^{\frac{1}{0.588}} \sim 13$. We therefore estimate that $L \sim 6.4\ nm$.

The Alexander–de Gennes approximation assumes a step profile for the volume fraction of the grafted polymer (ϕ). We can estimate this using the following equation (63):

$$\phi \approx \begin{cases} (\Gamma b^2)^{\frac{3\nu-1}{2\nu}} \, for \, z < L \\ 0 \, for \, z > L \end{cases} \qquad (Eq. 2.11)$$

where z is the distance from the bare particle surface. Using the same approximations as above we find $\phi \approx 0.43$.

Western blot of luminal contents

30-µm filtered small intestinal luminal fluid was reduced in sample buffer with 100 mM dithiotreitol DTT at 95 °C for 5 min (the luminal fluid was diluted 10-fold in the sample buffer). Gel electrophoresis was then run on 4–15% SDS/PAGE gels. The transfer was performed using wet electroblotting to a nitrocellulose membrane. For detection of MUC2, the primary antibody was diluted 1:1,000 (MUC2 polyclonal antibody, rabbit host, Biomatik, Wilmington, DE, USA) as a 1:10,000 in Odyssey blocking buffer (Li-Cor, Lincoln, NE, USA) with 0.2% Tween 20. The secondary antibody (Li-Cor IRDye 800CW Goat Anti-Rabbit IgG, Li-Cor) was diluted 1:10,000. For the detection of IgG and IgM, 1:10,000 dilutions of Li-Cor IRDye 800 CW Goat Anti-Mouse IgG and Li-Cor IRDye 800CW Goat Anti-Mouse IgM were used respectively. For detection of IgA, a 1:10,000 dilution of SouthernBiotech Goat Anti-Mouse IgA-unlabeled was used as the primary and a 1:10,000 dilution of Li-Cor IRDye 800CW Donkey Anti-Goat IgG was used as the secondary. All membranes were visualized using a Li-Cor Odyssey scanner.

Gel permeation chromatography

We used a Malvern OMNISEC RESOLVE connected to two Malvern A6000M columns (Malvern, Westborough, MA, USA) equilibrated with 1x PBS with 0.02% sodium azide, flow rate: 0.75 mL/min. For detection of the polymers, the OMNISEC REVEAL was used with a refractometer, UV detector, dual-angle light scattering detector, and a capillary viscometer. Luminal contents were 0.45-µm filtered as described above, and then diluted 10-fold in the running buffer (1x PBS with 0.02% sodium azide) before injection into the system. Prior to injection, samples were kept on the autosampler at 4 °C.

Synthesis of PEG-coated particles

We amended a previously published protocol (3) to synthesize PEG-coated particles; briefly, 2 mL of 1-µm fluorescent carboxylic-acid-terminated polystyrene beads (FluoroSpheres, Invitrogen, Thermo Fisher Scientific) at 2% v/v with 2 mM NaN_3 were rinsed at 3900g for 40 min using a centrifugal filter (Millipore Amicon Ultra-4 mL 100 K MWCO). Particles were removed from the filter using 4 mL of a solution of 15 mg/mL 1-Ethyl-3-(3-dimethylaminopropyl)carbodiimide (EDC, Sigma-Aldrich) and 15 mg/mL N-hydrosuccinimide (NHS, Aldrich), an excess concentration of NH_2-PEG-OMe (5 kDa, Creative PEGworks, Chapel Hill, NC, USA) in 1 mL increments using 100 mM borate buffer, pH 8.4. By an excess concentration of NH_2-PEG-OMe we mean ten-fold the concentration of PEG required to enter the polymer brush regime (see "Estimation of coverage and length of grafted PEG layer" section for details of calculation). This solution was tumbled on a rotary tumbler for 4 h at room temperature in a 15 mL falcon tube. Particles were washed three times to remove starting materials with 4 mL Milli-Q water in a centrifugal filter and re-suspended in 2 mL in Milli-Q water.

Synthesis of PEG-coated particles with "backfill."

12 mL of 1-µm fluorescent carboxylic-acid-terminated polystyrene beads at 2% v/v with 2 mM NaN_3 (FluoroSpheres 1-µm; 505/515, Invitrogen) were centrifuged to a pellet at 12,000g for 10 min. Beads were pelleted and rinsed three times with Milli-Q water. To the final pellet of particles, 12 mL of a solution of 6 mM EDC (10 mg/mL; Sigma-Aldrich) and 5 mM Sulfo-NHS (1.08 mg/mL, ThermoFisher), with 50x excess of the number of chains needed to enter the brush regime (see "Estimation of coverage and length of grafted PEG layer" for details of calculation) of NH_2-PEG-OMe (mPEG-Amine 2kDa; mPEG-Amine 5kDa; Creative PEGWorks) in 10x PBS, pH 7.4 (100 mM), was added. This solution was tumbled on a rotary tumbler for 4 h at room temperature. Tubes were vented every 30 min to release gas produced by the reaction. Particles were then pelleted and rinsed three times with Milli-Q water. The 12 mL sample was divided into four 3 mL aliquots for the remaining conditions. For condition without backfill, beads were quenched

with 50 mM Tris pH 7.4 overnight at room temperature with slow tilt rotation prepared from 10x Tris-buffered saline with Tween 20, pH 7.5 (Sigma-Aldrich). For particles with backfill, the 3-mL aliquot was re-suspended in with 50x excess of the number of chains needed to enter the brush regime (see "Estimation of coverage and length of grafted PEG layer" for details of calculation) of NH_2-PEG-OMe (mPEG-Amine 350; mPEG-Amine 1 kDa; mPEG-Amine 5kDa, Creative PEGWorks) in 100 mM PBS, pH 7.4 containing 6 mM EDC and 5 mM Sulfo-NHS for 4 h before quenching overnight with 50 mM TRIS buffered Saline with Tween 20, pH 7.5. All beads were washed three times with Milli-Q water before suspending in 3 mL sterile filtered PBS, pH7.4 with 1% BSA for storage.

NMR of PEG-coated particles with "backfill."

We took 400 µl of 2% w/v samples and lyophilized (~8 mg), then dissolved in deuterated chloroform (Cambridge Isotope Laboratories, Tewksbury, MA, USA) with 0.01% tetramethylsilane (Aldrich) immediately before measurement. Data were collected on a Varian Innova 600 MHz spectrometer without spinning, using a 45^o pulse width and 1 sec relaxation delay between scans. The concentration of PEG in each sample was determined by integrating the singlet at 3.64 pm and normalizing the integral to TMS internal standard at 0.0 ppm.

Zeta potential measurements on PEG-coated particles with "backfill."

Each particle solution was 0.1 mg/mL of particles in 1 mM KCl. Measurements were done on a Brookhaven NanoBrook ZetaPALS Potential Analyzer (Brookhaven Instruments Corporation, Holtsville, NY, USA). Three trials were done where each trial was 10 runs each and each run was 10 cycles. Values reported are the average zeta potential for the 30 runs.

Estimate of Weissenberg number for small intestine

The Weissenberg number (Wi), which weighs the relative contributions of elastic and viscous forces, can be written as (108):

$$Wi = \dot{\gamma}\lambda \qquad (Eq. 2.12)$$

where $\dot{\gamma}$ is the shear rate (in s^{-1}) and λ is the fluid relaxation time (in *s*). The shear rate in the human small intestine during peristaltic contractions has been estimated as $\dot{\gamma} \sim 29\ s^{-1}$ (109). For dilute aqueous polymeric solutions of polyacrylamide with MWs ranging from 10^4 to 10^7 Da, it has been found that $\lambda = 0.009$ to 0.45 s, with the relaxation time increasing with MW as $\lambda\, \alpha\, MW^{2/3}$(110). Using these values, we can estimate the Weissenberg number to be Wi ~ 0.3 to 10.

Author contributions

APS, SSD, and RFI designed the research; APS, SSD, JCR, and SRB performed the research; APS, SSD, TN, JCR, and SRB contributed new reagents/analytic tools; APS analyzed the data. All authors wrote the paper.

Acknowledgements

This work was supported in part by DARPA Biological Robustness in Complex Settings (BRICS) contract HR0011-15-C-0093, Army Research Office (ARO) Multidisciplinary University Research Initiative (MURI) contract #W911NF-17-1-0402, the Jacobs Institute for Molecular Engineering for Medicine, and an NSF Graduate Research Fellowship DGE-144469 (to APS). We acknowledge Michael Porter, Joong Hwan Bahng, Jacob Barlow, Zhen-Gang Wang, Julia Kornfield, David Tirrell, Justin Bois, and Greg Donaldson for useful discussions; the Beckman Institute Biological Imaging Facility, the Broad Animal Facility, and the Church Animal Facility for experimental resources; Jennifer Costanza,

Taren Thron, the Caltech Office of Laboratory Animal Resources, and the veterinary technicians at the California Institute of Technology for technical support; Joanne Lau for assistance with Western blot measurements; Emily Wyatt for assistance with zeta potential measurements; the Mazmanian laboratory for providing Rag1KO mice; the Eugene Chang Lab (University of Chicago) for providing the initial breeding pairs for the MUC2KO colony and Leonard H. Augenlicht at the Department of Oncology of Albert Einstein Cancer Center for providing the original MUC2KO line to them; and Natasha Shelby for contributions to writing and editing this manuscript.

Competing interests

The technology described in this publication is the subject of a patent application filed by Caltech.

Data availability statement

All source data and data codes are available from the Dryad Digital Repository: https://doi.org/10.5061/dryad.kd1qt0p.

References

1. Donaldson GP, Lee SM, Mazmanian SK. Gut biogeography of the bacterial microbiota. Nat Rev Microbiol [Internet]. 2015;14(1):20–32. Available from: http://www.nature.com/doifinder/10.1038/nrmicro3552

2. McGuckin MA, Lindén SK, Sutton P, Florin TH. Mucin dynamics and enteric pathogens. Nat Rev Microbiol [Internet]. 2011;9(4):265–78. Available from: http://dx.doi.org/10.1038/nrmicro2538

3. Maisel K, Ensign L, Reddy M, Cone R, Hanes J. Effect of surface chemistry on nanoparticle interaction with gastrointestinal mucus and distribution in the gastrointestinal tract following oral and rectal administration in the mouse. J Control Release. 2015;40(6):1301–15.

4. Goldberg M, Gomez-Orellana I. Challenges for the oral delivery of macromolecules. Nat Rev Drug Discov [Internet]. 2003;2(4):289–95. Available from: http://www.nature.com/doifinder/10.1038/nrd1067

5. Faisant N, Gallant DJ, Bouchet B, Champ M. Banana starch breakdown in the human small intestine studied by electron microscopy. Eur J Clin Nutr [Internet]. 1995;49(2):98–104. Available from: http://europepmc.org/abstract/MED/7743990

6. Millet YA, Alvarez D, Ringgaard S, von Andrian UH, Davis BM, Waldor MK. Insights into Vibrio cholerae intestinal colonization from monitoring fluorescently labeled bacteria. PLoS Pathog. 2014;10(10).

7. Lukic J, Strahinic I, Milenkovic M, Nikolic M, Tolinacki M, Kojic M, et al. Aggregation factor as an inhibitor of bacterial binding to gut mucosa. Microb Ecol. 2014;68(3):633–44.

8. Del Re B, Busetto A, Vignola G, Sgorbati B, Palenzona D. Autoaggregation and adhesion ability in a Bifidobacterium suis strain. Lett Appl Microbiol.

1998;27:307–10.

9. Kos B, Šušković J, Vuković S, Šimpraga M, Frece J, Matošić S. Adhesion and aggregation ability of probiotic strain Lactobacillus acidophilus M92. J Appl Microbiol [Internet]. 2003;94(6):981–7. Available from: http://doi.wiley.com/10.1046/j.1365-2672.2003.01915.x

10. Tzipori S, Montanaro J, Robins-Browne RM, Vial P, Gibson R, Levine MM. Studies with enteroaggregative Escherichia coli in the gnotobiotic piglet gastroenteritis model. Infect Immun. 1992;60(12):5302–6.

11. Howe SE, Lickteig DJ, Plunkett KN, Ryerse JS, Konjufca V. The uptake of soluble and particulate antigens by epithelial cells in the mouse small intestine. PLoS One [Internet]. 2014;9(1):e86656. Available from: http://www.ncbi.nlm.nih.gov/pubmed/24475164

12. Puri S, Friedman J, Saraswat D, Kumar R, Li R, Ruszaj D, et al. Candida albicans shed Msb2 and gost mucins affect the Candidacidal activity of salivary Hst 5. Pathogens [Internet]. 2015;4(4):752–63. Available from: http://www.mdpi.com/2076-0817/4/4/752/

13. Laux DC, McSweegan EF, Williams TJ, Wadolkowski E a, Cohen PS. Identification and characterization of mouse small intestine mucosal receptors for Escherichia coli K-12(K88ab). Infect Immun [Internet]. 1986;52(1):18–25. Available from: http://www.pubmedcentral.nih.gov/articlerender.fcgi?artid=262191&tool=pmcentrez&rendertype=abstract

14. Sajjan SU, Forstner JF. Characteristics of binding of Escherichia coli serotype O157:H7 strain CL-49 to purified intestinal mucin. Infect Immun. 1990;58(4):860–7.

15. Wanke C a., Cronan S, Goss C, Chadee K, Guerrant RL. Characterization of binding of Escherichia coli strains which are enteropathogens to small-bowel mucin. Infect Immun. 1990;58(3):794–800.

16. Sun J, Le GW, Shi YH, Su GW. Factors involved in binding of Lactobacillus plantarum Lp6 to rat small intestinal mucus. Lett Appl Microbiol. 2007;44(1):79–85.

17. Doe WF. The intestinal immune system. Gut. 1989;30:1679–85.

18. Peterson DA, McNulty NP, Guruge JL, Gordon JI. IgA response to symbiotic bacteria as a mediator of gut homeostasis. Cell Host Microbe. 2007;2(5):328–39.

19. Levinson KJ, Jesus M De, Mantis NJ. Rapid effects of a protective O-polysaccharide-specific monoclonal IgA on Vibrio cholerae agglutination, motility, and surface morphology. Infect Immun. 2015;83(4):1674–83.

20. Hendrickx APA, Top J, Bayjanov JR, Kemperman H, Rogers MRC, Paganelli FL, et al. Antibiotic-driven dysbiosis mediates intraluminal agglutination and alternative segregation of enterococcus faecium from the intestinal epithelium. MBio. 2015;6(6):1–11.

21. Endt K, Stecher B, Chaffron S, Slack E, Tchitchek N, Benecke A, et al. The microbiota mediates pathogen clearance from the gut lumen after non-typhoidal salmonella diarrhea. PLoS Pathog. 2010;6(9).

22. Bunker JJ, Erickson SA, Flynn TM, Henry C, Koval JC, Meisel M, et al. Natural polyreactive IgA antibodies coat the intestinal microbiota. Science (80-) [Internet]. 2017;358(6361):eaan6619. Available from: http://www.sciencemag.org/lookup/doi/10.1126/science.aan6619

23. Moor K, Diard M, Sellin ME, Felmy B, Wotzka SY, Toska A, et al. High-avidity

IgA protects the intestine by enchaining growing bacteria. Nature [Internet]. 2017;544(7651):498–502. Available from: http://www.nature.com/doifinder/10.1038/nature22058

24. Mantis NJ, Rol N, Corthésy B. Secretory IgA's complex roles in immunity and mucosal homeostasis in the gut. Mucosal Immunol [Internet]. 2011;4(6):603–11. Available from: http://www.nature.com/doifinder/10.1038/mi.2011.41

25. Donaldson GP, Ladinsky MS, Yu KB, Sanders JG, Yoo BB, Chou WC, et al. Gut microbiota utilize immunoglobulin A for mucosal colonization. Science (80-) [Internet]. 2018;800(May):eaaq0926. Available from: http://www.sciencemag.org/lookup/doi/10.1126/science.aaq0926

26. Bergström JH, Birchenough GMH, Katona G, Schroeder BO, Schütte A, Ermund A, et al. Gram-positive bacteria are held at a distance in the colon mucus by the lectin-like protein ZG16. Proc Natl Acad Sci [Internet]. 2016;113(48):13833–8. Available from: http://www.pnas.org/lookup/doi/10.1073/pnas.1611400113

27. Asakura S, Oosawa F. On interaction between two bodies immersed in a solution of macromolecules. J Chem Phys. 1954;22(1954):1255–6.

28. Asakura S, Oosawa F. Interaction between particles suspended in solutions of macromolecules. J Polym Sci. 1958;33:183–92.

29. Vrij A. Polymers at interfaces and the interactions in colloidal dispersions. Pure Appl Chem. 1976;48:471–83.

30. Gast AP, Hall CK, Russel WB. Polymer-induced phase separations in nonaqueous colloidal suspensions. J Colloid Interface Sci [Internet]. 1983 [cited 2018 Apr 19];96(1):251–67. Available from: https://ac.els-cdn.com/0021979783900279/1-s2.0-0021979783900279-main.pdf?_tid=92957995-976d-4b56-89e5-375e1f3503e6&acdnat=1524159252_a80a1a5abbd1c629ca137cfe2b85a79d

31. Prasad V. Weakly interacting colloid polymer mixtures. Harvard University; 2002.

32. Lu PJ, Conrad JC, Wyss HM, Schofield AB, Weitz DA. Fluids of clusters in attractive colloids. Phys Rev Lett. 2006;96(2):28306.

33. Ilett S, Orrock A, Poon W, Pusey P. Phase behavior or a model colloid-polymer mixtures. Phys Rev E. 1995;51(2):1344–53.

34. Valentine MT, Perlman ZE, Gardel ML, Shin JH, Matsudaira P, Mitchison TJ, et al. Colloid surface chemistry critically affects multiple particle tracking measurements of biomaterials. Biophys J. 2004;86(6):4004–14.

35. Wang Y-Y, Lai SK, Suk JS, Pace A, Cone R, Hanes J. Addressing the PEG mucoadhesivity paradox to engineer nanoparticles that “Slip” through the human mucus barrier. Angew Chemie-International Ed. 2008;47(50):9726–9.

36. Ensign LM, Cone R, Hanes J. Oral drug delivery with polymeric nanoparticles: the gastrointestinal mucus barrier. Adv Drug Deliv Rev. 2012;64(6):557–70.

37. Tirosh B, Rubinstein A. Migration of adhesive and nonadhesive particles in the rat intestine under altered mucus secretion conditions. J Pharm Sci. 1998;87(4):453–6.

38. Maisel K, Chattopadhyay S, Moench T, Hendrix C, Cone R, Ensign LM, et al. Enema ion compositions for enhancing colorectal drug delivery. J Control Release [Internet]. 2015;209:280–7. Available from: http://dx.doi.org/10.1016/j.jconrel.2015.04.040

39. Hasler W. Motility of the small intestine and colon. In: Alpers DH, Kalloo AN, Kaplowitz N, Owyang C, Powell DW, editors. Textbook of Gastroenterology, Fifth Edition. 5th ed. Blackwell Publishing; 2009. p. 231–263.

40. Lai SK, Wang YY, Hanes J. Mucus-penetrating nanoparticles for drug and gene delivery to mucosal tissues. Adv Drug Deliv Rev [Internet]. 2009;61(2):158–71.

Available from: http://dx.doi.org/10.1016/j.addr.2008.11.002

41. Rubio-Tapia A, Barton SH, Rosenblatt JE, Murray JA. Prevalence of small intestine bacterial overgrowth diagnosed by quantitative culture of intestinal aspirate in celiac disease. J Clin Gastroenterol. 2009;43(2):157–61.

42. O'Hara AM, Shanahan F. The gut flora as a forgotten organ. EMBO Rep. 2006;7(7):688–93.

43. Simon GL, Gorbach SL. Intestinal flora in health and disease. Gastroenterology [Internet]. 1984;86(1):174–93. Available from: http://www.gastrojournal.org/article/0016508584906061/fulltext

44. Padmanabhan P, Grosse J, Asad ABMA, Radda GK, Golay X. Gastrointestinal transit measurements in mice with 99mTc-DTPA-labeled activated charcoal using NanoSPECT-CT. EJNMMI Res [Internet]. 2013;3(1):60. Available from: http://www.pubmedcentral.nih.gov/articlerender.fcgi?artid=3737085&tool=pmcentrez&rendertype=abstract

45. Royall CP, Poon WCK, Weeks ER. In search of colloidal hard spheres. Soft Matter. 2013;9(1):17–27.

46. Pusey PN, Van Megen W. Phase behaviour of concentrated suspensions of nearly hard colloidal spheres. Nature. 1986;320(6060):340–2.

47. Lekkerkerker HNW, Poon WCK, Pusey PN, Stroobants A, Warren PB. Phase behavior of colloid + polymer mixtures. Europhys Lett. 1992;20(6):559.

48. Lu PJ, Zaccarelli E, Ciulla F, Schofield AB, Sciortino F, Weitz DA. Gelation of particles with short-range attraction. Nature. 2008;453(7194):499–503.

49. Zaccarelli E, Lu PJ, Ciulla F, Weitz DA, Sciortino F. Gelation as arrested phase separation in short-ranged attractive colloid-polymer mixtures. J Phys Condens

Matter. 2008;20(49).

50. Vincent B, Edwards J, Emmett S, Jones A. Depletion flocculation in dispersions of sterically-stabilised particles (“soft spheres”). Colloids and Surfaces. 1986;18(2–4):261–81.

51. Cowell C, Li-In-On R, Vincent B. Reversible flocculation of sterically-stabilised dispersions. J Chem Soc Faraday Trans 1 [Internet]. 1978;74(0):337. Available from: http://xlink.rsc.org/?DOI=f19787400337

52. Vincent B, Luckham PF, Waite FA. The effect of free Polymer on the stability of sterically stabilized dispersions. J Colloid Interface Sci. 1980;73(2):508.

53. Clarke J, Vincent B. Nonaqueous silica dispersions stabilized by terminally anchored polystyrene: The effect of added polymer. J Colloid Interface Sci. 1981;82(1):208–16.

54. Feigin RI, Napper DH. Depletion stabilization and depletion flocculation. J Colloid Interface Sci. 1980;75(2):525–41.

55. Vincent B, Clarke J, Barnett KG. The Flocculation of non-aqueous, sterically-stabilised latex dispersions in the presence of free polymer. Colloids and Surfaces. 1986;17(1):51–65.

56. Gast AP, Leibler L. Interactions of Sterically Stabilized Particles Suspended in a Polymer Solution. Macromolecules. 1986;19(3):686–91.

57. Jones A, Vincent B. Depletion flocculation in dispersions of sterically-stabilised particles 2. Modifications to theory and further studies. Colloids and Surfaces. 1989;42(1):113–38.

58. Napper DH. Polymeric stabilization of colloidal dispersions. 1983. 398-399 p.

59. Lindahl A, Ungell A-L, Knutson L, Lennernas H. Characterization of Fluids from the Stomach and Proximal Jejunum in Men and Women. Pharm Res. 1997;14(4):497–502.

60. Fuchs A, Dressman JB. Composition and physicochemical properties of fasted-state human duodenal and jejunal fluid: A critical evaluation of the available data. J Pharm Sci. 2014;103(11):3398–411.

61. Yethiraj A, Van Blaaderen A. A colloidal model system with an interaction tunable from hard sphere to soft and dipolar. Nature. 2003;421(6922):513–7.

62. Jones RAL. Colloidal dispersions. In: Soft Condensed Matter. 1st ed. New York: OXford University Press; 2002. p. 52–62.

63. Rubinstein M, Colby RH. Polymer Physics. New York: OUP Oxford; 2003.

64. Cai L-H. Structure and Function of Airway Surface Layer of the Human Lungs and Mobility of Probe Particles in Complex Fluids. Vol. PhD, Chemistry. [Chapel Hill]: University of North Carolina; 2012.

65. Burchard W. Structure formation by polysaccharides in concentrated solution. Biomacromolecules. 2001;2(2):342–53.

66. Joanny JF, Leibler L, De Gennes PG. Effects of polymer solutions on colloid stability. J Polym Sci Polym Phys Ed. 1979;17:1073–84.

67. Verma R, Crocker JC, Lubensky TC, Yodh AG. Entropic colloidal interactions in concentrated DNA Solutions. Phys Rev Lett. 1998;81(18):4004–7.

68. Armstrong JK, Wenby RB, Meiselman HJ, Fisher TC. The hydrodynamic radii of macromolecules and their effect on red blood cell aggregation. Biophys J. 2004;87(6):4259–70.

69. Tanford C. Physical Chemistry of Macromolecules. New York: Wiley; 1961.

70. Lee H, Venable RM, Mackerell AD, Pastor RW. Molecular dynamics studies of polyethylene oxide and polyethylene glycol: hydrodynamic radius and shape anisotropy. Biophys J [Internet]. 2008;95(4):1590–9. Available from: http://dx.doi.org/10.1529/biophysj.108.133025

71. Flory PJ. Principles of Polymer Chemistry. Ithaca, New York: Cornell University Press; 1953.

72. Brandup J, Immergut E. Polymer Handbook. 2nd ed. John Wiley; 1975.

73. Weitz D, Huang J, Lin M, Sung J. Dynamics of diffusion-limited kinetic aggregation. Phys Rev Lett. 1984;53(17):1657–60.

74. Ball RC, Weitz DA, Witten TA, Leyvraz F. Universal kinetics in reaction-limited aggregation. Phys Rev Lett. 1987;58(3):274–7.

75. Smoluchowski M. Drei Vortrage uber Diffusion, Brownsche Bewegung und Koagulation von Kolloidteilchen. Phys Zeit. 1916;17:557–85.

76. Ermund A, Schütte A, Johansson ME V, Gustafsson JK, Hansson GC, Schuette A. Gastrointestinal mucus layers have different properties depending on location - 1. Studies of mucus in mouse stomach, small intestine, Peyer's patches and colon. Am J Physiol Gastrointest Liver Physiol [Internet]. 2013;305(5):ajpgi.00046.2013-. Available from: http://ajpgi.physiology.org/content/early/2013/07/05/ajpgi.00046.2013.reprint

77. Johansson ME V, Ambort D, Pelaseyed T, Schütte A, Gustafsson JK, Ermund A, et al. Composition and functional role of the mucus layers in the intestine. Cell Mol Life Sci. 2011;68(22):3635–41.

78. Ambort D, Johansson ME V., Gustafsson JK, Nilsson HE, Ermund a., Johansson

BR, et al. Calcium and pH-dependent packing and release of the gel-forming MUC2 mucin. Proc Natl Acad Sci. 2012;109(15):5645–50.

79. Murphy K, Travers P, Walport M. Janeway's Immunobiology. 8th ed. Current Biology, Ltd.; 2004.

80. Kishimoto Y, Kanahori S, Sakano K, Ebihara S. The maximum single dose of resistant maltodextrin that does not cause diarrhea in humans. J Nutr Sci Vitaminol (Tokyo) [Internet]. 2013;59(4):352–7. Available from: http://www.ncbi.nlm.nih.gov/pubmed/24064737

81. Fibersol-2 FAQ's [Internet]. Available from: http://www.fibersol.com/products/fibersol-2/faqs/

82. Dongowski G, Lorenz A, Anger H. Degradation of pectins with different degrees of esterification by Bacteroides thetaiotaomicron isolated from human gut flora. Appl Environ Microbiol. 2000;66(4):1321–7.

83. Thakur BR, Singh RK, Handa AK. Chemistry and Uses of Pectin - A Review. Crit Rev Food Sci Nutr. 1997;37(1):47–73.

84. Holloway W, Tasman-Jones C, Maher K. Pectin digestion in humans. Am J Clin Nutr. 1983;37(2):253–5.

85. Coenen M, Mosseler A, Vervuert I. Fermentative gases in breath indicate that Inulin and Starch start to be degraded by microbial fermentation in the stomach and small intestine of the horse in contrast to pectin and cellulose. J Nutr. 2006;136(May):2108–10.

86. Saha D, Bhattacharya S. Hydrocolloids as thickening and gelling agents in food: A critical review. J Food Sci Technol. 2010;47(6):587–97.

87. Grey H, Abel C, Zimmerman B. Structure of IgA proteins. Ann New York Acad

Sci. 1971;190(1):37–48.

88. Kerr M. The structure and function of human IgA. Biochem J [Internet]. 1990;271(2):285–96. Available from: http://www.pubmedcentral.nih.gov/articlerender.fcgi?artid=1149552&tool=pmcentrez&rendertype=abstract

89. Secor PR, Michaels LA, Ratjen A, Jennings LK, Singh PK. Entropically driven aggregation of bacteria by host polymers promotes antibiotic tolerance in Pseudomonas aeruginosa. Proc Natl Acad Sci [Internet]. 2018;201806005. Available from: http://www.pnas.org/lookup/doi/10.1073/pnas.1806005115

90. Highgate D. Particle Migration in Cone-plate Viscometry of Suspensions. Nature. 1966;211:1390–1.

91. Michele J, Patzold R, Donis R. Alignment and aggregation effects in suspensions of spheres in non-Newtonian media. Rheol Acta. 1977;16(3):317–21.

92. Kim J, Helgeson ME. Shear-induced clustering of Brownian colloids in associative polymer networks at moderate Péclet number. Phys Rev Fluids [Internet]. 2016;1(4):43302. Available from: https://link.aps.org/doi/10.1103/PhysRevFluids.1.043302

93. Highgate DJ, Whorlow RW. Rheological properties of suspensions of spheres in non-Newtonian media. Rheol Acta [Internet]. 1970;9(4):569–76. Available from: https://doi.org/10.1007/BF01985469

94. Snijkers F, Pasquino R, Vermant J. Hydrodynamic interactions between two equally sized spheres in viscoelastic fluids in shear flow. Langmuir. 2013;29(19):5701–13.

95. USDA. The Food Supply and Dietary Fiber : Its Availability and Effect on Health.

Nutrition Insight 36. 2007.

96. USDA. 2015 – 2020 Dietary Guidelines for Americans [Internet]. 2015 – 2020 Dietary Guidelines for Americans (8th edition). 2015 [cited 2018 Jun 11]. Available from: http://health.gov/dietaryguidelines/2015/guidelines/

97. Datta SS, Preska Steinberg A, Ismagilov RF. Polymers in the gut compress the colonic mucus hydrogel. Proc Natl Acad Sci U S A [Internet]. 2016 Jun 28 [cited 2016 Jul 22];113(26):7041–6. Available from: http://www.ncbi.nlm.nih.gov/pubmed/27303035

98. Leary S, Underwood W, Anthony R, Cartner S. AVMA Guidelines for the Euthanasia of Animals: 2013 Edition [Internet]. American Veterinary Medical Association. 2013 [cited 2018 Jun 11]. p. 98. Available from: https://www.avma.org/kb/policies/documents/euthanasia.pdf

99. Otsu N. A threshold selection method from gray-level histograms. IEEE Trans Syst Man Cybern. 1979;SMC-9(1):62–6.

100. Bois J. BE / Bi 103 : Data Analysis in the Biological Sciences [Internet]. 2015. Available from: http://bebi103.caltech.edu.s3-website-us-east-1.amazonaws.com/2017/lecture_notes/l06_frequentist_methods.pdf

101. Ward FW, Coates ME. Gastrointestinal pH measurement in rats: Influence of the microbial flora, diet and fasting. Lab Anim. 1987;21(3):216–22.

102. Smith HW. Observations on the flora of the alimentary tract of animals and factors affecting its composition. J Pathol Bacteriol. 1965;89:95–122.

103. McConnell EL, Basit AW, Murdan S. Measurements of rat and mouse gastrointestinal pH, fluid and lymphoid tissue, and implications for in-vivo experiments. J Pharm Pharmacol [Internet]. 2008;60(1):63–70. Available from:

http://doi.wiley.com/10.1211/jpp.60.1.0008

104. de Gennes PG. Conformations of polymers attached to an interface. Macromolecules [Internet]. 1980;13(19):1069–75. Available from: http://pubs.acs.org/doi/abs/10.1021/ma60077a009

105. Israelachvili J. Intermolecular and Surface Forces. Intermolecular and Surface Forces. 2011.

106. Waters DJ, Engberg K, Parke-Houben R, Hartmann L, Ta CN, Toney MF, et al. Morphology of photopolymerized end-linked poly (ethylene glycol) hydrogels by small-angle X-ray scattering. Macromolecules. 2010;43(16):6861–70.

107. Kawaguchi S, Imai G, Suzuki J, Miyahara A, Kitano T, Ito K. Aqueous solution properties of oligo- and poly(ethylene oxide) by static light scattering and intrinsic viscosity. Polymer (Guildf). 1997;38(12):2885–91.

108. Arratia PE, Voth GA, Gollub JP. Stretching and mixing of non-Newtonian fluids in time-periodic flows. Phys Fluids. 2005;17(5):1–10.

109. Takahashi T. Flow Behavior of Digesta and the Absorption of Nutrients in the Gastrointestine. J Nutr Sci Vitaminol. 2011;57:265–73.

110. Arratia PE, Cramer LA, Gollub JP, Durian DJ. The effects of polymer molecular weight on filament thinning and drop breakup in microchannels. New J Phys. 2009;11(November).

Supplementary Information

Supplemental Figures

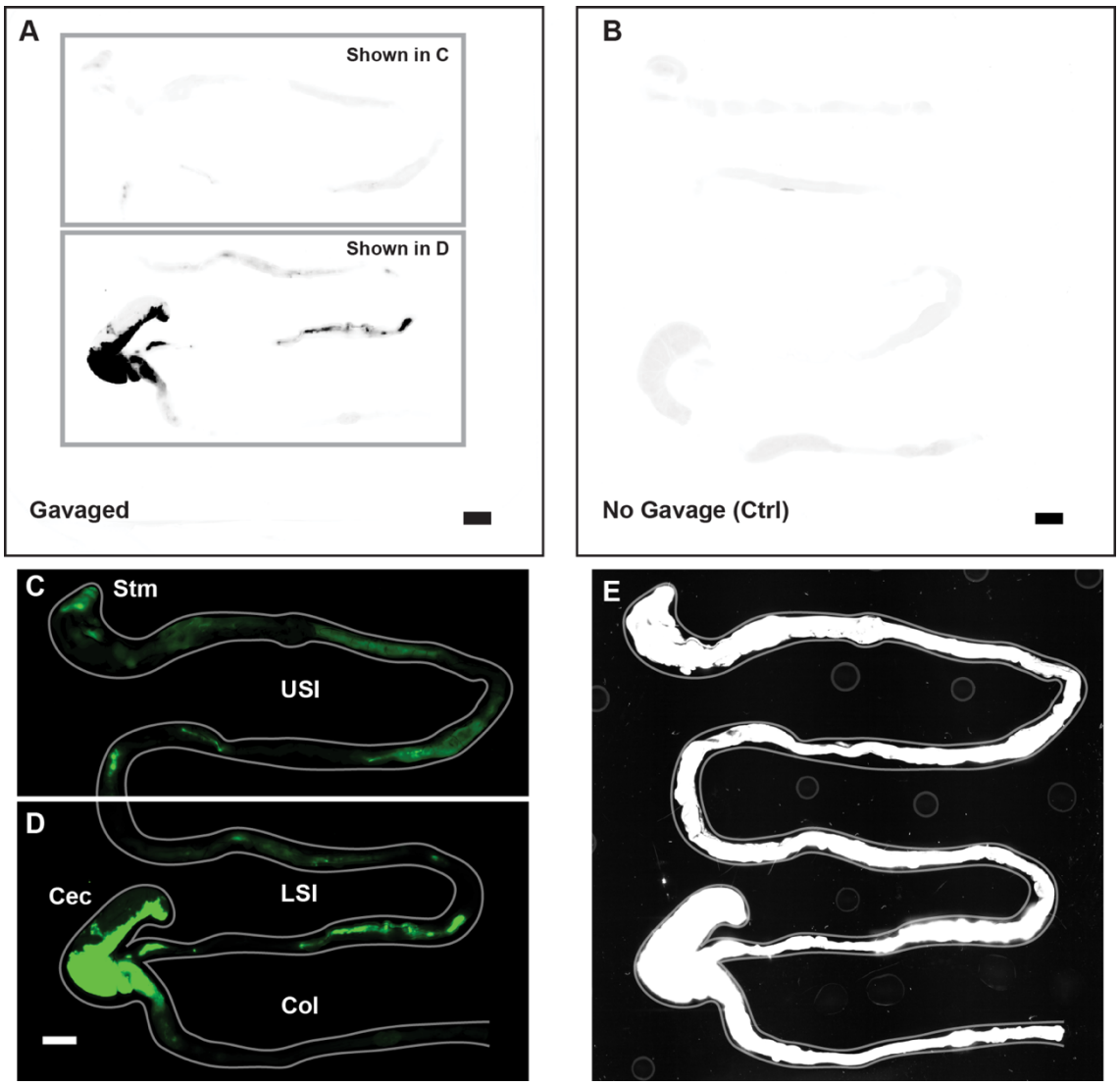

Figure 2.S1: Overview of image processing for fluorescent scanner images in Figure 2.1. (A) Unmodified fluorescent scanner images of the gastrointestinal tract of a mouse gavaged with 1 µm-diameter PEG-coated particles (prior to the contrast and color-adjustments shown in Figure 2.S1A–B). Scale bar is 0.5 cm. Boxes indicate the regions that are shown in panels C and D. (B) Unmodified fluorescent scanner image of the gut of a mouse that has not been gavaged with particles. Scale bar is 0.5 cm. (C and D). The contrast and color-adjusted images that appear in Figure 2.S1A–B. (E) Contrast-adjusted image of Figures 2.S1A-B that was used to trace the outline of the gut shown in Figure 2.S1A–B (and panel C and D of this figure). Outline of gut is shown in grey on both C, D, and E.

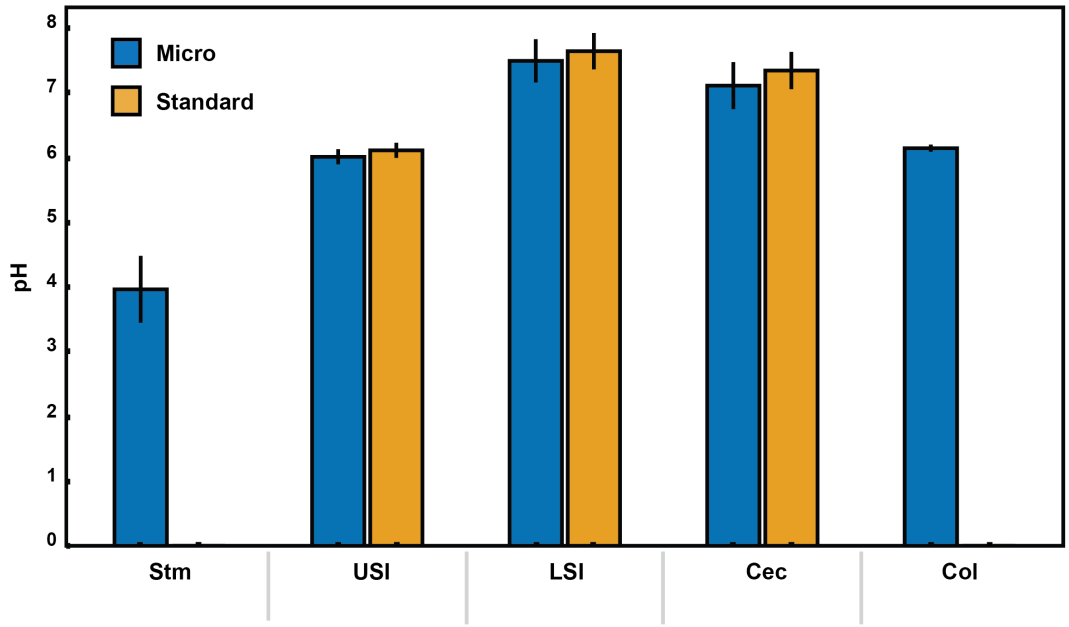

Figure 2.S2: pH measurements of luminal fluid from different sections of the gastrointestinal tract. Measurements were conducted on pooled samples of luminal fluid collected from two groups of mice. Each measurement was repeated three times, and the error bars are the standard deviation across the six trials (three trials per group). Micro (blue) indicates measurements that were conducted using a micro pH electrode. Standard (orange) indicates measurements that were conducted using a standard pH electrode. For the stomach and colon samples there was insufficient luminal fluid from both groups to submerge the tip of the standard pH electrode, so measurements were only taken with the micro pH electrode. Stm = stomach, USI = upper small intestine. LSI = lower small intestine, Cec = cecum, and Col = colon.

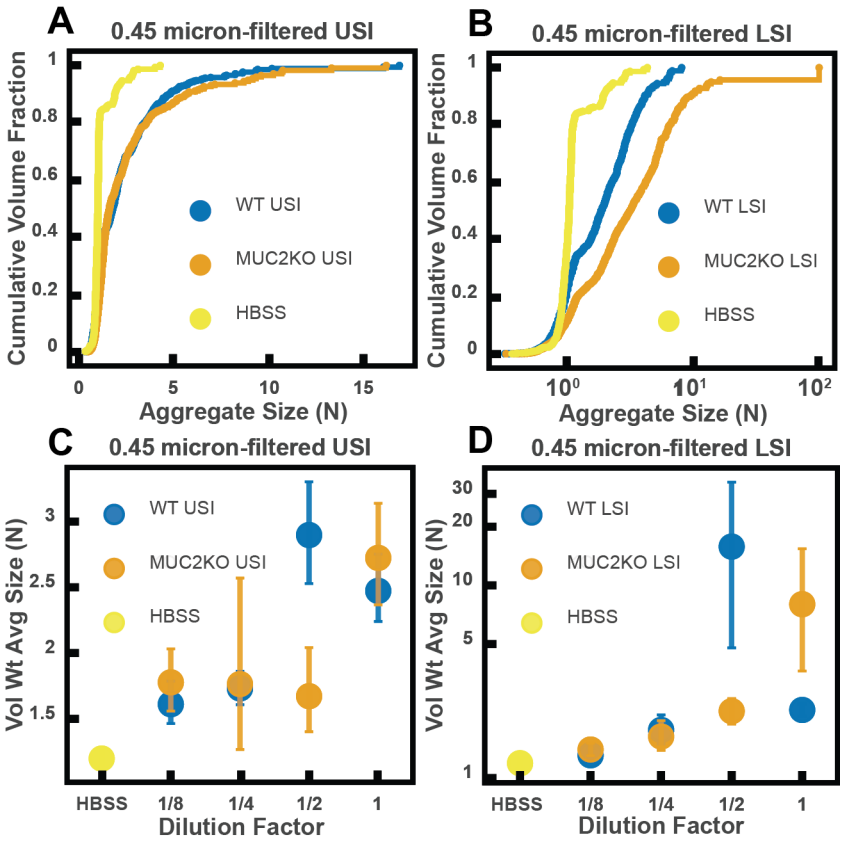

Figure 2.S3: *Ex vivo* aggregation in 0.45 µm-filtered luminal fluid from the small intestines (SI) of wild-type (WT) and MUC2 knockout (MUC2KO) mice. (**A** and **B**) Volume-weighted empirical cumulative distribution functions (ECDFs) comparing aggregation of the particles in undiluted, 0.45-µm-filtered samples from the upper (A) and lower (B) SI of two separate groups of WT and MUC2KO mice to the control (particles suspended in HBSS). The vertical axis is the cumulative volume fraction of the total number of particles in solution in an aggregate of a given size. The horizontal axis is aggregate size in number of particles per aggregate (N). (C and D) Volume-weighted average aggregate sizes (Vol Wt Avg Size) for serial dilutions of 0.45 µm-filtered samples from the upper (C) and lower (D) SI of two separate groups of WT and MUC2KO mice. Volume-weighted average sizes are plotted on the vertical axis in terms of number of particles per aggregate (N). The dilution factor is plotted on the horizontal axis, where a dilution factor of 1 is undiluted and ½ is a two-fold dilution. The control (particles suspended in HBSS) is plotted as a dilution factor of 0. The vertical error bars are 95% empirical bootstrap CI using the bootstrapping procedure described in *Materials and Methods*.

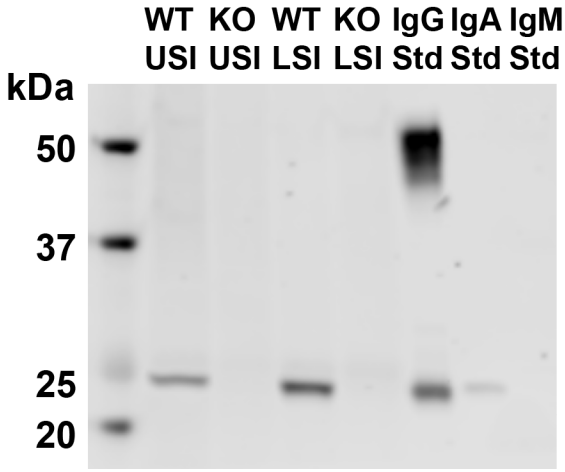

Figure 2.S4: Western blots of 30 µm-filtered samples from the small intestine (SI) of wild-type (WT) and Rag1 knockout (Rag1KO) mice. WT USI = WT upper SI; KO USI = KO lower SI; WT LSI = WT lower SI; KO USI = KO upper SI. For the detection of IgG, 1:10,000 dilutions of Li-Cor IRDye 800 CW Goat Anti-Mouse IgG was used. Because the Anti-IgG antibody appears to be binding to just the light chains (around 25 kDa), we suspect that it is mostly binding to IgA. Li-Cor's published validation (https://www.licor.com/bio/products/reagents/secondary_antibodies/irdye_800cw.html) found that the antibody binds to the heavy and light chains of IgG and just the light chains of IgA. Because we see binding of the antibody to both the heavy and light chains in the IgG standard, but only binding to a light chain in the SI samples and the IgA control, this suggests that we are detecting the light chains of IgA in the SI samples.

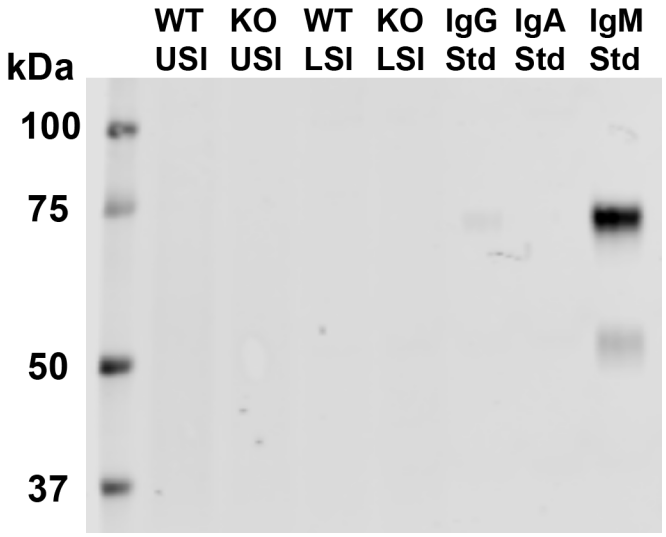

Figure 2.S5: Western blots of 30 µm-filtered samples from the small intestine (SI) of wild-type (WT) and Rag1 knockout (Rag1KO) mice. WT USI = WT upper SI; KO USI = KO lower SI; WT LSI = WT lower SI; KO USI = KO upper SI. For detection of IgM, 1:10,000 dilution of Li-Cor IRDye 800CW Goat Anti-Mouse IgM was used. We do not detect IgM in any of the SI samples.

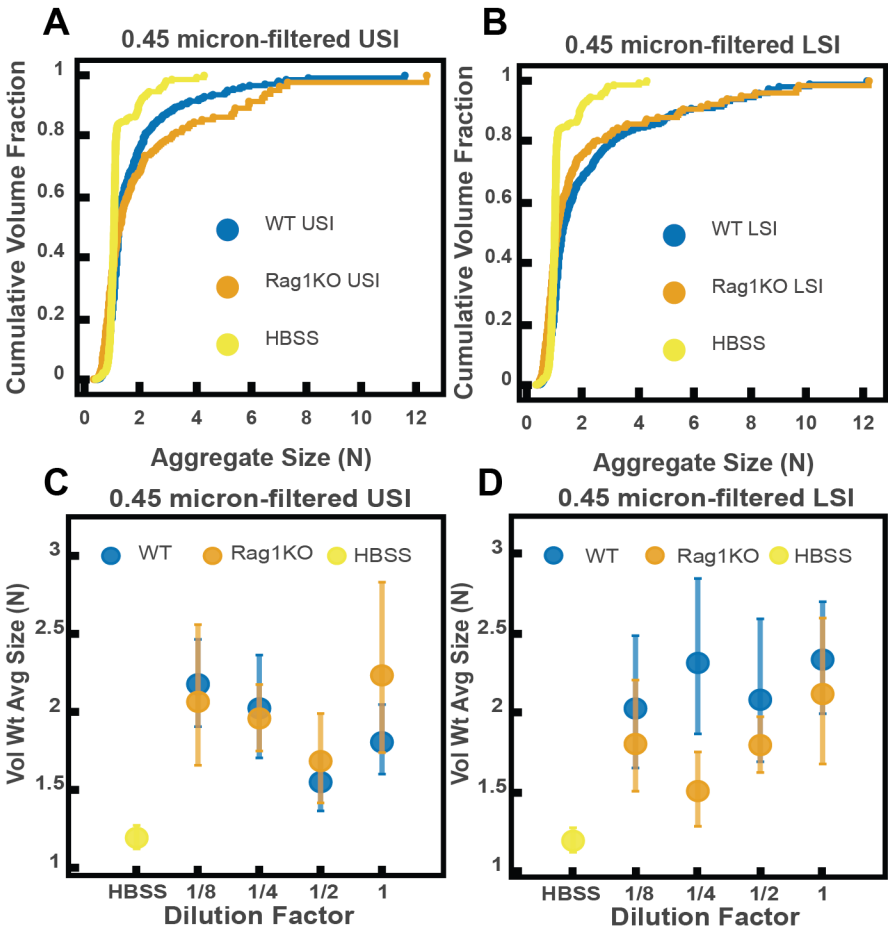

Figure 2.S6: *Ex vivo* aggregation in 0.45-µm-filtered luminal fluid from the small intestines (SI) of wild-type (WT) and Rag1 knockout (Rag1KO) mice. (A and B) Volume-weighted empirical cumulative distribution functions (ECDFs) comparing aggregation of the particles in undiluted, 0.45-µm-filtered samples from the upper (A) and lower (B) SI of two separate groups of WT and immunoglobulin-deficient (Rag1KO) mice to the control (particles suspended in HBSS). Plotted on the vertical axis is the cumulative volume fraction of the total number of particles in solution in an aggregate of a given size. Plotted on the horizontal axis are aggregate sizes in number of particles per aggregate (N). (C and D). Volume-weighted average aggregate sizes (Vol Wt Avg Size) for serial dilutions of 0.45-µm-filtered samples from the upper (C) and lower (D) SI of two separate groups of WT and Rag1KO mice. Volume-weighted average sizes are plotted on the vertical axis in terms of number of particles per aggregate (N). The dilution factor is plotted on the horizontal axis, where a dilution factor of 1 is undiluted and ½ is a two-fold dilution. The control (particles suspended in HBSS) is plotted as a dilution factor of 0. The vertical error bars are 95% empirical bootstrap CI using the bootstrapping procedure described in *Materials and Methods*.

Supplemental Tables

Table 2.S1: Estimates of physical parameters of polymers from gel permeation chromatography for liquid fractions from the upper small intestine of MUC2 knockout (MUC2KO) and wild-type (WT) mice.

Retention volume (mL)	**11 to 16**		**16 to 20**		**>20**	
Mouse type	WT	MUC2KO	WT	MUC2 KO	WT	MUC2 KO
M_w (kDa)	3,560±410	5,420±620	162±20	147±17	4.05±0.46	2.96±0.34
M_w/M_n	1.36	1.59	2.16	2.43	3.59	10.9
R_h (nm)	49.1	45.5	6.31	5.95	1.18	1.02
Fract. Conc. (mg/mL)	2.52±0.29	1.18±0.13	24.6±2.8	21.9±2.5	88.7±10.1	86.0±9.8

We calculated values with both dn/dc = 0.185 (for proteins) and dn/dc = 0.147 (pullulan). When the value varied with dn/dc, it is reported in the table as the mid-range values ± the absolute deviation between the two calculated values. M_w = the weight-average molecular weight; M_w/M_n = the dispersity; R_h = hydrodynamic radius; Fract. Conc. = Concentration of a given molecular weight fraction.

Table 2.S2: Estimates of physical parameters of polymers from gel permeation chromatography for liquid fractions from the lower small intestine of MUC2 knockout (MUC2KO) and wild-type (WT) mice

Retention volume (mL)	**11 to 16**		**16 to 20**		**>20**	
Mouse type	WT	MUC2KO	WT	MUC2KO	WT	MUC2KO
M_w (kDa)	4,730±540	5,180±590	219±25	155±18	13.7±1.6	5.93±0.68
M_w/M_n	1.24	1.80	1.91	1.84	1.88	2.03
R_h (nm)	57.0	49.2	8.45	7.58	1.89	1.35
Fract. Conc. (mg/mL)	3.42±0.39	2.36±0.27	23.0±2.6	22.8±2.6	54.8±6.3	63.3±7.2

We calculated values with both dn/dc = 0.185 (for proteins) and dn/dc = 0.147 (pullulan). When the value varied with dn/dc, it is reported in the table as the mid-range values +/- the absolute deviation between the two calculated values. M_w = the weight-average molecular weight; M_w/M_n = the dispersity; R_h = hydrodynamic radius; Fract. Conc. = Concentration of a given molecular weight fraction.

Table 2.S3: Estimates of physical parameters of polymers from gel permeation chromatography for liquid fractions from the upper small intestine of immunoglobulin-deficient (Rag1KO) and wild-type WT mice.

Retention volume (mL)	**11 to 16**		**16 to 20**		**>20**	
Mouse type	WT	Rag1KO	WT	Rag1KO	WT	Rag1KO
M_w (kDa)	1,480±170	2,140±250	108±12	74.2±8.5	2.84±0.32	1.91±0.22
M_w/M_n	1.09	1.14	2.62	2.42	1.59	1.54
R_h (nm)	31.8	39.8	4.77	2.51	1.078	0.936
Fract. Conc. (mg/mL)	1.07±0.12	1.13±0.13	14.3±1.6	13.9±1.6	66.1±7.6	70.5±8.1

We calculated values with both dn/dc = 0.185 (for proteins) and dn/dc = 0.147 (pullulan). When the value varied with dn/dc, it is reported in the table as the mid-range value +/- the absolute deviation between the two calculated values. M_w = the weight-average molecular weight; M_w/M_n = the dispersity; Rh = hydrodynamic radius; Fract. Conc. = Concentration of a given molecular weight fraction.

Table 2.S4: Estimates of physical parameters of polymers from gel permeation chromatography for liquid fractions from the lower small intestine of immunoglobulin-deficient (Rag1KO) and wild-type WT mice.

Retention volume (mL)	**11 to 16**		**16 to 20**		**>20**	
Mouse type	WT	Rag1KO	WT	Rag1KO	WT	Rag1KO
M_w (kDa)	1,080±120	2,490±290	66.9±7.7	91.6±10.5	3.64±0.42	3.72±0.43
M_w/M_n	1.18	1.05	1.71	1.98	2.09	1.98
R_h (nm)	34.6	47.1	4.67	4.85	1.116	1.09
Fract. Conc. (mg/mL)	1.52±0.17	1.89±0.22	15.8±1.8	14.1±1.6	49.5±5.7	55.1±6.3

We calculated values with both dn/dc = 0.185 (for proteins) and dn/dc = 0.147 (pullulan). When the value varied with dn/dc, it is reported in the table as the mid-range values +/- the absolute deviation between the two calculated values. M_w = the weight-average molecular weight; M_w/M_n = the dispersity; R_h = hydrodynamic radius; Fract. Conc. = Concentration of a given molecular weight fraction.

Table 2.S5: Gel permeation chromatography of Fibersol-2 and pectin in phosphate-buffered saline

Sample	Fibersol-2	Pectin
M_w (kDa)	3.48	232
M_w/M_n	10.5	1.97
R_h (nm)	1.24	25.4

Both fiber types were analyzed with dn/dc = 0.147 for polysaccharides**.** M_w = weight-average molecular weight; M_w/M_n = the dispersity; R_h = hydrodynamic radius

Table 2.S6: Estimates of physical parameters of polymers from gel permeation chromatography for liquid fractions from upper small intestine of pectin and Fibersol-2 fed mice

Retention volume (mL)	**11 to 16**		**16 to 20**		**>20**	
Mouse type	Pectin	Fibersol-2	Pectin	Fibersol-2	Pectin	Fibersol-2
M_w (kDa)	267±31	686±79	40.0±4.5	35.3±4.0	1.39±0.16	1.67±0.19
M_w/M_n	1.50	1.08	2.15	2.64	2.45	1.48
R_h (nm)	31.8	N/C**	5.52	2.88	0.819	N/C**
Fract. Conc. (mg/mL)	1.62±0.19	0.516±0.059	9.00±1.03	23.3±2.7	53.7±6.1	77.0±8.8

We calculated values with both dn/dc = 0.185 (for proteins) and dn/dc = 0.147 (pullulan). When the value varied with dn/dc, it is reported in the table as the mid-range values +/- the absolute deviation between the two calculated values. M_w = the weight-average molecular weight; M_w/M_n = the dispersity; R_h = hydrodynamic radius; Fract. Conc. = Concentration of a given molecular weight fraction. N/C** denotes values for which the concentration was too low to calculate.

Table 2.S7: Estimates of physical parameters of polymers from gel permeation chromatography for liquid fractions from lower small intestine of pectin and Fibersol-2-fed mice

Retention volume (mL)	**11 to 16**		**16 to 20**		**>20**	
Mouse type	Pectin	Fibersol-2	Pectin	Fibersol-2	Pectin	Fibersol-2
M_w (kDa)	282±32	1680±190	30.2±3.5	18.8±2.2	1.12±0.13	2.32±0.27
M_w/M_n	7.37	1.64	1.70	2.78	2.89	1.14
R_h (nm)	29.0	26.4	5.28	2.16	0.724	1.06
Fract. Conc. (mg/mL)	2.48±0.28	0.839±0.096	9.43±1.1	53.6±6.1	42.7±4.9	88.3 ±10.1

We calculated values with both dn/dc = 0.185 (for proteins) and dn/dc = 0.147 (pullulan). When the value varied with dn/dc, it is reported in the table as the mid-range values +/- the absolute deviation between the two calculated values. M_w = the weight-average molecular weight; M_w/M_n = the dispersity; R_h = hydrodynamic radius; Fract. Conc. = concentration of a given molecular weight fraction.

Table 2.S8: Zeta potential and NMR measurements of PEG-coated particles

Surface Modification of PS particles	Zeta potential (mV)	Nanomoles PEG/mg particles
mPEG 5 kDa	-18.87 ±1.78	5.5
mPEG 5 kDa w/ mPEG 1 kDa backfill	-7.66 ±2.12	4.6
mPEG 5 kDa w/ mPEG 350 Da backfill	-9.99 ± 1.65	4.3
mPEG 5 kDa w/ mPEG 5 kDa backfill	-14.56 ± 1.78	4.0
mPEG 2 kDa	-39.59 ± 2.41	9.4
Carboxylate-coated (no PEG)	-61.36 ± 12.40	0.0

For the zeta potential measurements, each particle solution was 0.1 mg/ml of particles in 1 mM KCl. Measurements were done on a Brookhaven NanoBrook ZetaPALS Potential Analyzer. Three trials were done where each trial was 10 runs each and each run was 10 cycles. Values reported are the average zeta potential for the 30 runs. NMR measurements were performed as described in *Materials and Methods*. Values are estimates of the nanomoles of polyethylene glycol (PEG) per milligrams of particles. To calculate this, we have to assume all the PEG on the surface is a single MW. It is therefore assumed all the PEG on the surface is PEG 5 kDa.

Detailed contributions from non-corresponding authors

A.P.S. co-designed all experiments and co-analyzed all experimental results; developed theoretical tools and performed all calculations; co-developed imaging analysis pipeline in ImageJ; developed computational tools for bootstrapping procedure; co-developed microscopy assay for examining luminal contents from mice gavaged particles used in Figure 2.1C and 1D; co-performed, designed, and analyzed data from experiments involving oral administration of particles in Figure 2.1; performed, designed, and analyzed data from all *ex vivo* aggregation experiments in SI fluid in Figures 2.2, 2.3, 2.5-7, 2.S2, and 2.S5; performed, designed, and analyzed data from all GPC measurements in Figures 2.3, 2.5-7, and Tables 2.S1-7; performed, designed, and analyzed data from all *in vitro* aggregation experiments with PEG solutions in Figure 2.4D, Figure 2.4 – figure supplements 1-2, and with dietary fiber in Figure 2.7A; developed a computational approach for theoretical calculations in 2.4H and 2.4I and performed all calculations; performed, designed, and analyzed data from Western blots in Figures 2.5E, 2.6E, 2.S3, and 2.S4; helped supervise animal husbandry of MUC2KO colony; performed animal husbandry for WT mice on autoclaved diets in Figure 2.6 and 2.S5; performed animal husbandry for mice on pectin and Fibersol-2 diets in Figure 2.7; performed, designed, and analyzed all zeta potential measurements in Table 2.S8; performed pH measurements on luminal fluid in Figure 2.S2; co-interpreted results; and co-wrote the paper.

S.S.D. conceived and co-planned the project; initially observed the aggregation phenomenon described in this work; co-designed and co-analyzed preliminary experiments; performed preliminary *ex vivo* and *in vitro* aggregation experiments; co-developed microscopy assay for examining luminal contents from mice gavaged particles used in Figure 2.1C and 2.1D; developed *ex vivo/in vitro* aggregation assay used in Figures 2.2-7; co-developed approach to extract liquid fraction of murine intestinal contents; co-developed protocol for NMR measurements on PEG-coated particles; organized transfer and initial set up of MUC2KO colony; co-interpreted results; and co-wrote the paper.

T.N. co-developed imaging analysis pipeline in ImageJ; co-analyzed *ex vivo* aggregation data in Figure 2.2; co-designed and co-analyzed preliminary *ex vivo* aggregation experiments with MUC2KO mice; provided useful advice on design of bootstrapping procedure; co-interpreted results; and co-wrote the paper.

J.C.R. developed protocol for NMR measurements on PEG-coated particles; performed synthesis of particles; performed NMR measurements in Table 2.S8; and co-wrote the paper.

S.R.B. co-performed preliminary experiments; developed fluorescent laser scanning approach for examining luminal contents of mice gavaged with particles appearing in Figure 2.1A and 2.1B; administered particles to mice in Figure 2.1; co-developed approach to extract liquid fraction of murine intestinal contents; co-organized transfer and initial set up of MUC2KO colony; set up genotyping of MUC2KO mice; helped supervise animal husbandry of MUC2KO colony; helped with interpretation of results; and co-wrote the paper.

Chapter 3

POLYMERS IN THE GUT COMPRESS THE COLONIC MUCUS HYDROGEL

1. S. S. Datta, A. Preska Steinberg, and R. F. Ismagilov. 2016 "Polymers in the gut compress the colonic mucus hydrogel." PNAS 113(26):7041-7046. doi: 10.1073/pnas.1602789113

Abstract

Colonic mucus is a key biological hydrogel that protects the gut from infection and physical damage and mediates host-microbe interactions and drug delivery. However, little is known about how its structure is influenced by materials it comes into contact with regularly. For example, the gut abounds in polymers like dietary fibers or administered therapeutics, yet whether such polymers interact with the mucus hydrogel, and if so, how, remains unclear. While several biological processes have been identified as potential regulators of mucus structure, the polymeric composition of the gut environment has been ignored. Here, we demonstrate that gut polymers do in fact regulate mucus hydrogel structure, and that polymer-mucus interactions can be described using a thermodynamic model based on Flory-Huggins solution theory. We found that both dietary and therapeutic polymers dramatically compressed murine colonic mucus *ex vivo* and *in vivo*. This behavior depended strongly on both polymer concentration and molecular weight, in agreement with the predictions of our thermodynamic model. Moreover, exposure to polymer-rich luminal fluid from germ-free mice strongly compressed the mucus hydrogel, while exposure to luminal fluid from specific-pathogen-free mice—whose microbiota degrade gut polymers—did not; this suggests that gut microbes modulate mucus structure by degrading polymers. These findings highlight the role of mucus as a responsive biomaterial, and reveal a new mechanism of mucus restructuring that must be integrated into the design and interpretation of studies involving therapeutic polymers, dietary fibers, and fiber-degrading gut microbes.

Significance statement

Hydrogels are critical components of biological systems; however, how these structures are impacted by polymers abundant in their environments—e.g. dietary fiber in the gut, soluble glycoproteins in tissues—remains unknown. Here we find that the colonic mucus hydrogel (a protective barrier and mediator of microbe-host interactions) is compressed by gut polymers. Surprisingly, the predictions of a simple thermodynamic model are able to describe our experiments on this complex biological system, providing insight into the underlying physics. Moreover, we find that gut microbes modulate mucus structure by degrading dietary polymers into smaller, non-compressing fragments. These findings reveal a new mechanism of mucus restructuring, and illustrate an unexpected interplay between diet, gut microbiota, and the biological structures that protect a host.

Introduction

Biological hydrogels (including mucus, blood clots, and the extracellular matrix) provide critical functions, yet little is known about how their structure is influenced by materials they come into contact with regularly. For example, the environments of many hydrogels abound in polymers, such as dietary fibers (1, 2) or administered therapeutics (3–5) in the gut and soluble glycoproteins in tissues. Whether such polymers interact with these hydrogels, and if so, how, remains unclear. An important example is the case of colonic mucus, which protects the gut from infection and physical damage (6–8), mediates drug delivery (9), and mediates host-microbe interactions (10) in a structure-dependent manner; for example, a "tighter" mesh could impede the infiltration of microorganisms from the intestinal lumen (6, 11–13). Mucus restructuring is typically attributed solely to changes in secretion (14–16), or to the activity of specific enzymes (8, 17), detergents (18), or dextran sulfate sodium-induced inflammation (19). However, the physicochemical properties of the gut environment itself—particularly its polymeric composition—have not been considered as a potential regulator of mucus structure. We therefore sought to characterize the structure of the colonic mucus hydrogel in the absence and in the presence of polymers.

Results

In vivo thickness of the colonic mucus hydrogel

To probe the in vivo thickness of murine colonic mucus, we developed a label-free technique that eliminates evaporation and avoids the use of any washing, fixative, labeling, or dehydrating agents that could alter mucus structure (SI Materials and Methods). We used freshly-excised colon explants obtained from mice at least 8 weeks old—whose mucus hydrogel has been found to be fully-developed and stable (20) — and gently removed the luminal contents using FC-40 oil, a fluorocarbon fluid that is immiscible with, and denser than, water. We opened each explant along the intestinal axis and mounted it flat, with its luminal surface facing upward and coated with FC oil. We then used an upright confocal microscope equipped with a dry objective lens to image, in three dimensions, the exposed epithelial surface and the oil overlying the adherent mucus hydrogel (Figure 3.1a).

We first identified both the epithelial surface (Figure 3.S1a-b) and the oil-mucus interface using confocal reflectance microscopy (Figure 3.1b-c); the distance between the two provided a measure of the mucus hydrogel thickness. We measured a comparable mucus thickness of 67 ± 7 μm or 55 ± 5 μm (mean ± SEM, n = 6 or 3, P = 0.3) for control mice fed a standard chow diet or a sucrose solution (Figure 3.1d), consistent with previous measurements (8). To investigate the role of polymers in altering mucus structure, we then fed mice the same sucrose solution, with added polyethylene glycol (PEG), an uncharged polymer that is well-characterized, is often used as a therapeutic in the gut (3, 4), and has minimal chemical interactions with biomolecules (21). We used PEG of an average molecular weight ~200 kDa and average radius of gyration $R_{g,p} \approx 22$ nm, denoted as PEG 200k. Unexpectedly, the mucus hydrogel was significantly thinner for these mice, 14 ± 2 μm (mean ± SEM, n = 6, P = 2 x 10-4; Fig. 1d). This finding demonstrates that such polymers can in fact alter the structure of mucus.

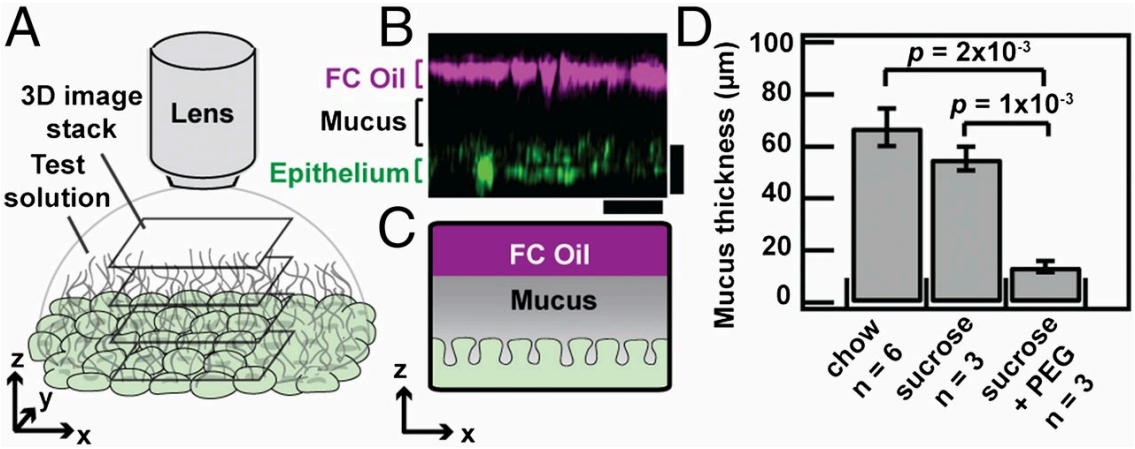

Figure 3.1: Polymers compress colonic mucus hydrogel in vivo. (a) Schematic depicting visualization of adherent colonic mucus hydrogel. (b) Sideview confocal micrograph showing FC oil-mucus interface (magenta) separated from the epithelial surface (green) by the adherent mucus hydrogel (depicted in black). Scale bars, 30 μm. (c) Schematic of sideview shown in (b). (d) FC oil mucus thickness measurements for colonic explants taken from SPF mice fed ad libitum on either a standard chow diet, 5% w/v sucrose in 1x PBS, or 5% w/v sucrose with 7% w/v PEG 200k in 1x PBS. Data show means ± SEM.

Ex vivo characterization of colonic mucus hydrogel

To better understand this phenomenon, we modified our imaging approach so we could directly image the mucus hydrogel ex vivo while simultaneously controlling the physicochemical composition of the aqueous solution to which mucus is exposed (SI Materials and Methods). We again used freshly-excised murine colon explants, cut open along the intestinal axis and mounted flat; instead of using FC oil as the test solution, we cleared the luminal contents and coated the luminal surface with cold saline to remove soluble components, including any polymers. We used a water-immersion objective lens to identify the epithelial surface (Figure 3.2a) and corroborated this with lectin staining (Figure 3.S1c-d). To identify the luminal surface of the mucus hydrogel, we deposited a solution of 1 μm diameter microparticle probes onto the explant surface. These probes did not penetrate, but instead settled on top of, the mucus hydrogel, indicating that they were larger than its mesh size (Figure 3.2c). Previous studies have validated that this region of probe exclusion corresponds to the adherent mucus hydrogel (11, 19, 22, 23); we further

confirmed this using lectin staining (Figure 3.S2). Measuring the distance between the excluded probes (Figure 3.S3) and the underlying epithelial surface thus provided a measure of the mucus thickness, 75 ± 30 μm (mean ± SD), consistent with the distance measured when we imaged using FC oil and consistent with other reported measurements (8). Hydrogel thickness did not change appreciably over an observation time of 2.5 h. We found similar results using probes of other sizes (Figure 3.S5a–b): all probes 250 nm in diameter or larger were excluded from the mucus, and yielded comparable mucus thickness values (Figure 3.2e). By contrast, probes 100 nm in diameter or smaller (Figure 3.S5c–d) penetrated the mucus and reached the underlying epithelium, indicating that they were smaller than the mesh size (Figure 3.2b, e). We concluded that the mesh size of the adherent mucus hydrogel was between 100–250 nm, in good agreement with measurements of the mesh size of other mucus hydrogels (24, 25).

Having established a method for characterizing mucus hydrogel structure ex vivo, we next tested the influence of polymers. We placed a solution of the same PEG onto the explant surface, continually monitoring the mucus hydrogel thickness using the deposited microparticles. The PEG penetrated the mucus and reached the underlying epithelium (Figure 3.S6) and this penetration was reversible, suggesting that strong PEG-mucus chemical interactions—such as complexation, which can play a role under different conditions than those explored here (SI Materials and Methods)—were absent (Figure 3.S7). Nevertheless, the mucus hydrogel compressed by approximately 50–60% of its initial thickness within ~5–20 min (Figure 3.2e), and the level of compression appeared to be stable over an observation time of at least ~100 min. We verified that any optical effects induced by the polymer solution did not appreciably affect the z measurements (Figure 3.S8). Interestingly, compression was at least partly reversible; the mucus hydrogel re-expanded to approximately 90% of its original thickness after PEG was removed by washing the explant. These findings suggest that the polymer-induced compression observed in the FC oil experiments could be reproduced and investigated further ex vivo.

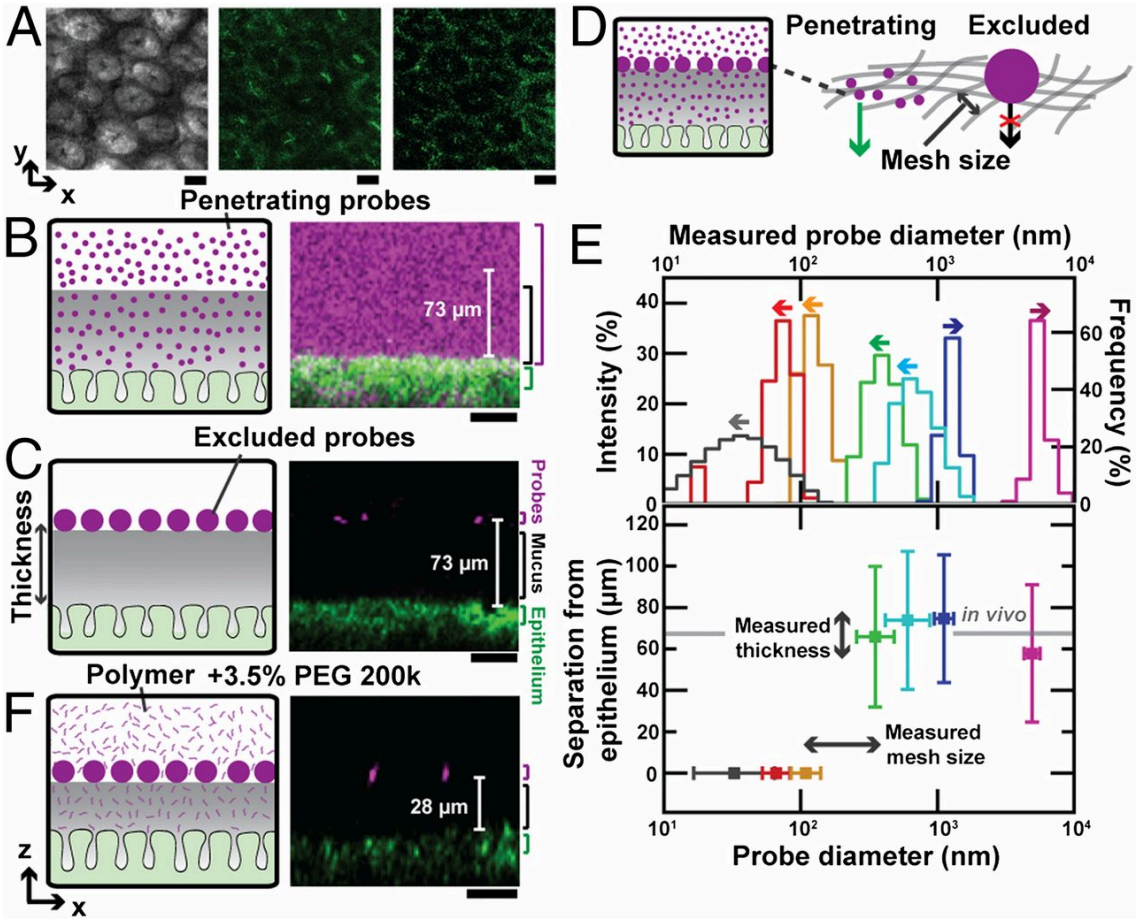

Figure 3.2: Polymers compress colonic mucus hydrogel ex vivo. (a) Bright-field (top), confocal reflectance (middle), and two-photon (bottom) micrographs of epithelial surface. Image levels were adjusted for clarity (SI Materials and Methods). Scale bars, 30 μm. (b, c, e) Left shows schematics, right shows sideview confocal micrographs. Scale bars, 10 μm. (b) Penetration of mucus by low concentration (0.05% w/v) of mPEG-FITC 200k. (c) Exclusion from mucus of 1 μm microparticle probes. (d) Schematic depicts mucus mesh structure, with penetrating probes on the left and larger non-penetrating probe on the right. (e) Top shows probe size distributions measured using dynamic light scattering (left axis, arrows to the left) or optical microscopy (right axis, arrows to the right). Bottom panel shows minimal probe separation from epithelial surface. Horizontal positions and error bars show geometric mean ± geometric SD of lognormal fits to size distributions. Vertical positions and error bars show mean ± SD. Grey bar shows mean of FC oil measurements of in vivo thickness for mice fed chow. Penetration measurements used fluorescently labeled polymers at concentrations below those that cause mucus compression. (f) Compression of colonic mucus by 3.5% w/v PEG 200k.

Flory-Huggins theory of polymer-induced compression

Large non-penetrating polymers have been used to osmotically compress synthetic hydrogels (26) and even the periciliary brush after mucus removal in the mammalian lung (27). However, the possibility that even polymers small enough to penetrate a hydrogel could compress it was first recognized by Brochard in 1981 (28), and was subsequently investigated both theoretically and experimentally (29, 30), further references are provided in SI Materials and Methods). In this case, hydrogel compression arises from a combination of enthalpic and entropic effects. For example, the polymers can reduce the effective solvent quality of the hydrogel environment, due to enthalpic interactions with the hydrogel network strands, forcing the hydrogel to reduce its hydrated volume and compress. Another effect arises from the free energy penalty associated with penetrating the hydrogel mesh: this can lead to an elevated polymer concentration, and therefore, an elevated osmotic pressure, outside the hydrogel, which similarly forces the hydrogel to compress. Clarifying the role of these, and other, different effects remains unresolved, even for the case of synthetic hydrogels; however, such effects can be described collectively using the classic Flory-Huggins theory of polymer solutions (29, 30). We therefore asked whether this physical framework could also describe polymer-induced compression of the colonic mucus hydrogel. Indeed, while the predictions of this theory have been experimentally verified using a few model synthetic hydrogels (30, 31), its applicability to the more complex case of biological hydrogels like colonic mucus is unclear. One signature of this form of compression is its tunability: more concentrated polymer solutions should induce more hydrogel compression (29, 30). Consistent with this prediction, we found that mucus compression was tunable by PEG concentration (green points, Figure 3.3b).

To test the applicability of Flory-Huggins theory, we used the same theoretical framework (30) to describe our experimental system (details and limitations of this theory are described in SI Materials and Methods). We first modeled the mucus as a swollen, cross-linked hydrogel. We then considered how the addition of polymers changes the extent to which the mucus hydrogel is swollen and its equilibrium thickness. We made the

simplifying assumption (30, 31) that the mucus behaves as an elastic gel on the timescale of our experiments, even though hydrogels, including colonic mucus, are known to be viscoelastic—they relax stresses over long times. This assumption is supported by our observations that the hydrogel thickness remained stable in either the uncompressed or polymer-induced compressed states (over observation times of at least ~100 min). It is further supported by the reversibility of the observed compression. We therefore calculated the total free energy of the ternary solvent-mucus-polymer system, G, as the sum of the elastic free energy, which accounts for deformations of the individual mucus network strands, and the free energy of mixing the polymer and the solvent with the mucus hydrogel. We then used this total free energy to calculate the chemical potentials of both the added PEG and the solvent, $\mu_P \equiv \partial G/\partial n_p$ and $\mu_S \equiv \partial G/\partial n_S$, respectively, both inside and outside of the mucus network; n_P and n_S are the respective numbers of moles:

$$\frac{\mu_S^{in}}{RT} = \frac{1}{N_M}\left(\nu_M^{\frac{1}{3}}\nu_M^{0\,\frac{2}{3}} - \frac{\nu_M}{2}\right) + ln\nu_S^{in} + 1 - \nu_S^{in} - \frac{\nu_P^{in}}{y}$$

$$+\left(\chi_{SM}\nu_M + \chi_{SP}\nu_P^{in}\right)\left(1 - \nu_S^{in}\right) - \chi_{MP}\nu_M\nu_P^{in}$$

(Eq. 3.1)

$$\frac{\mu_S^{out}}{RT} = \ln(1-\phi) + \phi\left(1 - \frac{1}{y}\right) + \chi_{SM}\phi^2$$

(Eq. 3.2)

$$\frac{\mu_P^{in}}{yRT} = \frac{1}{N_M}\left(\nu_M^{\frac{1}{3}}\nu_M^{0\,\frac{2}{3}} - \frac{\nu_M}{2}\right) + \frac{1}{y}ln\nu_P^{in} + \frac{1}{y}\left(1 - \nu_P^{in}\right) - \nu_S^{in}$$

$$+\left(\chi_{SP}\nu_S^{in} + \chi_{MP}\nu_M\right)\left(1 - \nu_P^{in}\right) - \chi_{SM}\nu_S^{in}\nu_M$$

(Eq. 3.3)

$$\frac{\mu_P^{out}}{yRT} = \frac{1}{y} ln\phi - 1 + \phi + \frac{1}{y}(1-\phi) + \chi_{SM}(1-\phi)^2$$

(Eq. 3.4)

Here, R is the gas constant, T is the temperature, ν_i is the volume fraction of species i, ν_M^0 is the mucus hydrogel volume fraction in its initial preparation state, $\varphi \equiv \nu_P^{out}$ is the volume fraction of the free polymer in external solution, N_M is the average number of segments in a mucus network strand, y is the number of segments in a polymer molecule, and χ_{ij} is the Flory-Huggins interaction parameter, which quantifies enthalpic interactions, between species i and j; we denoted solvent, mucus and free polymers as i = S, M, P, respectively. At thermodynamic equilibrium, $\mu_S^{in} = \mu_S^{out}$and $\mu_P^{in} = \mu_P^{out}$; these equalities enabled us to numerically calculate the equilibrium mucus thickness for a given PEG concentration (details of calculations, parameters used, and sensitivity to parameters are described in SI Materials and Methods). Consistent with our experimental observations, the Flory-Huggins model predicted that exposure to PEG compresses the adherent mucus hydrogel. Moreover, the model predicted (green curve, Figure 3.3a) a similar dependence of mucus compression on PEG concentration as we measured in our experiments using microparticles (green points, Figure 3.3b).

Another key prediction of the model is that the extent of mucus compression should depend on the polymer molecular weight: for a given PEG concentration, smaller polymers should compress the mucus hydrogel less (Figure 3.3a). One intuitive explanation for this is the free energy penalty paid by PEG to penetrate the mucus, which is smaller for smaller polymers; thus, even though they can exert a larger osmotic pressure, smaller polymers are less likely to be excluded from the mucus hydrogel (Figure 3.S9e), and are expected to compress it less (Figure 3.3c). To test this prediction, we measured the extent of mucus compression induced by two smaller polymers, PEG 6k and PEG 400, characterized by $R_{g,p} \approx$ 3 nm and 0.7 nm, respectively. These polymers again compressed the mucus hydrogel within 5 min, and the compression level appeared to be stable over an observation time of up to several hours. Despite the mean-field nature of the Flory-Huggins model,

which is not expected to capture the full complexity of the experiments, we observed qualitative similarities between the calculations (Figure 3.3a) and the experimental data (Figure 3.3b). We also found similar results for varying values of the model parameters (Figure 3.3a, Figure 3.S9a-d). Moreover, the observed compression was similar for mice of different genders and strains, for washed explants originating from germ-free or microbe-colonized mice, for different buffers, in the presence and the absence of Mg^{2+} ions, for buffers also containing protease inhibitor, for polymer solutions prepared using the liquid fraction of SPF mice colonic contents instead of buffer, for experiments performed at 22 ºC or 37 ºC, and for a similar, but charged, polymer, demonstrating that our results were not an artifact of the choice of the animal model or details of experimental conditions. The similarity between the theoretical predictions and the experimental data suggests that Flory-Huggins theory provides a physical description of the concentration and molecular weight-dependence of the polymer-induced compression of colonic mucus, and provides a foundation for more sophisticated modeling to better characterize the full complexity of this phenomenon (SI Materials and Methods).

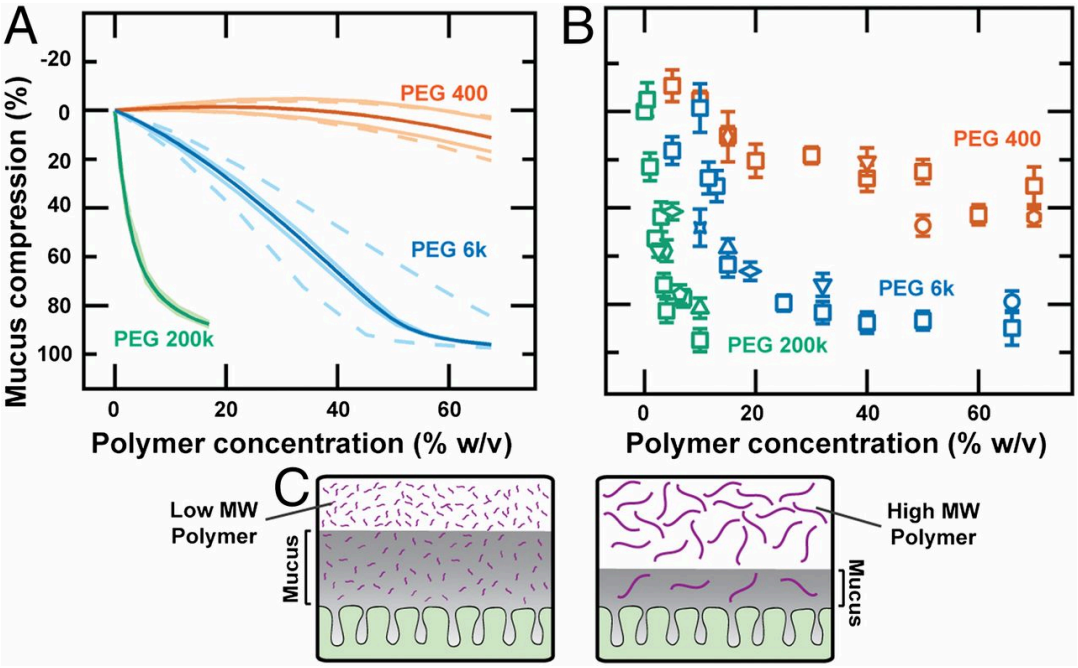

Figure 3.3: Tunable compression of colonic mucus hydrogel can be qualitatively described by Flory-Huggins theory. (a) Theoretically-predicted and (b) experimentally-measured (using 1 μm microparticles) mucus compression for varying polymer concentrations and molecular weights. Bold curves in (a) show model results for parameter values (SI Materials and Methods) $\chi_{SM} = 0$ and $\chi_{MP} = 0.3$; less opaque and dashed curves show sensitivity to variations in these parameters (upper and lower less opaque curves, $\chi_{SM} = 0.1$ and -0.1; upper and lower dashed curves, $\chi_{MP} = 0.2$ and 0.4). All mice, except for those indicated by upward triangles, were male. Symbols in (b) indicate different mouse types and experimental conditions: squares, C57BL/6 mice; circles, BALB/c mice; upward triangles, female C57BL/6 mice; vertical diamond, washed explants from GF mice; downward triangles, all solutions have added 2x Roche protease inhibitor cocktail; pentagons, all solutions have added 5mM MgSO4; horizontal diamonds, experiments performed at 37ºC instead of 22 ºC using a heated microscope stage; stars, polyacrylic acid of ~8 kDa average molecular weight instead of PEG; hexagons, HEPES buffer instead of PBS for all solutions. Each data point represents the mean of a series of five measurements on a single explant; error bars represent measurement uncertainty. (c) Schematic showing one effect potentially underlying mucus compression: molecular weight-dependent partitioning of the polymer.

Microbes can modulate mucus compression

Given the diversity of polymers abundant in fruits, vegetables, and food additives, we next asked whether dietary polymers could also compress colonic mucus. We tested three common dietary polymers: dextrin, pectin, and pullulan. Exposure to each of these polymer solutions caused the colonic mucus hydrogel to compress in a concentration-dependent manner (Figure 3.4A). Moreover, as with PEG, for a given polymer concentration, the larger polymers, pectin and pullulan, compressed the mucus more than the smaller polymer, dextrin. These observations demonstrate that, similar to the case of PEG, dietary polymers present in the gut can also induce mucus compression in a manner that depends on the physical properties of the polymers themselves.

Given our results indicating that mucus compression can depend on the polymer molecular weight, we hypothesized that microbial degradation of polymers into smaller fragments (1, 2) may actively modulate compression in vivo. Indeed, we found that while pectin strongly compressed the colonic mucus hydrogel (Figure 3.4a, blue points), a small molecule, acetate—a typical product of pectin degradation and fermentation by gut microbes—did not (500 mM acetate compressed the mucus only by ≈10%). Moreover, using the wash-free FC oil methodology as in Figure 3.1, we found that the adherent mucus of germ-free (GF) mice was only ≈25% as thick as that of specific-pathogen-free (SPF) mice in vivo (Figure 3.4b), consistent with previous observations (8, 32). Thicker SPF mucus was previously attributed solely to altered mucus secretion by the host in response to the presence of microbes, and not to the difference in polymeric composition of the gut fluid. Given our results, however, we hypothesized that mucus compression by intestinal polymers may also contribute to this phenomenon: these polymers remain intact in GF mice, which lack the gut microbiota that normally degrade these polymers into smaller non-compressing fragments. In agreement with this hypothesis, washing the GF explant with excess cold saline, which should dilute out any polymers present in the sample, restored the mucus to the thickness observed in SPF mice (Figure 3.4b). This result was surprising, because it could not have been the result of a host response to the presence of

microbes. To further test the effect of intestinal polymers on mucus compression, we isolated and analyzed the liquid fractions of the colonic contents of GF and SPF mice. As expected (Figure 3.S10), the GF contents were enriched in higher molecular weight polymers compared to the SPF contents, reflecting polymeric degradation by the SPF gut microbiota. We therefore predicted that the GF contents would compress colonic mucus more than the SPF contents. In agreement with this prediction, while SPF contents did not appreciably compress colonic mucus, the GF contents compressed colonic mucus by ≈70% of its initial washed thickness, for washed explants obtained from either SPF or GF mice (Figure 3.4c). This finding indicates that gut microbes, by modifying the polymeric composition of intestinal contents, can actively modulate the compression state of the colonic mucus hydrogel (Figure 3.4d).

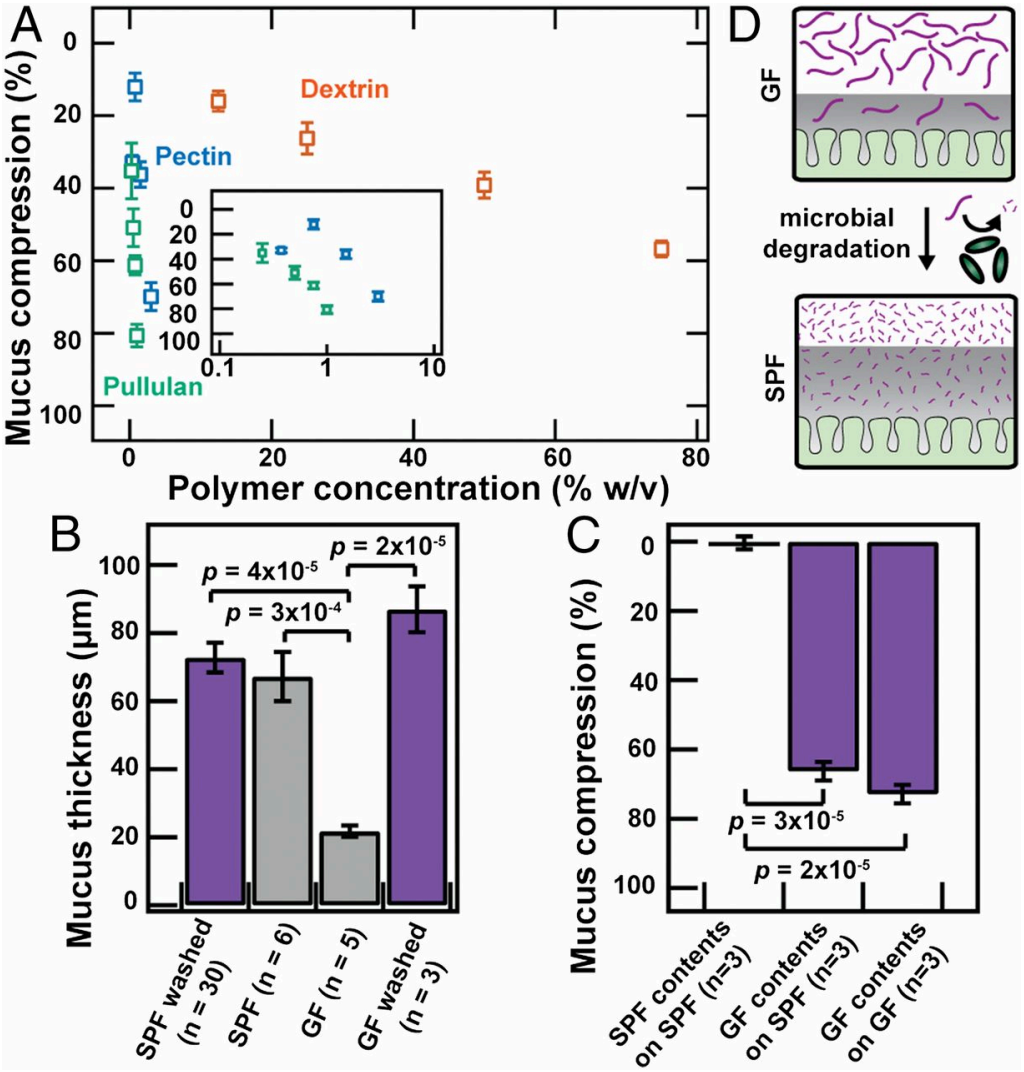

Figure 3.4: Gut microbes can modulate mucus compression by modifying the polymeric composition of intestinal contents. (a) Mucus compression induced by dietary polymers, determined using the ex vivo microparticle method. Each data point represents the mean of a series of five measurements on a single explant; error bars represent measurement uncertainty. Inset shows data for pectin and pullulan with semilogarithmic axes. (b and c) Mucus (b) thickness or (c) compression measurements determined using (purple) ex vivo microparticle method or (grey) FC oil method, for explants from SPF or GF mice. Last bar in (b) shows measurements for washed GF explants. Data are presented as means ± SEM. We also found using our ex vivo method that SPF contents only compressed mucus on a GF explant by 5 ± 2% (n=1). (d) Schematic depicting how microbial degradation of polymers alters mucus compression.

Discussion

This work highlights the role of mucus as a dynamic biomaterial that responds to the polymeric composition of its environment. Our experiments reveal a previously unknown mechanism by which polymers in the gut—including dietary fibers abundant in our diet and therapeutic polymers ingested to relieve intestinal distress—alter the structure of the colonic mucus hydrogel. We speculate that this phenomenon may play a role in studies involving dietary fibers or therapeutic polymers, or their metabolism by microbes, in the gut. This could potentially have considerable physiological consequences—e.g. altering the access of pathogens or endotoxins to the epithelium. Investigating these effects will be a valuable direction for future work.

The work presented here focused on mucus compression induced by PEG, an uncharged polymer that has minimal chemical interactions with biomolecules and is often used as a therapeutic in the gut. We also observed similar behavior for several dietary polymers, suggesting that exploring a wider range of gut polymers will be a useful direction for future experiments. Polymers are also commonly used for the fundamental characterization of mucus itself, with the assumption that they do not alter the hydrogel structure. For example, a polymer solution (e.g. “OCT” compound) is frequently used in cryosection experiments that seek to preserve mucus structure e.g. (33–36). The polymer-induced compression that we describe in this paper may impact such experiments; indeed, in preliminary experiments, we have found that OCT compound actually alters mucus structure considerably. Our work thus highlights the importance of understanding polymer-mucus interactions, and their resultant biological effects, in experimental design and interpretation.

Our data show that the extent of compression is strongly dependent on polymer concentration and molecular weight; this behavior is remarkably similar to the compression of synthetic hydrogels, which is known to arise from a combination of enthalpic and entropic effects. The role played by these different effects remains to be elucidated, even for the case of simple synthetic hydrogels. However, our data suggest that, similar to the

synthetic case, polymer-induced compression of mucus—a complex biological hydrogel—can be described using Flory-Huggins theory. Our results thus motivate further work studying the physics underlying hydrogel compression, and the theoretical description presented here provides a basis for more sophisticated biophysical modeling that could incorporate effects such as non-isotropic structure of the mucus network (37), viscoelastic relaxation of the mucus hydrogel, or electrostatic interactions (further outlined in SI Materials and Methods). This could lead to new strategies for designing polymer-based therapeutics to controllably and predictably alter the morphology of gut mucus. Moreover, this work provides a general biophysical framework for investigating similar, previously overlooked, polymer-induced effects in other biological hydrogels, such as airway mucus, cervico-vaginal mucus, or extracellular matrix in tissues.

Materials and Methods

Details of animals used. Except where otherwise noted, all mice were male or female specific pathogen free (SPF) or germ-free (GF) C57BL/6 mice between 2-6 months of age, fed a standard solid chow diet and given water ad libitum. The mice given only sucrose or only sucrose + PEG were first raised on a standard solid chow diet and given water ad libitum, then maintained on a restricted diet consisting only of 5% w/v sucrose or 5% w/v sucrose + 7% w/v PEG 200k in 1x phosphate buffered saline (PBS, pH 7.4, without calcium and magnesium, Corning, Corning, NY, USA) given ad libitum for the 24 h period preceding euthanasia. All animal experiments were approved by the Caltech IACUC.

Details of microscopy

All imaging was performed using a Zeiss LSM 510 upright confocal microscope, or a Zeiss LSM 880 upright confocal microscope, using either brightfield microscopy, confocal fluorescence microscopy (543 nm excitation / 560 nm long-pass filter, or 488 nm excitation / 505 nm long-pass filter), confocal reflectance microscopy (514 nm excitation / 505 nm long-pass filter), or two-photon microscopy (800 nm excitation / 650 nm long-pass filter). We collected 3D stacks consisting of multiple xy slices at different z positions.

Imaging of unwashed tissue

We euthanized each mouse, removed the colon and immediately flushed it gently with Fluorinert FC 40 oil (3M, St. Paul, MN, USA), which is immiscible with the aqueous contents of the colon. We then immediately cut the colon segment open along the longitudinal axis, and mounted the opened tissue (luminal surface facing upward) onto a glass slide or a Petri dish using GLUture topical tissue adhesive (Abbott, Abbott Park, IL, USA). We then gently deposited ~0.5-2 mL of additional FC 40 oil onto the exposed luminal surface. The FC 40 is immiscible with water and with the mucus hydrogel; this procedure thus retained the adherent mucus in its in vivo "unwashed" state and prevented it from dehydrating.

Imaging of washed tissue

We euthanized each mouse, removed the colon and immediately flushed it gently with ice-cold 1x PBS, and placed ~1 cm long segments of the mid-colon in ice-cold PBS. We then cut and mounted the colon segments as described for unwashed tissues, always ensuring the explant surface was covered in PBS to prevent any dehydration. We then gently deposited the test solution onto the explant.

Thickness measurements of washed mucus hydrogel

In each experiment, after placing a suspension of 1 μm diameter microparticles onto the exposed luminal surface, we incubated the tissue at 4 ºC for 1-2 h. We simultaneously imaged both the epithelium and the deposited microparticles using confocal or two-photon reflectance microscopy, and determined the mucus thickness by measuring the distance between the epithelial surface and the deposited microparticles.

Quantifying polymer-induced compression of washed mucus hydrogel

After measuring the initial washed mucus thickness, we gently deposited ~ 0.2-2mL of the test polymer solution onto the exposed luminal surface, then collected the same 3D stacks

at the same xy fields of view, and re-measured the distance between the epithelial surface and the deposited microparticles.

Flory-Huggins model of compression

We used the Flory-Huggins theory of polymer solutions to describe polymer interactions with the mucus hydrogel, treating the mucus as a cross-linked hydrogel swollen in a good solvent. First, we calculated the total free energy of the ternary solvent-mucus-polymer system, G, given by the sum of the elastic free energy, G_{el}, which accounts for deformations of the individual mucus network strands, and the free energy of mixing the polymer and the solvent with the mucus hydrogel, G_m. The total change in free energy is then $\Delta G = \Delta G_m + \Delta G_{el}$ where ΔG_m is given by the Flory-Huggins (30, 38, 39) free energy of mixing and ΔG_{el} is given by rubber elasticity. At equilibrium, the chemical potentials of both the solvent and the free polymer, $\mu_S \equiv \partial G/\partial n_S$ and $\mu_P \equiv \partial G/\partial n_P$, must be equal inside and outside of the mucus network; these equalities provided Eqs. 3.1-4 shown in the main text, which represent the central result of the Flory-Huggins model and have been successfully used to describe polymer-induced compression of synthetic hydrogels (30).

Experiments using liquid fraction of colonic contents. Immediately after euthanizing a mouse, we collected its colonic contents in a polypropylene spin column with a 30 μm pore size filter (Thermo Scientific Pierce, Waltham, MA, USA), always kept on ice, and centrifuged at 17,000g for 100 min at 4 ºC. We then collected the liquid supernatant from the collection tube. For each of the experiments shown in Fig. 4c, we incubated a washed explant with 1 μm microparticles and used two-photon microscopy to first measure the initial, washed mucus thickness. We then gently deposited 100 μL of the liquid fraction of colonic contents on the exposed luminal explant surface, and re-imaged to measure the change in mucus thickness.

Acknowledgments

This work was supported in part by DARPA Biological Robustness in Complex Settings (BRICS) contract HR0011-15-C-0093, the National Science Foundation's Emerging Frontiers in Research and Innovation Award under Grant No. 1137089 and NSF Graduate Research Fellowship DGE-1144469 (to A.P.S.). We acknowledge Said Bogatyrev, Andres Collazo, Elaine Hsiao, Julia Kornfield, Octavio Mondragon-Palomino, Ahmad Omar, Alexandre Persat, David Tirrell, Zhen-Gang Wang, and David Weitz for useful discussions; the Beckman Institute Biological Imaging Facility, the Broad Animal Facility, and the Church Animal Facility for experimental resources; the veterinary technicians at the California Institute of Technology for experimental assistance; Jennifer R. Keeffe for assistance with DLS measurements; Dorothy Pan for assistance with GPC measurements; and Natasha Shelby for contributions to writing and editing this manuscript.

References

1. Macfarlane S, Macfarlane GT, Cummings JH (2006) Review article: prebiotics in the gastrointestinal tract. Aliment Pharmacol Ther 24(5):701–714.

2. Hooper L V, Midtvedt T, Gordon JI (2002) How host-microbial interactions shape the nutrient environment of the mammalian intestine. Annu Rev Nutr 22:283–307.

3. DiPalma JA, DeRidder PH, Orlando RC, Kolts BE, Cleveland M V (2000) A randomized, placebo-controlled, multicenter study of the safety and efficacy of a new polyethylene glycol laxative. Am J Gastroenterol 95(2):446–450.

4. Dipalma JA, Brady CE (1989) Colon cleansing for diagnostic and surgical procedures: polyethylene glycol-electrolyte lavage solution. Am J Gastroenterol 84(9):1008–1016.

5. Wu L, et al. (2004) High-molecular-weight polyethylene glycol prevents lethal sepsis due to intestinal Pseudomonas aeruginosa. Gastroenterology 126(2):488–498.

6. Cone RA (2009) Barrier properties of mucus. Adv Drug Deliv Rev 61(2):75–85.

7. Atuma C, Strugala V, Allen A, Holm L (2001) The adherent gastrointestinal mucus gel layer: thickness and physical state in vivo. Am J Physiol Liver Physiol 280(5):G922–G929.

8. Johansson ME V, et al. (2008) The inner of the two Muc2 mucin-dependent mucus layers in colon is devoid of bacteria. Proc Natl Acad Sci U S A 105(39):15064–15069.

9. Khanvilkar K (2001) Drug transfer through mucus. Adv Drug Deliv Rev 48(2-3):173–193.

10. Johansson ME V, Larsson JMH, Hansson GC (2011) The two mucus layers of colon are organized by the MUC2 mucin, whereas the outer layer is a legislator of host-microbial interactions. Proc Natl Acad Sci U S A 108:4659–4665.

11. Johansson ME V, et al. (2014) Bacteria penetrate the normally impenetrable inner colon mucus layer in both murine colitis models and patients with ulcerative colitis. Gut 63(2):281–291.

12. Bergstrom KSB, et al. (2010) Muc2 protects against lethal infectious colitis by disassociating pathogenic and commensal bacteria from the colonic mucosa. PLoS Pathog 6(5). doi:10.1371/journal.ppat.1000902.

13. Olmsted SS, et al. (2001) Diffusion of macromolecules and virus-like particles in human cervical mucus. Biophys J 81(4):1930–1937.

14. Barcelo A, et al. (2000) Mucin secretion is modulated by luminal factors in the isolated vascularly perfused rat colon. Gut 46(2):218–224.

15. Brownlee IA, Havler ME, Dettmar PW, Adrian A, Pearson JP (2003) Colonic mucus: secretion and turnover in relation to dietary fibre intake. Proc Nutr Soc 62(1):245–249.

16. Shimotoyodome A, Meguro S, Hase T, Tokimitsu I, Sakata T (2001) Sulfated polysaccharides, but not cellulose, increase colonic mucus in rats with loperamide-induced constipation. Dig Dis Sci 46(7):1482–1489.

17. Lidell ME, Moncada DM, Chadee K, Hansson GC (2006) Entamoeba histolytica cysteine proteases cleave the MUC2 mucin in its C-terminal domain and dissolve the protective colonic mucus gel. Proc Natl Acad Sci U S A 103(24):9298–303.

18. Lai SK, Wang YY, Cone R, Wirtz D, Hanes J (2009) Altering mucus rheology to "solidify" human mucus at the nanoscale. PLoS One 4(1):6.

19. Johansson ME V, et al. (2010) Bacteria penetrate the inner mucus layer before inflammation in the dextran sulfate colitis model. PLoS One 5(8). doi:10.1371/journal.pone.0012238.

20. Johansson MEV, et al. (2015) Normalization of Host Intestinal Mucus Layers Requires Long-Term Microbial Colonization. Cell Host Microbe:1–11.

21. Valentine MT, et al. (2004) Colloid surface chemistry critically affects multiple particle tracking measurements of biomaterials. Biophys J 86(6):4004–4014.

22. Jakobsson HE, et al. (2015) The composition of the gut microbiota shapes the colon mucus barrier. EMBO Rep 16(2):164–177.

23. Gustafsson JK, et al. (2012) An ex vivo method for studying mucus formation, properties, and thickness in human colonic biopsies and mouse small and large intestinal explants. Am J Physiol Gastrointest Liver Physiol 302(4):G430–8.

24. Matsui H, et al. (2006) A physical linkage between cystic fibrosis airway surface dehydration and Pseudomonas aeruginosa biofilms. Proc Natl Acad Sci U S A 103(48):18131–18136.

25. Lai SK, et al. (2007) Rapid transport of large polymeric nanoparticles in fresh undiluted human mucus. Proc Natl Acad Sci U S A 104(5):1482–1487.

26. Boyer RF (1945) Deswelling of gels by high polymer solutions. J Chem Phys 13(9):363–372.

27. Button B, et al. (2012) A periciliary brush promotes the lung health by separating the mucus layer from airway epithelia. Science 337(6097):937–941.

28. Brochard F (1981) Polymer networks swollen by a homopolymer solution. J Phys 42(3):505–511.

29. Vasilevskaya V V, Khokhlov AR (1992) Swelling and collapse of polymer gel in polymer solutions and melts. Macromolecules 25(1):384–390.

30. Kayaman N, Okay O, Baysal B (1997) Phase transition of polyacrylamide gels in PEG solutions. Polym Gels Networks 5:167–184.

31. Saunders BR, Crowther HM, Vincent B (1997) Poly[(methyl methacrylate)- co -(methacrylic acid)] microgel particles: swelling control using pH, cononsolvency, and osmotic deswelling. Macromolecules 30(3):482–487.

32. Li H, et al. (2015) The outer mucus layer hosts a distinct intestinal microbial niche. Nat Commun 6:8292.

33. Kobayashi K, Ogata H, Morikawa M, Iijima S, Harada N, Yoshida T, Brown WR, Inoue N, Hamada Y, Ishii H, Watanabe M HT (2002) Distribution and partial characterisation of IgG Fc. Gut 51:169–177.

34. Zindl CL, et al. (2013) IL-22-producing neutrophils contribute to antimicrobial defense and restitution of colonic epithelial integrity during colitis. Proc Natl Acad Sci U S A 110(31):12768–73.

35. Heazlewood CK, et al. (2008) Aberrant mucin assembly in mice causes endoplasmic reticulum stress and spontaneous inflammation resembling ulcerative colitis. PLoS Med 5(3):0440–0460.

36. Engevik M a., et al. (2015) Human Clostridium difficile infection: altered mucus production and composition. Am J Physiol - Gastrointest Liver Physiol 308(6):G510–G524.

37. Ambort D, et al. (2012) Calcium and pH-dependent packing and release of the gel-forming MUC2 mucin. Proc Natl Acad Sci 109(15):5645–5650.

38. Flory PJ (1953) Principles of Polymer Chemistry (Cornell University Press, Ithaca, New York).

39. Rubinstein M, Colby RH (2003) Polymer Physics (OUP Oxford, New York).

40. Wang Y-Y, et al. (2008) Addressing the PEG Mucoadhesivity Paradox to Engineer Nanoparticles that “Slip” through the Human Mucus Barrier. Angew Chemie-International Ed 47(50):9726–9729.

41. Lotfy S (2009) Controlling degradation of low-molecular-weight natural polymer “dextrin” using gamma irradiation. Int J Biol Macromol 44(1):57–63.

42. White DR, Hudson P, Adamson JT (2003) Dextrin characterization by high-performance anion-exchange chromatography--pulsed amperometric detection and size-exclusion chromatography--multi-angle light scattering--refractive index detection. J Chromatogr A 997(1-2):79–85.

43. Pal S, Nasim T, Patra A, Ghosh S, Panda AB (2010) Microwave assisted synthesis of polyacrylamide grafted dextrin (Dxt-g-PAM): Development and application of a novel polymeric flocculant. Int J Biol Macromol 47(5):623–631.

44. Sun J, Zhao R, Zeng J, Li G, Li X (2010) Characterization of destrins with different dextrose equivalents. Molecules 15(8):5162–5173.

45. Kim JH, Kim MR, Lee JH, Lee JW, Kim SK (2000) Production of high molecular weight pullulan by Aureobasidium pullulans using glucosamine. Biotechnol Lett 22(12):987–990.

46. Buliga GS, Brant DA (1987) Temperature and molecular weight dependence of the unperturbed dimensions of aqueous pullulan. Int J Biol Macromol 9(2):71–76.

47. Kato T, Katsuki T, Takahashi A (1984) Static and dynamic solution properties of pullulan in a dilute solution. Macromolecules 17(1):1726–1730.

48. Lazaridou A, Roukas T, Biliaderis CG, Vaikousi H (2002) Characterization of pullulan produced from beet molasses by Aureobasidium pullulans in a stirred tank reactor under varying agitation. Enzyme Microb Technol 31(1-2):122–132.

49. Wiley BJ, et al. (1993) Control of molecular weight distribution of the biopolymer pullulan produced by Aureobasidium pullulans. J Environ Polym Degrad 1(1):3–9.

50. Stephen AM, Phillips GO (2006) Food Polysaccharides and their Applications (CRC Press, Boca Raton).

51. Kawaguchi S, et al. (1997) Aqueous solution properties of oligo- and poly(ethylene oxide) by static light scattering and intrinsic viscosity. Polymer (Guildf) 38(12):2885–2891.

52. Raynal BDE, Hardingham TE, Sheehan JK, Thornton DJ (2003) Calcium-dependent protein interactions in MUC5B provide reversible cross-links in salivary mucus. J Biol Chem 278(31):28703–28710.

53. Maisel K, et al. (2015) Enema ion compositions for enhancing colorectal drug delivery. J Control Release 209:280–287.

54. Mestecky J, et al. (2005) Mucosal Immunology (Elsevier Science, San Diego).

55. Verdugo P (2012) Supramolecular dynamics of mucus. Cold Spring Harb Perspect Med 2(11). doi:10.1101/cshperspect.a009597.

56. Ambort D, Johansson ME V, Gustafsson JK, Ermund A, Hansson GC (2012) Perspectives on mucus properties and formation- lessons from the biochemical world. Cold Spring Harb Perspect Med 2(11). doi:10.1101/cshperspect.a014159.

57. Sellers L a., Allen A, Morris ER, Ross-Murphy SB (1991) The rheology of pig small intestinal and colonic mucus: weakening of gel structure by non-mucin components. BBA - Gen Subj 1115(2):174–179.

58. Rubinstein M, Colby RH, Dobrynin A V. (1994) Dynamics of semidilute polyelectrolyte solutions. Phys Rev Lett 73(20):2776–2779.

59. Lieleg O, Vladescu I, Ribbeck K (2010) Characterization of particle translocation through mucin hydrogels. Biophys J 98(9):1782–1789.

60. Li H (2010) Smart Hydrogel Modelling (Springer-Verlag Berlin Heidelberg, New York).

61. Sing CE, Zwanikken JW, de la Cruz MO (2013) Effect of ion-ion correlations on polyelectrolyte gel collapse and reentrant swelling. Macromolecules 46(12):5053–5065.

62. Philippova OE, Rumyantsev AM, Kramarenko EY, Khokhlov AR (2013) New type of swelling behavior upon gel ionization: Theory vs experiment. Macromolecules 46(23):9359–9367.

63. Dobrynin A V., Rubinstein M (2005) Theory of polyelectrolytes in solutions and at surfaces. Prog Polym Sci 30(11):1049–1118.

64. Perez-Vilar J (2007) Mucin granule intraluminal organization. Am J Respir Cell Mol Biol 36(2):183–190.

65. Lai SK, Wang Y-Y, Wirtz D, Hanes J (2009) Micro- and macrorheology of mucus. Adv Drug Deliv Rev 61(2):86–100.

66. Georgiades P, Pudney PD, Thornton DJ, Waigh TA (2014) Particle tracking microrheology of purified gastrointestinal mucins. Biopolymers 101(4):366–377.

67. Cai L-H (2012) Structure and Function of Airway Surface Layer of the Human Lungs and Mobility of Probe Particles in Complex Fluids. Dissertation (University of North Carolina, Chapel Hill).

68. Szycher M (1991) High Performance Biomaterials: A Complete Guide to Medical and Pharmaceutical Applications (Taylor & Francis, Lancaster).

69. Lentle RG, Janssen PWM (2011) Mucins. The Physical Processes of Digestion (Springer Science & Buisness Media, 2011).

70. Sobota JA, Ferraro F, Back N, Eipper BA, Mains RE (2006) Not all secretory granules are created equal: partitioning of soluble content proteins. Mol Biol Cell 17:5038–5052.

71. Quillin ML, Matthews BW (2000) Accurate calculation of the density of proteins. Acta Crystallogr Sect D Biol Crystallogr 56(7):791–794.

72. Shogren R, Gerken TA, Jentoft N (1989) Role of glycosylation on the conformation and chain dimensions of O-linked glycoproteins: light-scattering studies of ovine submaxillary mucin. Biochemistry 28(13):5525–5536.

73. Aksoy N, Sheehan J (2002) Determination of polydispersity of a human colonic mucus glycoprotein using rate-zonal centrifugation and laser light-scattering. Turk J Med Sci 32:373–378.

74. Mikkelsen A, Stokke BT, Christensen BE, Elgsaeter A (1985) Flexibility and length of human bronchial mucin studied using low-shear viscometry, birefringence relaxation analysis, and electron microscopy. Biopolymers 24(9):1683–1704.

75. Jentoft N (1990) Why are proteins O-glycosylated? Trends Biochem Sci 15(8):291–294.

76. Bansil R, Stanley HE, Lamont JT (1995) Mucin biophysics. Annu Rev Physiol 57:635–657.

77. Sheehan JK, et al. (2000) Physical characterization of the MUC5AC mucin: a highly oligomeric glycoprotein whether isolated from cell culture or in vivo from respiratory mucous secretions. Biochem J 347:37–44.

78. Prasitnok K, Wilson MR (2013) A coarse-grained model for polyethylene glycol in bulk water and at a water/air interface. Phys Chem Chem Phys 15(40):17093–17104.

79. Fischer J, Paschek D, Geiger A, Sadowski G (2008) Modeling of aqueous poly (oxyethylene) solutions . 2 . Mesoscale simulations. J Phys Chem B:13561–13571.

80. Selser C, et al. (1991) Asymptotic behavior and long-range interactions in aqueous solutions of poly(ethylene oxide). Macromolecules 24:5943–5947.

81. Ziębacz N, Wieczorek SA, Kalwarczyk T, Fiałkowski M, Hołyst R (2011) Crossover regime for the diffusion of nanoparticles in polyethylene glycol solutions: influence of the depletion layer. Soft Matter 7(16):7181.

82. Kienberger F, et al. (2000) Static and dynamical properties of single poly (ethylene glycol) molecules investigated by force spectroscopy. Single Mol 1(2):123–128.

83. Poon WCK, Andelman D (2006) Soft Condensed Matter Physics in Molecular and Cell Biology (CRC Press, Boca Raton).

84. Waters DJ, et al. (2010) Morphology of photopolymerized end-linked poly (ethylene glycol) hydrogels by small-angle X-ray scattering. Macromolecules 43(16):6861–6870.

85. Dondi F, Guiochon G (2012) Theoretical Advancement in Chromatography and Related Separation Techniques (Springer Netherlands, Ferrara).

86. Tanford C (1961) Physical Chemistry of Macromolecules (Wiley, New York).

87. Mijnlieff PF, Wiegel FW (1978) Intrinsic viscosity and friction coefficient of polymer molecules in solution: Porous sphere model. J Polym Sci Polym Phys Ed 16(2):245–263.

88. Brandup J, Immergut E (1975) Polymer Handbook (John Wiley). 2nd Ed.

89. Momii T, Nose T (1989) Concentration-dependent collapse of polymer gels in solution of incompatible polymers. Macromolecules 22(3):1384–1389.

90. Ishidao T, Akagi M, Sugimoto H, Iwai Y, Arai Y (1993) Swelling behaviors of poly(N-isopropylacrylamide) gel in poly(ethylene glycol)-water mixtures. Macromolecules 26(26):7361–7362.

91. Ishidao T, et al. (1995) Swelling equilibria of poly(N-isopropylacrylamide) gel in glucose and starch aqueous solution. Fluid Phase Equilib 104:119–129.

92. Ito T, Yamazaki M, Ohnishi S (1989) Poly(ethylene glycol)-induced shrinkage of Sephadex gel. A model system for quantitative analysis of osmoelastic coupling. Biophys J 56(4):707–711.

93. Kiefer J, Naser M, Kamel A, Carnali J (1993) Osmotic deswelling of microgels by linear polyelectrolytes. Colloid Polym Sci 271(3):253–261.

94. Adachi H, Nishi S, Kotaka T (1982) Structure and Mechanical Properties of Sequential Interpenetrating Polymer Networks II. Complex-Forming Polyoxyethylene: Poly(acrylic acid) Systems. Polym J 14(12):985–992.

95. Nishi S, Kotaka T (1985) Complex-Forming Poly(oxyehtylene):Poly(acrylic acid) Interpenetrating Polymer Networks. 1. Preparation, Structure and Viscoelastic Properties. Macromolecules 18(8):1519–1525.

96. Chen H-L, Morawetz H (1982) Kinetics of Polymer Complex Interchange in Poly(acrylic acid)-Poly(oxyethylene) Solutions. Macromolecules 15:1445–1447.

97. Bednar B, Morawetz H, Shafer J (1984) Kinetics of the Cooperative Complex Formation and Dissociation of Poly(acrylic acid) and Poly(oxyethylene). Macromolecules 17:1634–1636.

98. Philippova OE, Karibyants NS, Starodubtzev SG (1994) Conformational Changes of Hydrogels of Poly(methacrylic acid) Induced by Interaction with Poly(ethylene glycol). Macromolecules 27(9):2398–2401.

99. Sonnenburg JL (2005) Glycan foraging in vivo by an intestine-adapted bacterial symbiont. Science (80-) 307(5717):1955–1959.

100. Loesche WJ (1969) Effect of bacterial contamination on cecal size and cecal contents of gnotobiotic rodents. J Bacteriol 99(2):520–526.

101. Høverstad T, Midtvedt T (1986) Short-chain fatty acids in germfree mice and rats. J Nutr 116(9):1772–1776.

102. Heneghan J (2012) Germfree Research: Biological Effect of Gnotobiotic Environments (Elsevier Science, New York).

103. Spiro RG (1970) Glycoproteins. Annu Rev Biochem 39(1):599–638.

Supporting Information

Details of animals used

Except where otherwise noted, all mice were male or female specific pathogen free (SPF) or germ-free (GF) C57BL/6 mice between 2-6 months of age, fed a standard solid chow diet and given water ad libitum. The GF chow was autoclaved and was formulated to have similar nutritional profile after autoclaving as the SPF chow. The mice given only sucrose or only sucrose + PEG were first raised on a standard solid chow diet and given water ad libitum, then maintained on a restricted diet consisting only of 5% sucrose or 5% sucrose + 7% PEG 200k in 1x phosphate buffered saline (PBS, pH 7.4, without calcium and magnesium, Corning, Corning, NY, USA) given *ad libitum* for the 24 h period preceding euthanasia. Four hours after we started administering each of the restricted liquid diets, we moved each test mouse to a new, clean cage to minimize the effects of coprophagy.

Details of microscopy

All imaging was performed using a Zeiss LSM 510 upright confocal microscope, or a Zeiss LSM 880 upright confocal microscope, using either brightfield microscopy, confocal fluorescence microscopy (543 nm excitation / 560 nm long-pass filter, or 488 nm excitation / 505 nm long-pass filter), confocal reflectance microscopy (514 nm excitation / 505 nm long-pass filter or 505-735 nm detection), or two-photon microscopy (800 nm excitation / 650 nm long-pass filter). We collected 3D stacks consisting of multiple xy slices at different z positions.

Imaging of unwashed tissue

We euthanized each mouse, removed the colon and immediately flushed it gently with Fluorinert FC 40 oil (3M, St. Paul, MN, USA), which is immiscible with the aqueous contents of the colon. We then immediately cut the colon segment open along the longitudinal axis, and mounted the opened tissue (luminal surface facing upward) onto a glass slide or a Petri dish using GLUture topical tissue adhesive (Abbott, Abbott Park, IL,

USA). We then gently deposited ~0.5-2 mL of additional FC 40 oil onto the exposed luminal surface. The FC 40 is immiscible with water and with the mucus hydrogel; this procedure thus retained the adherent mucus in its in vivo "unwashed" state and prevented it from dehydrating. We imaged the explant with two-photon microscopy. For some mice, we took multiple explant samples, and for some explant samples we collected multiple 3D stacks at different fields of view.

We determined the mean mucus thickness (grey bars in Figures 3.1 and 3.4) for each stack obtained from an explant by measuring the distance between the epithelial surface (Figure 3.S1a-b) and the FC oil-hydrogel interface at five random positions in xy. In some cases this was repeated for multiple fields of view. When multiple colonic explants were obtained from a single mouse, we calculated the mean mucus thickness of an individual mouse. In Figures 3.1 and 3.4, the thickness values reported are the mean values of the individual mice thicknesses. The error bar on each value reported in Figures 3.1 and 3.4 is the standard error of the mean (SEM), calculated by taking the standard deviation of mucus thickness for a single mouse and dividing by $\sqrt{n}$ (n, number of different mice).

Imaging of washed tissue

We euthanized each mouse, removed the colon and immediately flushed it gently with ice-cold 1x PBS, and placed ~1 cm long segments of the mid-colon in ice-cold PBS, ensuring that the ionic composition was homogenized throughout the mucus hydrogel environment. We then cut and mounted the colon segments as described for unwashed tissues, always ensuring the explant surface was covered in PBS to prevent any dehydration or ionic imbalance, and surrounding (but not contacting) the tissue with >10 ~10 μL drops of water to maintain a humid environment. The measured mucus hydrogel thickness was consistent with the distance measured when we imaged using FC oil and consistent with other reported measurements (8), did not change appreciably over an observation time of 2.5 h, and was similar for probes of other sizes (250 nm in diameter or larger) as discussed in the main text, further confirming the validity of our approach. We then gently deposited an additional ~10-200 μL drop of test solution containing the fluorescent probes onto the

explant. We imaged the explant with confocal reflectance or two-photon microscopy. For some mice, we took multiple explant samples and for some explant samples, we collected multiple 3D stacks at different fields of view. The levels of the images in Figure 3.2a were non-linearly adjusted in Adobe Illustrator for clarity in print using the following input and output levels: 82, 1, 246 / 0, 255 (bright field), 34, 0.78, 172 / 0, 205 (confocal reflectance), 51, 0.91, 140 / 0, 255 (two-photon).

Thickness measurements of washed mucus hydrogel

In each experiment, after placing a suspension of 1 μm diameter microparticles onto the exposed luminal surface, we incubated the tissue at 4 ºC for 1-2 h, longer than the time required for the microparticles to diffuse across the vertical extent of the mucus in free solution (40 min). This ensured that the microparticles deposited onto the mucus hydrogel surface. We simultaneously imaged both the epithelium and the deposited microparticles using brightfield, confocal reflectance, or two-photon reflectance microscopy.

To determine the mean mucus thickness for tissue obtained from a single mouse (green, light blue, dark blue and pink points in the bottom graph of Figure 3.2d), for each stack on a washed explant, we measured the distance between the epithelial surface and the center of the deposited microparticles at five random positions in xy spanning the entire field of view. In some cases this process was repeated for multiple fields of view. If multiple colonic explants were obtained from the same mouse, the thickness was measured in the same way. We then took each of these individual thickness measurements at each xy position from all the individual mice, explants and fields of view and calculated the mean and standard deviation. The thickness values reported in Figure 3.2d are these mean values, and the error bars are the associated standard deviation. The washed values and error bars reported Figure 3.4 (purple bars), were determined as described in the section of the Methods: “Imaging of unwashed tissue.”

Experiments with probes of different sizes. We used (all in 1x PBS): Methoxyl polyethylene glycol-FITC (mPEG-FITC, Nanocs, Boston, MA, USA), weight averaged

molecular weight 350, 1.2 x 10-2 mg/mL; mPEG-FITC (Nanocs), weight averaged molecular weight 5 kDa, 3.3 x 10-2 mg/mL; mPEG-FITC (Nanocs), weight averaged molecular weight 200 kDa, 0.6 mg/mL; FITC–dextran (Sigma-Aldrich, St. Louis, MO, USA), average molecular weight 2 MDa, 0.1 mg/mL; Fluorescent polystyrene microparticles (micromer, from micromod GmbH, Rostock, Germany), coated with PEG 300 to render them chemically inert (40), 0.02-0.2% volume fraction of manufacturer-reported average diameters 100 nm, 250 nm, 500 nm, 1 μm, or 5 μm. Penetration measurements used fluorescently labeled polymers at concentrations below those that cause mucus compression.

We characterized probes or polymers 500 nm or smaller using dynamic light scattering performed on 200-500 μL of each sample with a Wyatt Dynapro NanoStar instrument. The data were collected and analyzed using Wyatt DYNAMICS software 7.1. Hydrodynamic radii were determined by fitting the data using a regularization analysis. The wavelength of the laser was 658 nm and the scattering angle was 90º. The microparticle solutions were unfiltered, while we filtered the polymer solutions using either a 0.2 μm Fisherbrand (PEG 400, PEG 6 kDa, PEG 200 kDa, fluorescent PEG 200 kDa, fluorescent dextran 2 MDa, fluorescent PEG 5 kDa) or a 0.45 μm Puradisc (pullulan, dextrin) syringe filter. All samples were dispersed in 1x PBS, and we used the following concentrations or volume fractions: 3 mg/mL (fluorescent PEG 200 kDa), 1 mg/mL (fluorescent dextran 2 MDa), 0.1% v/v (100 nm particles), 0.01% v/v (250 nm particles), 0.02% v/v (500 nm particles), 100 mg/mL (PEG 400), 10 mg/mL (PEG 6 kDa), 0.5 mg/mL (PEG 200 kDa), 10 mg/mL (pullulan), 10 mg/mL (dextrin), 0.25 mg/mL (fluorescent PEG 5 kDa). The acquisition time was 5 s, and 10-20 acquisitions were taken for each sample. We characterized the 1 μm and 5 μm microparticles using optical microscopy.

Polymers used for compression measurements. We used (all in 1x PBS): PEG 400, weight-averaged molecular weight 380-420 Da (Acros Organics, Pittsburgh, PA, USA); PEG 6k, weight-averaged molecular weight 5.6-6.6 kDa (Acros Organics); PEG 200k, viscosity-averaged molecular weight 200 kDa (Sigma-Aldrich); Dextrin, average molecular weight

between ~1-70 kDa (41–44) (Walgreens, Deerfield, IL, USA); Pullulan from Aureobasidium pullulans, average molecular weight between ~50 kDa – 4 MDa (45–49) (Sigma-Aldrich); Pectin from apple, weight averaged molecular weight ~100 kDa (50) (Sigma-Aldrich). We estimated the average radius of gyration, Rg,p, of the PEG 400, 6k, and 200k as ≈ 0.7 nm, 3 nm, and 22 nm, respectively, using published measurements (51) and our own dynamic light scattering measurements.

Quantifying polymer-induced compression of washed mucus hydrogel

After measuring the initial washed mucus thickness, we gently deposited ~ 0.2-2mL of the test polymer solution onto the exposed luminal surface and then collected the same 3D stacks at the same xy fields of view. To measure the "percent compression", or the overall percentage change in the thickness, of the colonic mucus after exposure to the polymer solution, we measured the thickness before and after exposure to the solution at the same five xy positions, using the distance between the epithelial surface and the deposited microparticles in the 3D stacks. To calculate the percentage compression, we calculated the percentage change in the thickness measured, as well as the measurement uncertainty (using the optical slice thickness as the experimental uncertainty in the measured thickness), at each of these five xy positions. We then calculated the percentage compression as the mean of these five measured values. The error bars show the uncertainty in the percentage compression measurement, which was calculated using the experimental uncertainty in each of the five strain measurements.

To explore the generality of the observed compression, we tested a number of different conditions, and found similar behavior (as shown in Figure 3.3b) for mice of different genders and strains, for washed explants originating from germ-free or microbe-colonized mice, for different buffers (PBS or HEPES), for buffers also containing protease inhibitor, for polymer solutions prepared using the liquid fraction of SPF mice colonic contents instead of buffer, for experiments performed at 22ºC or 37ºC, for a similar, but charged, polymer, and in the presence and the absence of Mg^{2+} ions. We note that other multivalent cations (e.g. Ca^{2+}) have been found to induce additional structural changes in mucins,

although no measurable changes were reported for Mg^{2+} (52). We also note that, in vivo, water may be absorbed from the lumen into the epithelium depending on the delivery medium e.g. as reported in (53). We speculate that this could concentrate the polymer in the lumen, possibly enhancing the mucus compression we measured ex vivo.

Flory-Huggins model of compression

We used the Flory-Huggins theory of polymer solutions to describe polymer interactions with the mucus hydrogel. The adherent mucus is a hydrogel with a network (10, 37, 54) comprised of MUC2 proteins having alternating hydrophilic, densely-glycosylated regions, which make up the strands of the hydrogel network, and hydrophobic, non-glycosylated regions, which help to cross-link the network, which is also cross-linked via physical entanglements, electrostatic interactions, and chemical cross-links such as disulfide bonds (55, 56). We therefore modeled the mucus as a cross-linked hydrogel swollen in a good solvent. For simplicity, we treated this hydrogel as being structurally isotropic; our model does not incorporate any possible supramolecular structuring of the colonic mucus hydrogel (37). We made the simplifying assumption that the mucus behaves as an elastic gel; while hydrogels, including colonic mucus, are known to be viscoelastic—they relax stresses over long times—the reversibility of the observed polymer-induced compression, and the observed unchanging thickness of the hydrogel after compression, suggest that the colonic mucus is elastic on the timescale of our experiments. This idea is supported by rheological measurements on a scraped porcine colonic mucus hydrogel, which exhibits elastic behavior for timescales of at least ~100 s (57). Moreover, this assumption has been successfully used to describe the compression of synthetic hydrogels that also contain chemical cross-links (30, 31). However, we note that the exact details of mucus hydrogel rheology remain unknown; we therefore chose to describe the mucus hydrogel as "viscoelastic" in the text for the sake of generality, thereby including any possible elastic or viscous response. Incorporating further details of mucus hydrogel rheology into our theoretical model, such as any possible viscous relaxation at long timescales and the

relative importance of the different forms of cross-linking in the network, will be an important direction for future work.

First, we calculated the total free energy of the ternary solvent-mucus-polymer system, G, given by the sum of the elastic free energy, G_{el} —which accounts for deformations of the individual mucus network strands, thus inhibiting the unphysical case of full mixing of the mucins and solvent—and the free energy of mixing the polymer and the solvent with the mucus hydrogel, G_m. The buffered aqueous solutions are characterized by a high ionic concentration (ionic strength ≈ 170 mM) and therefore a Debye screening length ≈ 0.7 nm, over two orders of magnitude smaller than the hydrogel mesh size, suggesting that electrostatic interactions may not play a significant role in our system. Indeed, theoretical predictions for charged semidilute polymer solutions reduce to those for uncharged semidilute polymer solutions when the solvent has a high ionic concentration such as ours e.g. (58). This idea is also supported by experimental measurements of charged particle diffusion in a mucus hydrogel, which show results similar to the case of uncharged particles at high ionic concentrations similar to ours (59). We therefore did not consider electrostatic effects (58, 60–63) in our work; considering these effects will be an interesting direction for future work.

The total change in free energy can thus be written as

$$\Delta G = \Delta G_m + \Delta G_{el}$$

(Eq. 3.5)

and ΔG_m is given by the Flory-Huggins (30, 38, 39) free energy of mixing,

$$\Delta G_m = RT\left(\sum_i n_i ln\nu_i + \sum_{i<j} n_i \nu_j \chi_{ij}\right)$$

(Eq. 3.6)

where R is the gas constant, T is the temperature, n_i is the number of moles of species i, ν_i is the volume fraction of species i, and χ_{ij} is the Flory-Huggins interaction parameter between species i and j; here, we denote solvent, mucus and free polymers as $i = S, M, P$, respectively. To describe the free energy of elastic deformation we used rubber elasticity, assuming affine deformation of the network (30, 38):

$$\Delta G_{el} = \frac{3}{2}\frac{RT}{N_M V_S}\left[\left(\frac{\nu_M^0}{\nu_M}\right)^{\frac{2}{3}} - 1 - ln\left(\frac{\nu_M^0}{\nu_M}\right)^{\frac{1}{3}}\right]$$

(Eq. 3.7)

where ν_M is the mucus hydrogel volume fraction, ν_M^0 is the mucus hydrogel volume fraction in its initial preparation state, V_S is the molar volume of the solvent, and N_M is the average number of mucin Kuhn segments, the stiff segments making up each mucin network strand, between cross-links of the network. More sophisticated forms of the elastic free energy would be interesting to explore in future work; we note that the exact choice of the elastic energy may not impact the calculated hydrogel compression trends considerably (29, 30).

At equilibrium, the chemical potentials of both the solvent and the free polymer, $\mu_S \equiv \partial G/\partial n_S$ and $\mu_P \equiv \partial G/\partial n_P$, must be equal inside and outside of the mucus network:

$$\mu_S^{in} = \mu_S^{out}$$

(Eq. 3.8)

$$\mu_P^{in} = \mu_P^{out}$$

(Eq. 3.9)

By substituting equations 3.6 and 3.7 into equation 3.5, and differentiating with respect to the number moles of solvent and free polymer, we obtained Eqs. 3.1-4 shown in the main

text, which represent the central result of the Flory-Huggins model and have been successfully used to describe polymer-induced compression of synthetic hydrogels (30). These equations are also subject to the constraints $\nu_S^{in} + \nu_M + \nu_P^{in} = 1$ and $\nu_S^{out} + \varphi = 1$.

We first treated the polymer-free case ($\phi = 0$), which describes the initial swollen state of the mucus hydrogel. The system is described by Eq. 1 with $\mu_S^{in} = \mu_S^{out} = 0$ and $\nu_P^{in} = 0$; this provided us with a relationship between ν_M^0 , χ_{SM}, N_M, and the mucus volume fraction in this initial swollen state, which we denote as ν_M^s . Direct measurements of ν_M^s are lacking; we chose a value of $\nu_M^s = 0.01$, well within in the range of estimates (64–68) of the volume fraction of swollen mucus, and tested the sensitivity of our results to variations in the numerical parameters used, with the constraint relating ν_M^0 , χ_{SM}, N_M, and ν_M^s (Figure 3.S9). As a simplifying assumption, we took ν_M^0 to be approximately equal to the mucin volume fraction when initially packed in secretory granules, before being released into the intestinal lumen to form the swollen, cross-linked adherent hydrogel. We found in our sensitivity analysis (Figure 3.S9) that our results are only weakly sensitive to the choice of the value of ν_M^0. We therefore chose a value $\nu_M^0 = 0.13$, within the range of published measurements (69–71) for mucin and other similar secretory granules. However, more work is required to quantitatively determine the exact value of ν_M^0. We expect water to be a good solvent for the mucin network strands, due to the preponderance of hydroxyl, carboxyl and sulfate groups in the glycosylated domains; we therefore chose $\chi_{SM} = 0$. We estimated N_M using published measurements in two different ways. In the first approach, we used measured values (64, 72–75) of the MUC2 radius of gyration,$R_{g,M}$, and Kuhn length, b_M, combined with the relationship for mucus strands swollen in a good solvent (39, 67, 76, 77), $R_{g,M} \approx b_M N_M^{3/5}$. In the second approach, we used our direct measurements of the mucus hydrogel mesh size, combined with the published measurements of b_M, to estimate N_M. In both cases, we found $N_M \approx 20 - 10{,}000$. The values of ν_M^0, χ_{SM}, and ν_M^s, together with Eq. 3.1, yielded $N_M \approx 1000$, in this estimated range; we therefore chose $N_M \approx 1000$. Again, we found qualitatively similar results for different values of N_M (Figure 3.S9).

We next investigated how added polymer ($\phi > 0$) changed the extent to which the mucus hydrogel is swollen, and therefore, its equilibrium thickness. We numerically solved Eqs. 3.8-9 for ν_M and ν_P^{in}, varying ϕ; this yielded the curves presented in Figure 3.3a. We focused on the case in which the added polymer is PEG 400, 6k, or 200k, as used in our experiments. We took the number of segments of each PEG, y, to be the number of PEG Kuhn segments, and estimated this (39) using the relationship $R_{g,P} \approx b_P y^{\alpha}$, where $R_{g,P}$ and b_P are the PEG radius of gyration and Kuhn length, respectively, choosing $\alpha = 0.58$, consistent with the measured range (39, 51, 78–81) $\alpha = 0.537 - 0.588$. Published measurements (82–84) yield $b_P \approx 0.76 - 1.8\,nm$; we therefore chose $b_P = 1.28\,nm$, in this range. We estimated $R_{g,P}$ using our measurements of the PEG 400, 6k, and 200k hydrodynamic radii, and converted these to radii of gyration using the Kirkwood-Riseman relationship (85–87). The relationship between $R_{g,P}$, b_P, and y thus yielded y = 1, 4, and 146 for PEG 400, 6k, and 200k, respectively, which we used for the main simulations (Fig. 3a). Based on published measurements for PEG (30, 88), we set $\chi_{SP} = 0.45$. The chemical interactions between PEG and mucins are thought to be slightly attractive or neutral. We therefore estimated χ_{MP} to be between 0 and 0.5, and chose $\chi_{MP} = 0.3$.

This Flory-Huggins framework has been successfully applied to qualitatively describe polymer-induced compression of a number of synthetic hydrogels (30, 31, 89–93). However, it is a simple mean-field theory, does not take into account correlations between monomers, and assumes affine deformation of a homogeneous gel. We therefore did not expect strong quantitative agreement between the experiments and numerical calculations. However, we observed similar behavior between the two, using parameters that are consistent with experimentally measured values. In particular, the Flory-Huggins calculations showed that the free polymer does induce compression of the network, even though in the calculations the polymer could penetrate into the mucus hydrogel, and the trends we observed experimentally are qualitatively similar to those predicted by the model. Moreover, we found that polymers of higher molecular weights required a lower monomer volume fraction to compress the network, consistent with our experimental observations. One reason for this is the entropic penalty paid by PEG to penetrate the

mucus; because this penalty is larger for larger polymers, they are more likely to be excluded from the mucus hydrogel, and therefore can compress it more by elevating the difference between external and internal osmotic pressure. Consistent with this expectation, we found that the higher molecular weight PEG was more likely to be excluded from the mucus hydrogel (Figure 3.S9e).

More sophisticated modeling could build on the work presented here by incorporating effects such as structuring of the colonic mucus hydrogel (37), viscoelastic relaxation of the mucus network, chemical adhesion (40) or electrostatic interactions, or polymer complex formation. For example, PEG has been observed to form complexes with polycarboxylic acids (30, 94–98), via hydrogen bonding between the ether oxygen of PEG and un-dissociated carboxylic groups; similar effects could play a role in our experimental system. We note, however, that at the physiological pH explored in our work, the carboxyl groups found on the sialic acid residues of mucins are negatively charged (54, 56) and complexation is unlikely (Figure 3.S7).

Experiments using liquid fraction of colonic contents. Immediately after euthanizing a mouse, we collected its colonic contents in a polypropylene spin column with a 30 μm pore size filter (Thermo Scientific Pierce, Waltham, MA, USA), always kept on ice, and centrifuged at 17,000g for 100 min at 4ºC. We then collected the liquid supernatant from the collection tube. We combined the liquid fraction thus obtained from multiple mice, both male and female, 3-4 months in age, to obtain enough sample for the experiments, and stored aliquots at -20 ºC until experimental use.

To test whether luminal contents could affect the polymer-induced mucus compression reported here, we used our ex vivo approach to also test compression induced by polymer solutions prepared in the thawed liquid fraction of SPF mice colonic contents instead of buffer. We tested both 3.1% w/v PEG 200k and 48.5% w/v dextrin, using the SPF liquid fraction as the solvent in both cases. In both cases, we verified that addition of the polymer to the SPF liquid fraction did not result in the formation of precipitates. In each case, we incubated a washed explant with 1 μm microparticles and used confocal reflectance

microscopy to first measure the initial, washed mucus thickness. We then gently deposited 65-75 μL of the test solution on the exposed luminal explant surface, and re-imaged to measure the change in mucus thickness. We found that the mucus hydrogel compressed by 55 ± 2% in the case of PEG 200k and 52 ± 2% in the case of dextrin, similar to the compressed measured for the same polymers in saline (as shown in Figures 3.3b and 3.4a). This result suggests that additional luminal contents do not mask the effect of polymers in the gut. Further investigations along these lines will be an interesting extension of our work.

For each of the experiments shown in Figure 3.4c, we incubated a washed explant with 1 μm microparticles and used two-photon microscopy to first measure the initial, washed mucus thickness. We then thawed the frozen liquid fraction of colonic contents, gently deposited 100 μL of it on the exposed luminal explant surface, and re-imaged to measure the change in mucus thickness. We then obtained successive 3D stacks to verify that the thickness did not change in time over a time period of ~10-30 minutes. We also collected multiple 3D stacks at different fields of view on the same tissue explant, and for different tissue explants obtained from multiple mice. The difference between the SPF and GF chromatograms in Figure 3.S10a-b suggested that, as expected (99–103), the GF contents were enriched in polymers of higher molecular weight compared to the SPF contents, and that these polymers were comparable in size to ~200-700kDa pullulan standards. As described in the main text, we found that the SPF contents did not appreciably compress colonic mucus, indicating that any residual polymers present in the SPF contents (after microbial degradation) were insufficient to compress the hydrogel; this result is also consistent with our observation that SPF mice and mice maintained on a sucrose diet had colonic mucus hydrogels of comparable thickness (Figure 3.1, $p = 0.3$). By contrast, we found that the GF contents compressed colonic mucus by ≈70% of its initial washed thickness, for washed explants obtained from either SPF or GF mice (Figure 3.4c). This finding indicates that gut microbes, by modifying the polymeric composition of intestinal contents, can actively modulate the compression state of the colonic mucus hydrogel (Figure 3.4d).

Detailed contributions from noncorresponding authors

A.P.S. codesigned all experiments and coanalyzed all experimental results; codeveloped theoretical tools and coperformed the experiments and calculations; performed some of the FC oil measurements and analyzed some of the results in Figures 3.1 and 3.S1; performed some of the ex vivo experiments and analyzed some of the results in Figures 3.2–4 and 3.S3–S7; codeveloped the theoretical model; cooptimized and coperformed calculations for the theoretical model and coanalyzed results in Figure 3.3; performed a sensitivity analysis for the theoretical model shown in Figure 3.S9; performed dynamic light scattering measurements of polymers and probes; designed and performed GPC measurements in Figure 3.S10; and cowrote the paper.

S.S.D. coplanned the project; codesigned all experiments and coanalyzed all experimental results; codeveloped theoretical tools and coperformed the experiments and calculations; set up polymer-fed animal experiments (Figure 3.1); performed some of the FC oil measurements and analyzed some of the results in Figures 3.1 and 3.S1; developed the ex vivo experimental approach; performed the ex vivo experiment of WGA-stained mucus (Figure 3.S2); performed some of the ex vivo experiments and analyzed some of the results in Figures 3.2–4 and 3.S3–S7; tested optical properties of test solutions (Figure 3.S8); codeveloped the theoretical model; developed a computational approach for the theoretical model calculations; cooptimized and coperformed calculations for the theoretical model and coanalyzed results in Figure 3.3; developed an approach to extract liquid fraction of murine colonic contents; and cowrote the paper.

Supplemental Figures

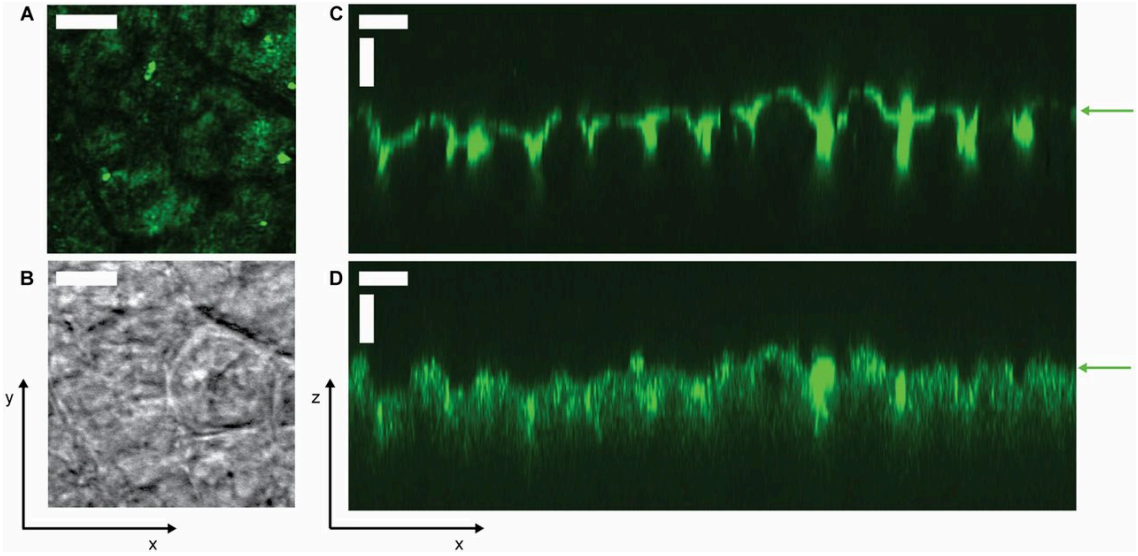

Figure 3.S1: Images of murine epithelium in the xy and xz planes. (a) Two-photon and (b) bright-field micrographs of unwashed epithelium from a mouse fed standard chow, imaged under FC oil. (c, d) Sideviews of lectin-stained epithelium washed with saline and imaged under aqueous solutions. Staining was performed by incubating a colon explant with 200 µL of a test solution of 2 mg/mL Rhodamine Ulex Europaeus Agglutinin I (Vector Laboratories, Burlingame, CA, USA), which stains α-L-fucose residues on the surface of epithelial cells, in HEPES buffer in a sealed petri dish for 10 min at 4 ºC, then washing the exposed luminal side with several milliliters of ice-cold 1x PBS. We then immediately imaged the explant surface using (c) confocal fluorescence microscopy (543 nm excitation / 560 nm long-pass filter) and (d) confocal reflectance microscopy (514 nm excitation / 505 nm long-pass filter). Epithelial surface is indicated by green arrows, confirming that the position of the epithelium agrees between the different imaging modalities. The adherent mucus hydrogel overlies the epithelium in the direction of increasing z above the green arrows. All scale bars, 30 µm.

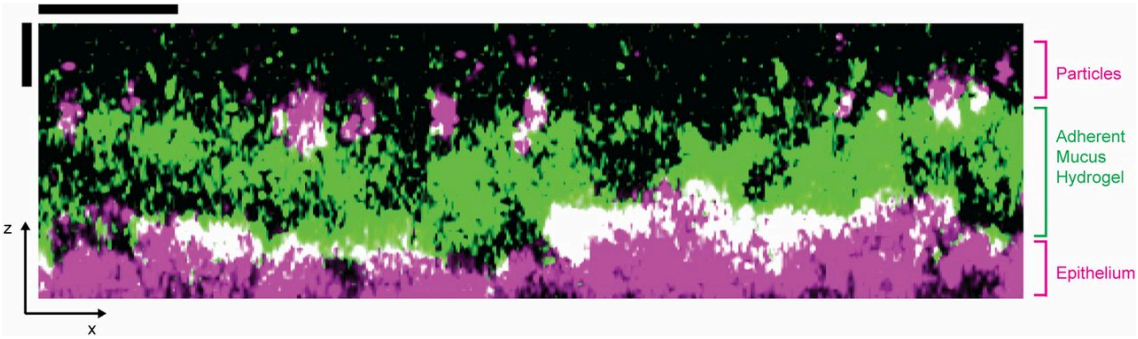

Figure 3.S2: False-color sideview showing WGA-stained adherent mucus hydrogel. We first deposited 1 μm diameter microparticles onto the explant surface of a freshly excised, washed, and mounted colonic explant. After incubating for 1 h at 4 ºC, we then stained the colonic mucus with wheat germ agglutinin (WGA), a fluorescent lectin that specifically binds to sialic acid sugar residues in the mucins. We prepared 10 μg/mL of WGA-Oregon Green (Invitrogen, Grand Island, NY, USA) in 1x PBS, placed a ~0.5 mL drop on the exposed surface of the explant and incubated the sealed petri dish for 5 min at room temperature. We then washed the exposed surface with several milliliters of ice-cold 1x PBS and immediately imaged the explant surface (lower magenta surface) and the deposited 1 μm microparticles (upper magenta circles) using confocal reflectance microscopy, and the stained mucus hydrogel using confocal fluorescence microscopy (488 nm excitation / 505 nm long-pass filter). Image is a superimposition of two separate, parallel sideviews taken at two neighboring positions in the xy plane. We observed that the position of the deposited microparticles agrees with the top of the stained mucus hydrogel. Scale bars, 30 μm.

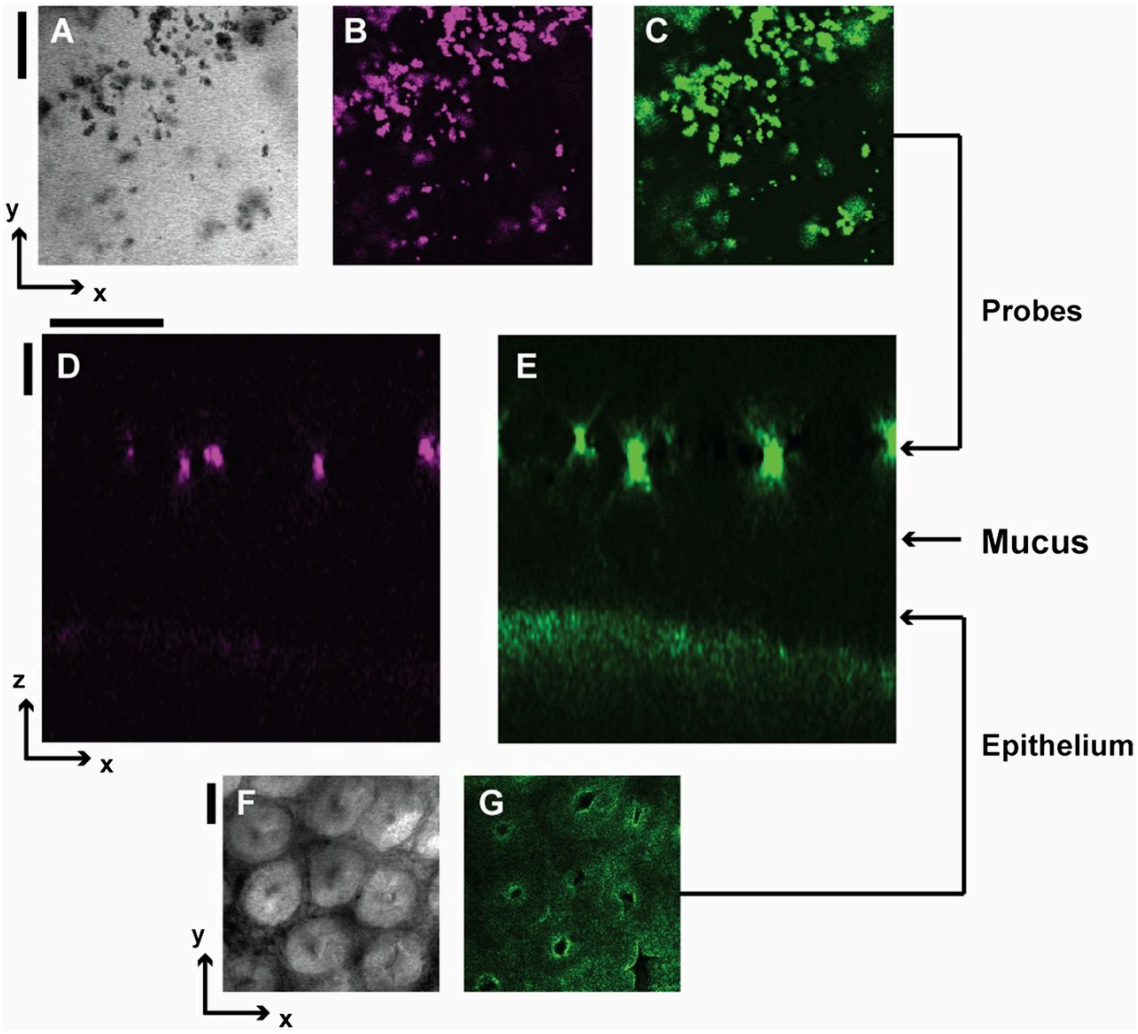

Figure 3.S3: Co-localization of signal from microparticle probes and epithelium from different imaging modalities. (a) Brightfield, (b) fluorescence excitation and (c) reflectance images of 1 μm probes of the same xy slice. (d) An xz sideview of fluorescence signal from 1 μm probes. (e) The same xz sideview as in panel d but of the reflectance signal from 1 μm probes and epithelial surface. (f) Brightfield and (g) reflectance images of the epithelial surface of the same xy slice. The arrow linking panel (c) to panel (e) indicates the vertical position of the xy slice shown in panels (a)-(c). The arrow linking panel (g) to panel (e) indicates the vertical position of the xy slice shown in panels (f)-(g). Scale bars, 30 μm. This confirms that the positions of the microparticles given by confocal reflectance and confocal fluorescence microscopy agree.

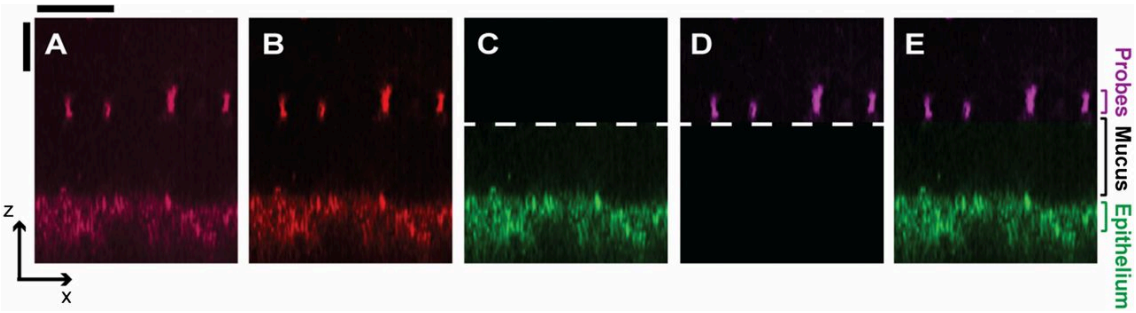

Figure 3.S4: Overview of image processing of confocal sideviews. To eliminate artifacts associated with staining and accelerate image acquisition, we used label-free confocal reflectance microscopy to simultaneously image the underlying epithelium (lower surface) and the microparticles deposited on the adherent mucus hydrogel (upper bright spots). To obtain the false-color sideviews, we first thresholded each sideview; (a) shows a representative xz sideview before processing, while (b) shows image after thresholding, with uniform enhancement of brightness and contrast across the entire image. The image was then split into two parts, and the epithelium was false-colorized green (c) and the deposited microparticles or oil-mucus interface (for imaging of unwashed tissues with FC oil) were false-colorized magenta (d). Dashed lines indicate where images (c)–(d) were split. Merging these two channels produced the sideview images shown, exemplified by (e). Scale bars, 30 μm. Unless otherwise noted, all of our experiments mapped z ranges spanning from below the epithelial surface to well above the mucus hydrogel surface. Each of the sideview images presented in this paper was cropped and scaled in xz for clarity (indicated by the x and z scale bars), to focus on the region corresponding to the mucus hydrogel.

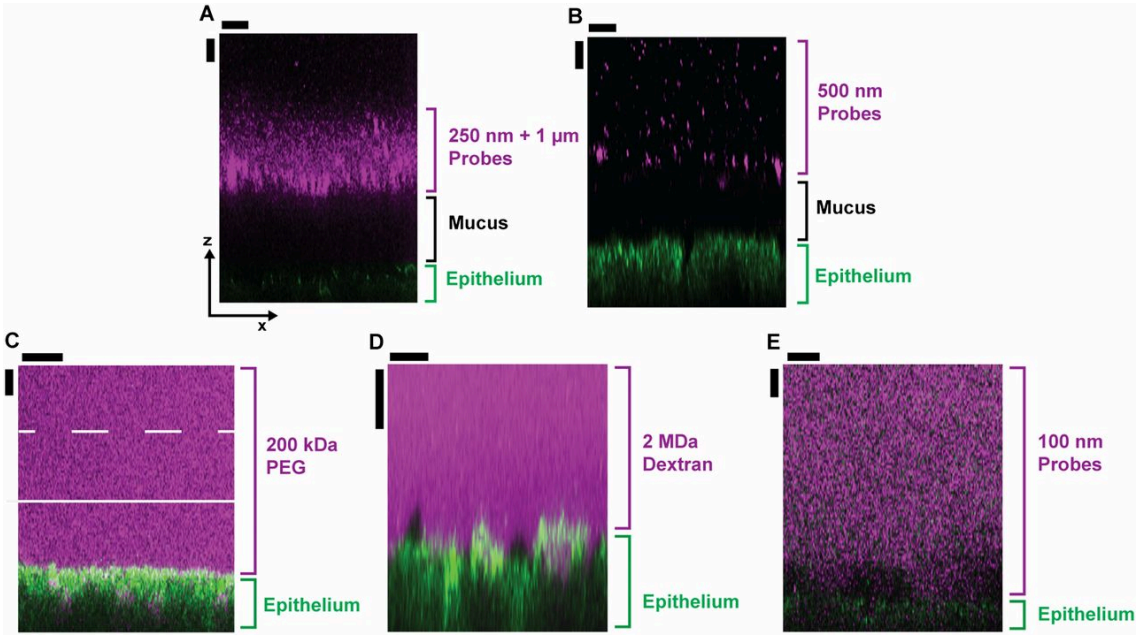

Figure 3.S5: False-color sideviews (xz plane) of 3D stacks showing probes excluded from (top row) or penetrating (bottom row) the mucus hydrogel. (a) Mixture of both 250 nm and 1 µm microparticles and (b) 500 nm particles were excluded from the adherent mucus hydrogel. The probes (magenta) were unable to diffuse through the mucus, and instead deposited on top of the hydrogel. The probes and the epithelium were simultaneously imaged using (a) 514 nm excitation / 505 nm long-pass filter and (b) 800 nm excitation / 650 nm long-pass filter. (c) Fluorescent PEG 200 kDa, (d) fluorescent dextran 2 MDa, (e) fluorescent 100 nm microparticle probes all penetrate the hydrogel. Note that polymers in (a) and (b) were used at concentrations below those that cause mucus compression. The probes (magenta) diffused through the mucus and reached the underlying epithelium (green), except for some isolated regions immediately adjacent to the epithelium observed in some experiments (dark patches). The probes were imaged using confocal fluorescence microscopy (488 nm excitation / 505 nm long-pass filter) and the epithelium was imaged using confocal reflectance microscopy. The adherent mucus hydrogel overlies the epithelium in the direction of increasing z above the green arrows; solid and dashed white lines in panel (c) indicate the approximate average and maximal positions of the top of the mucus, measured using 1 µm microparticles. Scale bars, 30 µm. In each experiment using probes of different sizes, after placing the test solution onto the exposed luminal surface, we incubated the tissue at 4 ºC for 1–2 h before imaging the explant. We estimated the time required for probes 100 nm or smaller to diffuse through the mucus as being < 10 min, and the time required for the 250 nm probes to diffuse across the vertical extent of the mucus in free solution as being ~10 min, both much shorter than the incubation time. We thus deduce that the fluorescent probes smaller than the measured mucus mesh size had sufficient time to diffuse through the mucus to the underlying epithelium, and that the measured exclusion of the larger probes reflects the presence of the adherent mucus hydrogel.

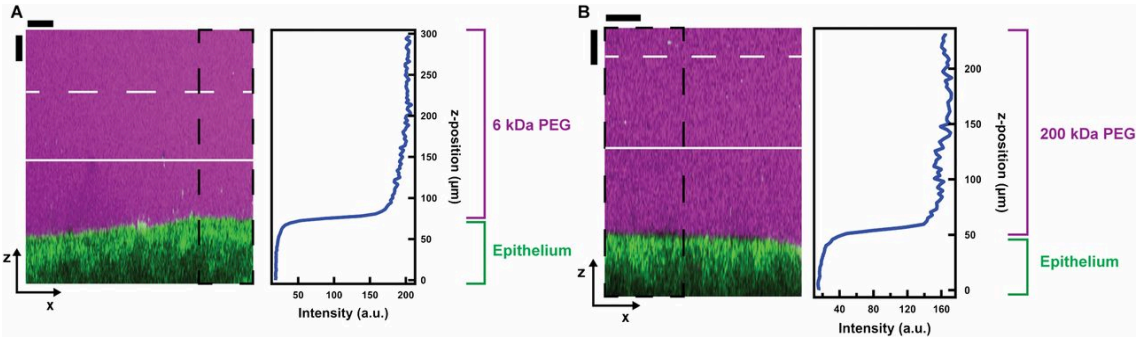

Figure 3.S6: Sideview showing penetration of mucus hydrogel by polymers. The polymer self-diffusion coefficient in the free solution outside the mucus, D_{free}, is represented by D_0 for the dilute polymer solutions, and can be estimated as $D_{free} \approx D_0 \left(\frac{c}{c^*}\right)^{-7/4}$ for the polymer solutions that were above their overlap concentration c^*. Our experiments spanned $D_0 \approx 10^{-11}$ to 3 x 10^{-10} m^2/s and $c/c^* \approx$ 0-10, therefore $D_{free} \approx 2 \times 10^{-13} - 3 \times 10^{-10}$ m^2/s. The characteristic time taken for the polymers to diffuse through the mucus can thus be estimated as ranging from ~ 1 s to 1 h, shorter than the time taken to perform the experiments. We thus assume that the polymer molecules were able to diffuse through the mucus hydrogel before imaging commenced in all of the experiments. To study the steady-state penetration of the PEG into the adherent mucus hydrogel, we imaged two representative test solutions: (a) 13% w/v PEG 6k spiked with 0.5 mg/mL FITC-PEG 5k, and (b) 3% w/v PEG 200k spiked with 0.6 mg/mL FITC-PEG 200k. Consistent with our expectation, in both cases, the polymer penetrated through the adherent mucus hydrogel and reached the underlying epithelium. Traces show the spatial variation of the x-averaged probes fluorescence intensity for the region indicated by the dashed black box. The probes (magenta) diffused through the mucus and reached the underlying epithelium (green). The probes were imaged using confocal fluorescence microscopy and the epithelium was imaged using confocal reflectance microscopy. The adherent mucus hydrogel overlies the epithelium in the direction of increasing z above the epithelium; solid and dashed white lines show the average and maximal positions of the top of the mucus, measured using 1 μm microparticles. Scale bars, 30 μm.

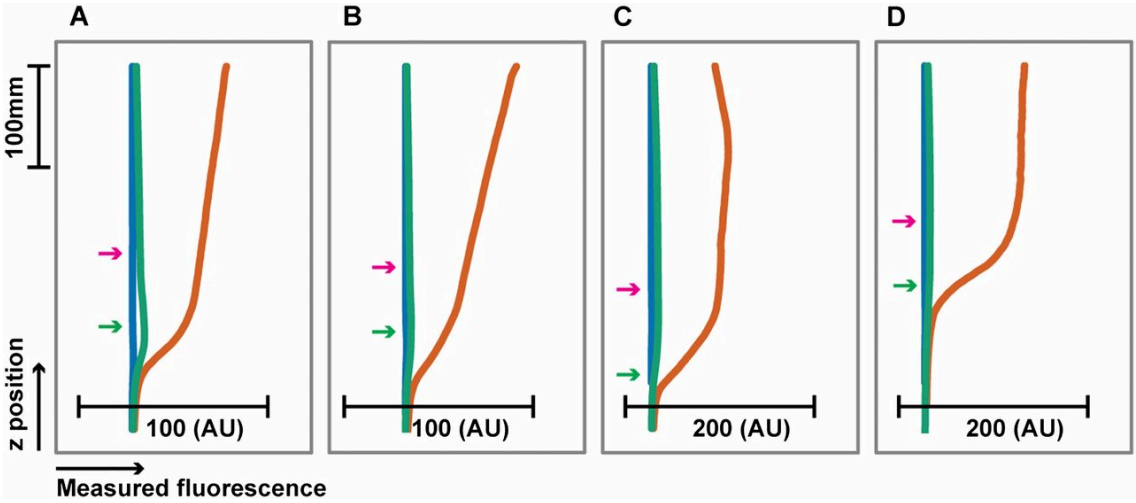

Figure 3.S7: Fluorescence profiles of test solutions deposited on mucus hydrogel, before and after washing. We expect that the carboxyl groups on the mucin sialic acid residues were negatively charged in our experiments (pH ~ 7), and therefore, complexation between the added PEG and the mucins is minimal. Moreover, we took care to not expose PEG solutions to light and keep them at low temperatures when not in use, to minimize oxidation. To confirm that labeled PEG molecules were not chemically cross-linked to the mucus hydrogel as they diffused through the hydrogel, we performed four sets of fluorescence measurements, using as test solutions (a) 5μM fluorescein, (b) 15μM FITC-PEG 350, (c) 6 μM FITC-PEG 5k, (d) 15μM FITC-PEG 350 in 60% w/v PEG 400. Four different explants were incubated with 1μm microparticles for >1 h, then imaged using confocal reflectance (to identify epithelial surface and microparticles on mucus) and confocal fluorescence (to quantify fluorescence of deposited test solution). Curves show fluorescence profiles of test solutions: horizontal axis shows measured fluorescence, averaged over a 450 μm x 450 μm xy field of view, while vertical axis shows z position. Green and magenta arrows show average positions of epithelial surface and probes deposited on the mucus hydrogel surface. We first used PBS as the test solution to provide a measure of background fluorescence (blue curves). We then deposited dyed test solution on the mucus (orange curves). We then washed the explant with saline (green curves). Fluorescence profiles returned to background levels after washing, suggesting that strong chemical interactions (such as covalent reactions) between the labeled PEG and the mucus hydrogel do not occur. We used the same gain settings before and after.

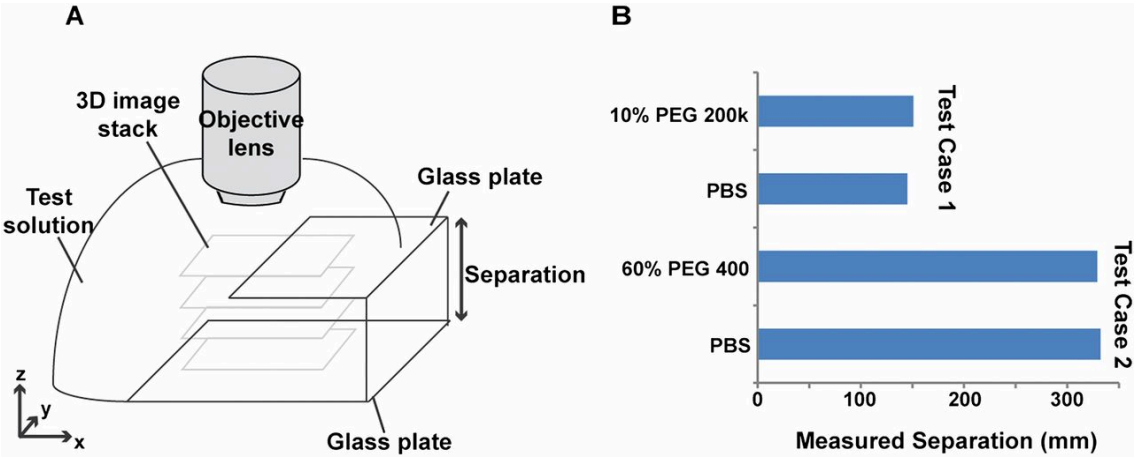

Figure 3.S8: Optical properties of polymer solutions do not appreciably affect z measurements. (a) Schematic showing set up of control experiments, measuring separation between two parallel glass plates using the same confocal reflectance microscopy approach. The test solution infiltrated the open gap between the two plates. (b) We first quantified separation using PBS as the test solution filling the space between the two plates, and then used either 10% PEG 200k (test case 1), or 60% PEG 400 (test case 2) as the test solution. Introduction of the polymer solution did not change the measured z separation appreciably, indicating that optical effects due to the presence of the polymer solution did not significantly affect the z measurements.

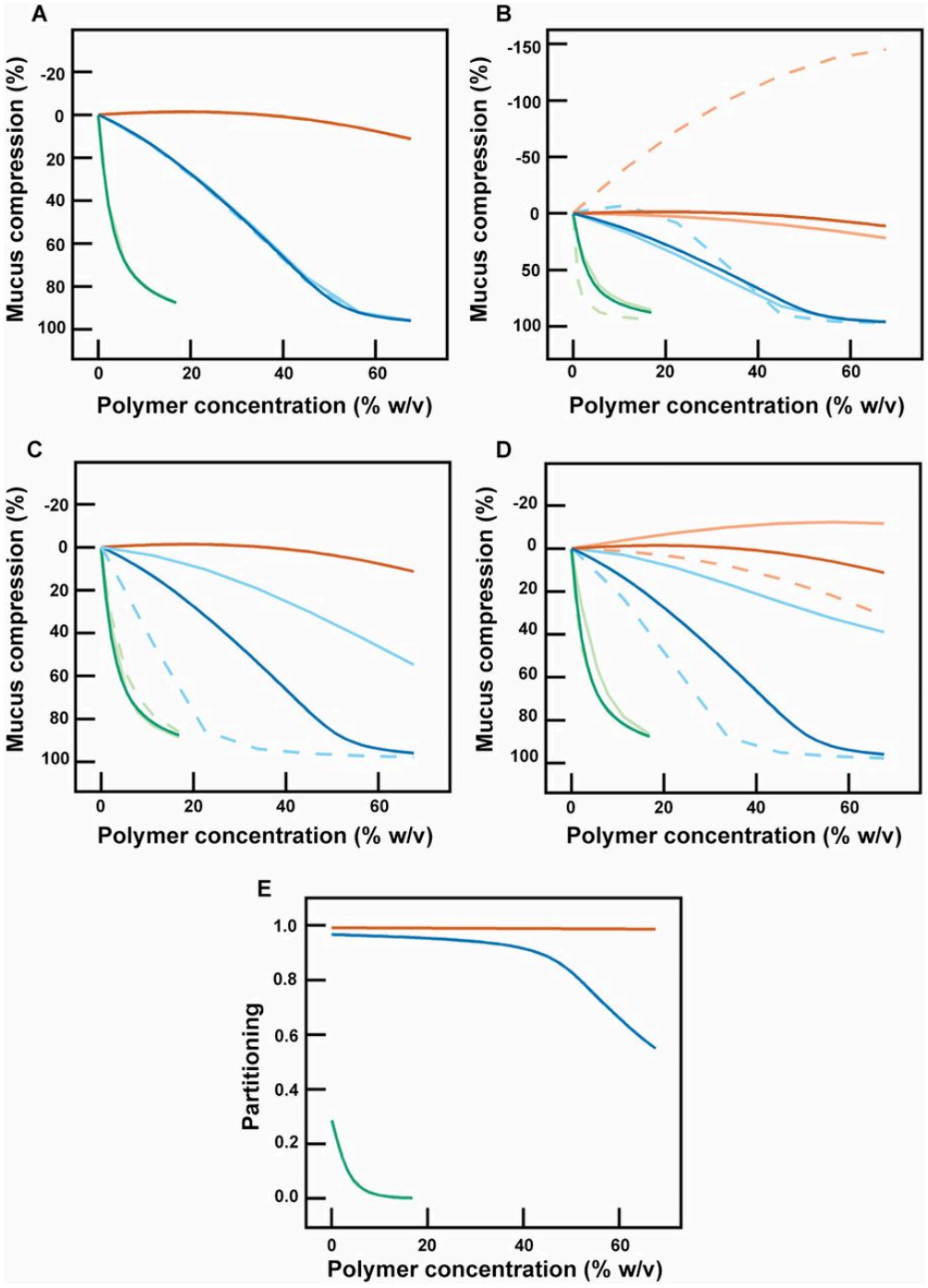

Figure 3.S9: Sensitivity of model predictions to variations in numerical parameters. Each panel shows numerical calculations (*Materials and Methods*) of the mucus hydrogel compression for different concentrations of PEG 400 (orange), 6k (blue), and 200k (green). Note that due to the constraint derived in the initial polymer-free case, some of the

parameters are coupled and cannot be varied independently. (a) v^0_M values are varied and corresponding values of N_M are adjusted to satisfy the initial polymer-free constraint. Light, solid traces correspond to v^0_M = 0.07 and N_M = 628, and light, dashed traces correspond to v^0_M = 0.35 and N_M = 2026. Note the overlap between the solid and dashed traces. (b) χSM values are varied and corresponding values of N_M are adjusted to satisfy the initial polymer-free constraint. Light, solid traces correspond to χ_{SM} =-0.2 and N_M = 715, and light, dashed traces correspond to χ_{SM} =0.45 and N_M = 9425. Upper and lower less opaque curves in Figure 3.2A, which correspond to χ_{SM} = 0.1 and -0.1, were characterized by N_M = 1247 and N_M = 833. (c) The number of Kuhn segments y for each PEG molecule is varied. Light, solid traces correspond to y = 1, 2, and 76, and light, dashed traces correspond to y = 1, 11 and 611 for PEG 400, 6k, and 200k respectively. (d) χ_{MP} is varied. Light, solid traces correspond to χ_{MP} = 0 and light, dashed traces correspond to χ_{MP} = 0.5. In each panel, the dark solid traces are the simulations presented in Fig. 2a. In all cases, we observed similar trends of compression with polymer concentration and molecular weight as in the experiments. (e) Numerical calculations showing the partitioning between the hydrogel and solution phase for PEG 400 (orange), 6k (blue), and 200k (green). The ratio of PEG inside and outside the hydrogel (v^P_{in}/ϕ, denoted "Partitioning") is plotted against the PEG concentration outside the hydrogel. Consistent with our expectation, the higher molecular weight polymer is more likely to be excluded from the mucus hydrogel.

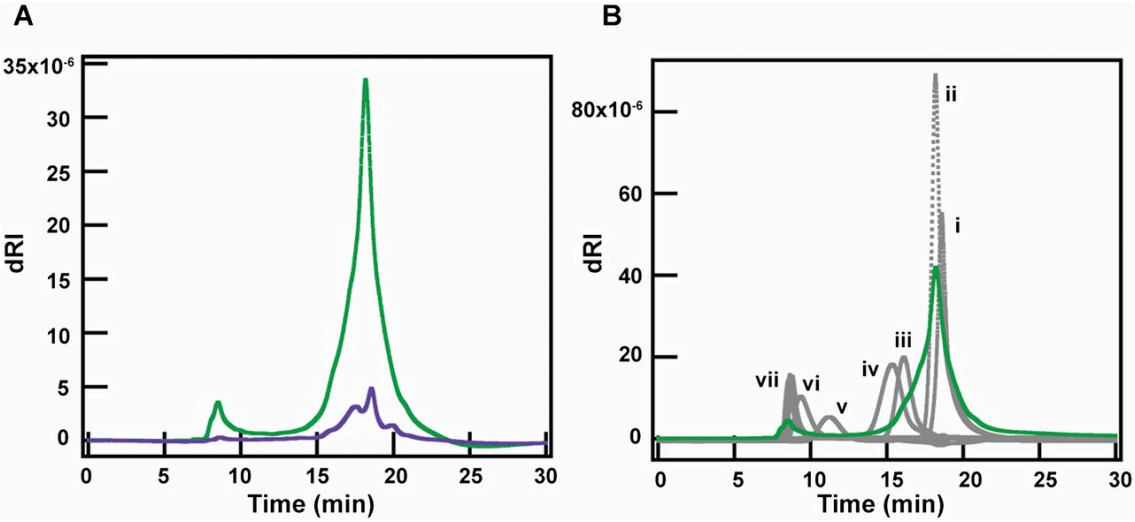

Figure 3.S10: Gel permeation chromatography of luminal contents from SPF and GF mice. We used an Agilent 1100 HPLC with a binary pump and auto-sampler, which was connected to a Tosoh TSKgel G3000SWxl column equilibrated with 1x PBS, pH 7.4, flow rate: 0.7 ml/min. For detection of the polymers, a Wyatt DAWN HELEOS light scattering instrument with a Wyatt Optilab Rex refractive index detector was used. Detected peaks were analyzed using ASTRA V software. For the pullulan standards, the Agilent PL 2090-0101 Pullulan polysaccharide calibration kit (Agilent, Wilmington, DE, USA) was used. An injection volume of 50 µL was used for each. All samples were prepared in 1x phosphate buffered saline and run through a sterile syringe filter (Polyvinylidene Fluoride, 13 mm diameter, pore size of 0.22 µm, Fisherbrand, Pittsburgh, PA, USA) before injection. For luminal contents, on the day of the experiment, frozen liquid fractions were warmed to room temperature for 10–20 min, then diluted two-fold with 1x PBS. Samples were centrifuged at 12,000 g at 4 ºC for 2 h in sterile centrifugal filters (Polyvinylidene Fluoride, pore size 0.22 µm, from EMD Millipore, Billerica, MA, USA). After centrifugation, samples were allowed to equilibrate to room temperature for 30 min before injection. For all liquid fraction samples, an injection volume of 10 µL was used. If multiple runs were performed on the same sample, the remaining sample volume was stored at 4 ºC until prior runs were complete. (a) Chromatograms of luminal contents from four, 3-month-old SPF males (purple) and two male and one female, 4-month-old GF (green) mice. Differential refractive index (dRI) is plotted against time (min). Both runs were run on the same day. (b) Chromatograms of luminal contents of GF mice (green) and pullulan standards (grey). Differential refractive index (dRI) is plotted against time (min). Concentrations and peak average MWs of the standards used were: (i) 5 mg/ml 180 Da, (ii) 8 mg/ml 667 Da, (iii) 4 mg/ml 6,100 Da, (iv) 4 mg/ml 9,600 Da, (v) 1 mg/ml 47,100 Da, (vi) 1 mg/ml 107,000 Da, and (vii) 1 mg/ml 194,000 Da, 344,000 Da and 708,000 Da.

Chapter 4

FOOD POLYELECTROLYTES COMPRESS THE COLONIC MUCUS HYDROGEL BY A DONNAN MECHANISM

1. A. Preska Steinberg, Z.-G. Wang, R. F. Ismagilov. 2019 “Food polyelectrolytes compress the colonic mucus hydrogel by a Donnan Mechanism”. Submitted.

Abstract

Systems consisting of a polyelectrolyte solution in contact with a cross-linked polyelectrolyte network are ubiquitous (e.g., biofilms, drug-delivering hydrogels, and mammalian extracellular matrices), yet the underlying physics governing these interactions is not well understood. Here, we find that carboxymethyl cellulose (CMC), a polyelectrolyte commonly found in processed foods and associated with inflammation and obesity, compresses the colonic mucus hydrogel (a key regulator of host-microbe interactions and a protective barrier) in mice. The extent of this polyelectrolyte-induced compression is enhanced by the degree of polymer negative charge. Through animal experiments and numerical calculations, we find that this phenomenon can be described by a Donnan mechanism. Further, the observed behavior can be quantitatively described by a simple, one-parameter model. This work suggests that polymer charge should be considered when developing food products because of its potential role in modulating the protective properties of colonic mucus.

Introduction

In this work, we sought to understand how polymer charge influences polymer-driven mucus compression. The colonic mucus hydrogel is a critical barrier in the colon—it is the nexus of host-microbe interactions and it protects against microbial infiltration and physical insults.[1] This hydrogel, which lines the walls of the colon, is composed primarily of high molecular weight (MW) glycoproteins (~1.2 MDa) known as mucins and is held together by physical entanglements, chemical cross-links, and electrostatic interactions.[2,3] Although the microbiology and chemical-biology communities have exhaustively studied how microbes interact with this hydrogel and its biochemical composition,[1,2,4,5] the underlying physics that governs the structural features of the colonic mucus hydrogel has only recently begun to be explored.[6] In particular, it is vital to understand what influences the de-swelling or compression of this hydrogel, because several studies have found correlations between changes in the mesh size and thickness of colonic mucus and changes in host health.[7,8] Our recent work has found that neutral or uncharged polymers can compress the colonic mucus hydrogel by a mechanism that can be described using a simple, first-principles thermodynamics model based on Flory-Huggins solution theory.[6] It was shown that for these uncharged polymers, the extent of polymer-induced mucus compression is increased by either increasing the polymer concentration or by increasing the polymer MW at a given polymer concentration. However, the human diet contains many charged polymers (i.e. polyelectrolytes) which are predominately negatively charged.[9,10]

One polyelectrolyte that is commonly placed in food and is "generally regarded as safe" (GRAS) by the U.S. Food & Drug Administration (FDA) is carboxymethyl cellulose (CMC).[11] This polyelectrolyte is a cellulose-derivative that has a negative charge in the gut due to carboxymethyl groups attached to some of its monomer units.[12] Interestingly, although many charged versions of CMC exist, the FDA allows only up to a degree of substitution (DS) of 9 charged groups per 10 monomers (abbreviated as "DS 0.9"). There

is no existing literature explaining how changing the charge of these polymers affects the design of food products. CMC is added to processed foods because of its ability to enhance the viscosity of food and to stabilize emulsions by slowing droplet coalescence,[9,13] which leads to it often being mistakenly called an "emulsifier" even though it is not a surfactant but a high-MW polyelectrolyte. Recent biological studies found that feeding mice CMC resulted in low-grade inflammation and obesity. CMC feeding was also correlated with a thin mucus layer that allowed for microbial encroachment upon the host.[14,15] In addition, it has been shown that acute exposures to CMC (by direct injection into the small intestine) can alter the structure of the small-intestine mucus layer in rats.[16] However, mechanistic understanding of these effects is lacking; it is unclear if, *in vivo,* colonic mucus is thinner because it is disrupted or compressed. We hypothesize that the thin colonic mucus layer in mice fed CMC was the result of mucus compression.

Many studies have covered the physical chemistry of polyelectrolyte solutions,[17,18] polyelectrolyte hydrogels,[19,20] complex coacervation between oppositely charged polyelectrolytes,[21,22] and complexation between polyelectrolytes with oppositely charged objects.[23,24] In contrast, the interactions between systems composed of polyelectrolyte solutions and polyelectrolyte gels remain vastly understudied,[25] both experimentally and theoretically. Here, we seek to untangle the physical interactions between colonic mucus (a biological polyelectrolyte gel) and CMC (a polyelectrolyte).

Materials and Methods

Details of animals used. All mice were 2-6 months old, male or female specific pathogen free (SPF) C57BL/6 mice (RRID: IMSR_JAX:000664). In our previous study, we did not observe any differences in mucus compression related to age (in the same age range as this study) or gender.[6] We justified the use of both male and female mice because an experimental study found that ~3 month old C57BL/6 mice had similar mucus thickness and morphology regardless of sex.[26] We justified the use of a range of ages of mice

because, although it has been reported that 19 month old C57BL/6 mice had thinner colonic mucus compared to 2.5-3 month old C57BL/6 mice, 19 months old is well outside the age range of this study.[26,27] Mice used in *ex vivo* experiments in Figure 4.2-4 and Figure 4.S1 were maintained on a solid chow diet (PicoLab Rodent Diet 20) and were given food and water *ad libitum*. Mice used in experiments in Figure 4.1 were maintained on chow diet until the day of the experiment. Starting 23 h before euthanization, these mice were restricted (no chow or water) to a solution of 1% w/v carboxymethyl cellulose (carboxymethylcellulose sodium, USP grade, medium viscosity, PN: C9481-500G) with 5% w/v sucrose (USP grade, PN: S3929) in water or a solution of 1% v/v Tween (Polysorbate 80, Food Grade, Sigma Aldrich, PN: W291706) with 5% sucrose in water. For these 23 h, mice were kept on mesh-bottom cages to prevent re-ingestion of chow-derived polymeric contents from fecal matter. All mice were obtained from Jackson Labs (The Jackson Laboratory, Bar Harbor, ME, USA) and were then housed at Caltech's animal facility. All animal experiments were approved by the California Institute of Technology (Caltech) Institutional Animal Care and Use Committee (IACUC; protocol #1691) and the U.S. Army's Animal Care and Use Review Office (ACURO; protocol #70905-LS-MUR.03). Mice were euthanized via CO_2 inhalation as approved by the Caltech IACUC in accordance with the American Veterinary Medical Association Guidelines on Euthanasia.[28]

Details of Microscopy. Images were acquired by taking z-stacks on a Zeiss LSM 880 upright confocal microscope using confocal fluorescence to image particles (488 nm excitation/505-736 band pass filter), confocal reflectance to image the epithelium (561 nm excitation/505-736 nm band pass filter), bright-field for epithelium and particles, or two-photon for FC-oil layer and epithelium (700 or 750 nm excitation/650-758 nm band pass filter).

Imaging of samples using "FC-oil approach." Sample preparation and imaging were carried out as described previously in ref. 6 (in ref. 6, see *SI Materials and Methods*, section "Imaging of Unwashed Tissue").

Imaging of samples using "micro-particle approach." Sample preparation and imaging were carried out as described previously in ref. 6 (in ref. 6, see *SI Materials and Methods*, sections "Imaging of Washed Tissue" and "Thickness Measurements of Washed Mucus Hydrogel"). The protocol was modified such that the fluorescent 1-μm-diameter polystyrene beads coated with polyethylene glycol (PEG) with a molecular weight (MW) of 5kDa were used as the micro-particles (created as described in ref. 29). These were imaged using fluorescence in addition to confocal reflectance (488 nm excitation/505-736 band pass filter). For the thickness measurements obtained using the "micro-particle approach" appearing in Figure 4.1, determination of mucus thickness was done in the same way as the "FC oil approach".

Compression measurements. Compression measurements were carried out as described in ref. 6 (in ref. 6, see *SI Materials and Methods*, section "Quantifying Polymer-induced Compression of Washed Mucus Hydrogel"). In this work, we define "% compression" as: *% compression = [Δt/t₀]*100%,* where t_0 is the initial mucus thickness and $\Delta t = t_0 - t_f$, and t_f is the final mucus thickness. We modified the protocol such that each compression measurement in this work represents the mean of compression measurements taken on colonic explants from three separate mice. The compression value from each individual explant is the average of compression measurements in five different positions on that explant. The error bars are standard error of the mean with n = 3. For measurements done with 1x phosphate buffered saline (PBS), we diluted 10x PBS (Corning 10x PBS, pH 7.4$\pm$0.1, without calcium and magnesium, RNAse-/DNAse- and protease-free, Product No. 46-013-CM) ten-fold with Milli-Q water. In the compression experiments in Figure 4.4 with polymers in 10x PBS, the tissue was incubated with microparticles in 1x PBS for ~1 hour before placing on the polymers in 10x PBS. Final thickness was then measured after 10 min. This was done to prevent prolonged exposure (1 hour or longer) to 10x PBS (which after long times could cause tissue deterioration due to the salt imbalance) while the microparticles sedimented down on top of the mucus hydrogel.

Polymers Used for Compression measurements. We used carboxymethyl cellulose (CMC) with a degree of substitution (DS) of 7 charged monomers per 10 monomers (DS 0.7) (Sigma Aldrich, PN: 419311), CMC DS 0.9 (Sigma Aldrich, PN: 419303), and hydroxyethyl cellulose (HEC) (Sigma, PN: 308633).

Gel permeation chromatography (GPC) of polymers. GPC was used to measure the MW and hydrodynamic radii (R_h) was used to confirm that the CMC used in the mouse feeding experiements in Fig. 1 and the CMC and HEC used in all other figures were approximately the same MW and R_h (measurements shown in Figure 4.S3 & Table 4.S1). GPC measurements were conducted as described in ref. 29. CMC derivatives were analyzed using a refractive index increment (dn/dc) of $\frac{dn}{dc} = 0.163$.[30] HEC was analyzed using $\frac{dn}{dc} = 0.150$.[31]

Curve Fitting in Figure 4.3. For the curve fitting presented in Figure 4.3, we used the "scipy.optimize.curve_fit" function in Python 3.6.4, which is included as a supplemental file to the manuscript.

Results and Discussion

Carboxymethyl cellulose (CMC) compresses mucus reversibly *in vivo*. We first sought to test two hypothesis: (1) the colonic mucus hydrogel is thin when mice are fed CMC because the mucus hydrogel is compressed; and (2) the mechanism by which CMC interacts with mucus is different than that of an emulsifier—Polysorbate 80 (Tween 80)—because of the differences in their physicochemical properties (CMC is a high-MW polyelectrolyte whereas Tween is a low-MW, non-ionic surfactant).

To test these two hypotheses, we devised a simple experiment, in which we fed one group of specific-pathogen-free (SPF) mice a solution of 1% w/v CMC and another group 1% w/v Tween 80 for 23 h and then measured the thickness of the mucus hydrogel. We justified the removal of the standard chow diet because our previous work with different dietary polymers suggested that the components of chow do not contribute to mucus compression

in SPF mice.[6] We tested this in ref. 6 by measuring mucus compression on colonic explants using polymers in buffer and comparing it to compression induced by the same polymers prepared in extracted luminal fluid from chow-fed SPF mice. In these experiments, we found similar amounts of compression in both sets of samples. Additional evidence supporting this in ref. 6 was that the addition of luminal fluid from chow-fed SPF mice to colonic explants did not induce mucus compression and that, for chow-fed SPF mice, the mucus thickness on explants remained the same when luminal contents were removed. In this work, for our experiment to test the differences between feeding 1% w/v CMC and 1% w/v Tween 80, we first measured the thickness of the mucus hydrogel using our "fluorocarbon (FC) oil approach" (Figure 4.1A,B; see ref. 6 for further details). In brief, this method allows us to avoid washing colonic explants with buffer (which could cause the loss of polymeric contents that are in contact with the mucus hydrogel) and it eliminates the use of a fixative (which could alter mucus structure). Instead, we remove luminal contents with FC-40 oil, which is immiscible with and denser than water, and coat the explant with FC-40 oil, which sits on top of mucus. The FC oil approach has the further advantage of preventing dehydration of the mucus layer, allowing us to measure the extent of compression as it would be *in vivo.* The thickness is then obtained by measuring the difference in position of the epithelial cells under mucus (identified using bright-field and confocal reflectance) and the position of the FC oil–hydrogel interface (identified using confocal reflectance). We found that both the CMC and Tween 80 groups had a thin mucus layer (Figure 4.1D, gold bars) compared with previous thickness (t) measurements we had done with groups of mice fed a standard chow diet, where we measured $t = 67 \pm 7\ \mu m$ (ref. 6; Figure 4.1D, grey bar).

The FC oil approach allows us to measure the mucus thickness in an environment that approximates the "native state" of the adherent, colonic mucus hydrogel when it is in contact with *in vivo* gut contents (see ref. 6 for further details and validation of this approach). However, we wanted to test whether the mucus was thin because it was disrupted or whether it was compressed. We therefore used a different tissue-preparation approach that allowed us to measure the mucus thickness after washing out the *in vivo* gut

contents (including polymers or and other molecules that could disrupt or compress mucus). We took two more groups of mice and fed them the same solutions, but this time before imaging we washed the tissue with phosphate buffered saline (PBS) to remove any colonic polymeric contents that could compress mucus. We then quantified the mucus thickness using the "microparticle approach" (Figure 4.1B,C; *Materials and Methods*). This and similar approaches have been used previously to quantify the thickness of the adherent, inner colonic mucus layer *ex vivo*.[6,7,32] Briefly, in the microparticle approach, after removing all gut contents, a solution of microparticles (in PBS) with a diameter (d) larger than the mucus mesh size (ξ) is allowed to sediment down on top of the mucus hydrogel. These microparticles were coated with polyethylene glycol (PEG), as PEG-coating has been previously shown to reduce the mucoadhesivity of particles.[33] Because $d > \xi$, the microparticles are excluded from the hydrogel (which we confirmed in our previous work[6]), and we can determine the thickness by measuring the difference in the position of the epithelium (using confocal reflectance and bright-field) and the position of the microparticles (using fluorescence). Using the microparticle approach, we observed that the mucus layer was substantially thicker in the CMC group than in the Tween group (Figure 4.1D, blue bars). Furthermore, we observed that the mucus in the "washed" CMC-fed group was substantially thicker than the mucus in the "unwashed" CMC-fed group. This suggests that the mucus hydrogel in CMC-fed groups is compressed reversibly, springing back when "compressive" polymeric contents are washed out with buffer. Another potential factor is that the gut microbiota has been shown to degrade colonic mucus in different contexts.[4] However, because the mucus thickness in the "washed" CMC-fed group agreed with our previous measurements of the inner mucus layer in chow-fed mice (i.e., the "normal" mucus thickness in healthy, SPF mice) it suggests that the colonic mucus hydrogel is not degraded by the gut microbiota over the course of our experiments. For the Tween-fed groups, our data showed that both the washed and unwashed Tween-fed groups had thinner mucus compared with the washed CMC-fed group (Figure 4.1D) and our previous measurements of mucus in chow-fed mice. Because the "normal" thickness of the inner mucus layer cannot be recovered, it suggests that in the

Tween-fed groups, mucus is irreversibly "thinned." In total, these experiments suggest that not only does CMC compress the colonic mucus hydrogel reversibly *in vivo*, but the physical mechanism by which it interacts with mucus is different than that of Tween. This observation was unexpected because polyelectrolytes and emulsifiers have been considered to be similar in previous gut studies.[14,15,34] We therefore sought to understand the mechanism by which CMC compresses the colonic mucus hydrogel.

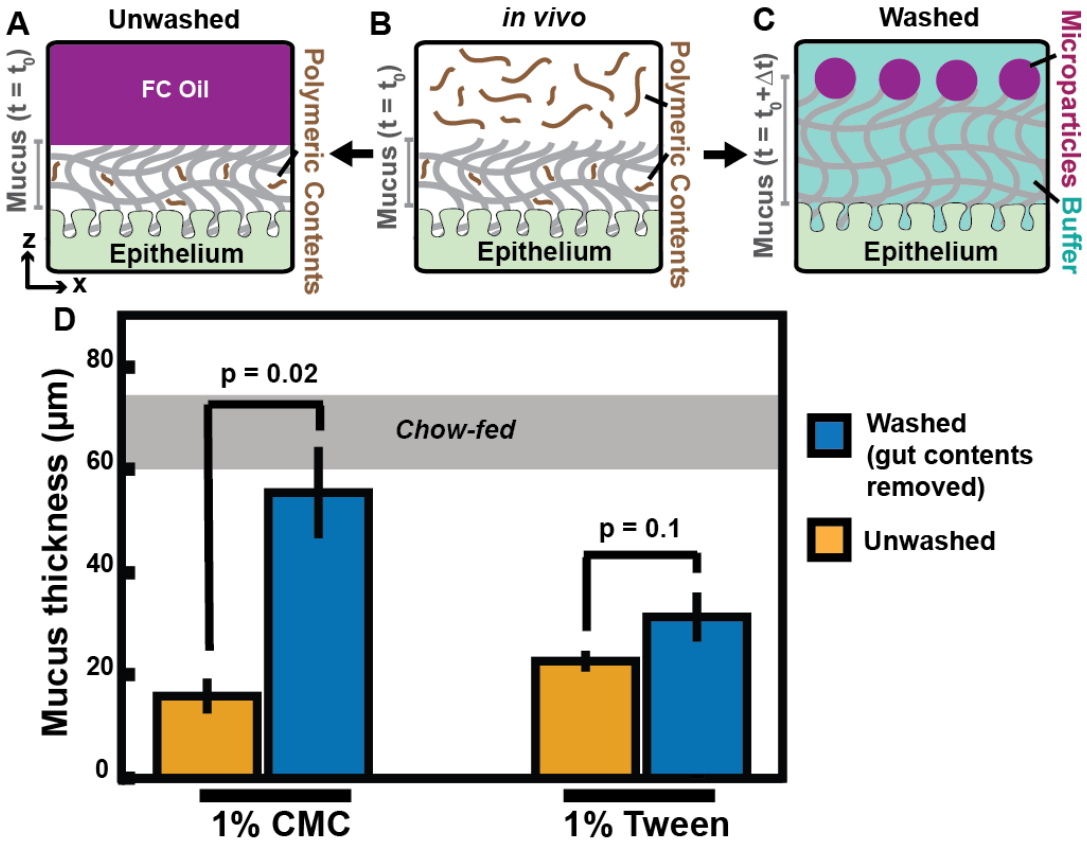

Figure 4.2: Carboxymethyl cellulose (CMC) compresses the colonic mucus hydrogel *in vivo.* (A–B) Cartoon side-view depicting the fluorocarbon (FC) oil imaging setup (A) which retains polymeric contents in contact with colonic mucus, prevents dehydration, and maintains mucus at a similar thickness (t) to that of initial *in vivo* thickness (t_0). *In vivo* (*B*), the mucus hydrogel is in contact with polymeric contents that can compress mucus. (C) Cartoon side-view depicting the microparticle imaging setup in which polymeric contents are washed away with buffer and particles with a diameter (d) greater than the mucus mesh size (ξ) are used to measure mucus thickness. Mucus thickness increases (Δt) from *in vivo* when "compressive" polymers are absent. (D) Mucus thickness measurements from mice fed either a solution of 1% CMC + 5% sucrose (1% CMC) or a solution of 1%

Tween + 5% sucrose (1% Tween) for 23 h. Mucus thickness is plotted on the vertical axis (in μm) for different groups of mice. Measurements using the microparticle approach ("washed (gut contents removed)") are blue; thickness measurements obtained using the FC-oil approach ("unwashed") are orange (see ref. 6 for details and validation of approach). Thickness measurements represent the average thickness measured on explants from individual mice. Error bars are standard error of the mean (SEM) where n = the number of mice. All groups contained at least 3 mice. P-values were obtained using Welch's t-test. Grey bar across figure indicates mucus thickness measured for chow-fed mice using FC oil approach from our previous study,[6] where we measured $t = 67 \pm 7\ \mu m$ (mean ± SEM). Bottom of bar is $t = 60\ \mu m$, top of bar is $t = 74\ \mu m$.

Carboxymethyl cellulose (CMC) degree of charge increases extent of mucus compression. We next sought to understand the mechanism by which CMC compresses the colonic mucus hydrogel. Here, we aimed to test whether modulating the amount of charge on CMC could influence the extent of mucus compression. We first tested if CMC compressed mucus *ex vivo*. We used our microparticle approach to measure the initial thickness of mucus (t_0) on a colonic explant, then placed the explant in a solution of 1% w/v CMC DS 0.7 (Figure 4.2A), waited 10 min, and measured the thickness (t_f) (Figure 4.2B). We found that CMC compressed the mucus hydrogel (Figure 4.2A) and that the extent of compression remained constant over the course of 30 min (Figure 4.S2), suggesting that the system had reached a steady state. Similarly, in our previous study, we found compression by an uncharged polymer (polyethylene glycol) was constant over the course of 60 min.[6] Additionally, for CMC, the compression was reversible—by washing out the CMC solution with buffer, the hydrogel returned to its initial thickness (Figure 4.S2).

To understand how polymer negative charge affects the extent of compression, we next compared how mucus compression differed as a function of polymer concentration for CMC DS 0.7, CMC DS 0.9 (a derivative of CMC that is more charged than CMC DS 0.7), and hydroxyethyl cellulose (HEC, a cellulose derivative with the same chemical backbone but no charge). Each polymer was added in a range of concentrations that are approved by the FDA for addition to food[11] and commonly used in processed foods.[9]

Generally, the extent of mucus compression increased with increased polymer concentration for all three polymers (Figure 4.2C). We found that at most polymer concentrations, the more highly negatively charged polymer (CMC DS 0.9) induced the most compression (Figure 4.2C). In contrast, the neutral polymer (HEC) generally induced the least compression at any given polymer concentration (Figure 4.2C). These data suggest that, generally, the negative charge of the polymer increases the extent of mucus compression.

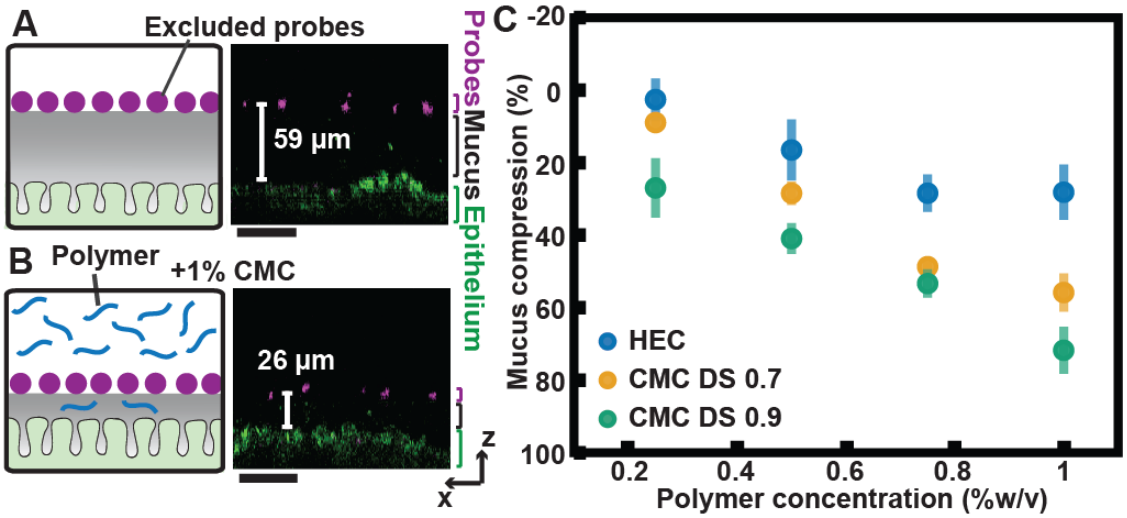

Figure 4.3: Negatively charged CMC compresses mucus *ex vivo* more than uncharged polymers. (A-B) Cartoons (left) and images (right) in side-view show the 1-µm-diameter particles (purple) sitting on top of the mucus before (A) and after (B) the addition of 1% w/v CMC solution. Epithelium is shown in green. (C) Plot of mucus compression (where % compression = $[\Delta t/t_0]*100\%$, further details in *Materials and Methods*) as a function of polymer concentration (% w/v). Each data point represents the average of compression measured on three independent replicates (three explants from different mice), where the compression from an individual replicate is the average of 5 compression measurements at lateral positions on the explant. Error bars are SEM with n = 3. HEC = hydroxyethyl cellulose, CMC DS 0.7 = CMC with a degree of substitution of 7 negatively charged groups per 10 monomers, and CMC DS 0.9 = CMC with a degree of substitution of 9 negatively charged groups per 10 monomers. Images shown in side-views were processed as described in ref. 6 and Figure 4.S1.

Mucus compression due to charged polymers is consistent with a Donnan mechanism.

We knew from previous studies with the colonic mucus hydrogel and the perciliary brush

that the polymer-induced compression of biological polymer networks can be driven by the differences in osmotic pressure between the external polymer solution and the solution phase within the cross-linked polymer network.[6,35] In such scenarios, the osmotic pressure difference (ΔΠ) drives the flux of water out of the polymer network, causing the network to shrink or compress; the equilibrium gel volume is determined by the balance between ΔΠ on one hand, and the mixing pressure (due to the change in free energy from mixing the gel with solvent and free polymer) and the pressure associated with the elastic deformation of the network chains on the other.[36] Polyelectrolyte solutions and gels can also preferentially partition ions between phases,[19,37,38] causing an increase in the osmotic pressure of the polyelectrolyte phase compared with the external solution phase with which it is in contact. This is what is known as Donnan partitioning or a Donnan mechanism. Given that both CMC and the colonic mucus hydrogel itself are both negatively charged, we therefore hypothesized that the theory of Donnan partitioning could be used to explain the enhancement of mucus compression we observed with increased polymer charge.

Before testing our hypothesis with numerical calculations, we first wanted to understand if mucus exhibits Donnan partitioning in a simple scenario, when the colonic mucus hydrogel is placed in a buffered solution without CMC. First, we write down the condition of electroneutrality for both the external buffer solution (ext) and inside mucus (int):[39,40]

$$c_+^{ext} = c_-^{ext} = c_0 \tag{4.1}$$

$$c_+^{int} = c_-^{int} + m \tag{4.2}$$

where c_+ denotes the molar concentration of mobile cations, c_- is the molar concentration of mobile anions, c_0 is the concentration of monovalent salt, and m is the molar concentration of charges on mucus (this analysis assumes that the polyelectrolyte

counterions are the same as the salt cations. In this case the cation for CMC is Na^+ and the cation in the buffer is predominantly Na^+, as explained below). Invoking the equality of electrochemical potential for the mobile ions and combining eq 4.1-2 gives us:

$$\frac{c_+^{int}}{c_0} = \frac{m}{2c_0} + \sqrt{\left(\frac{m}{2c_0}\right)^2 + 1}$$

(4.3)

Eq 4.3 gives the fractional increase of positively charged ions inside the mucus hydrogel due to Donnan partitioning. In our experiments, we use PBS as the buffer, which by molar concentration is ~90% NaCl. Therefore, we approximated the ionic strength to be equal to the molar concentration of NaCl: $c_0 = 137\ mM$. We can estimate the molar concentration of negative charges on mucus by estimating the volume fraction of mucus (ϕ_m) to be $\phi_m \sim 1\%$ (this is consistent with results from the literature: refs. 6,41–43) which, combined with the amount of charged groups per mucin,[40] yields $m \sim 5\ mM$. This yields: $\frac{c_+^{int}}{c_0} \cong 1.02$. We can therefore assume that any differential salt partitioning by the colonic mucus hydrogel itself at physiological ionic strengths is negligible.

Our previous numerical results for polymer-induced mucus compression[6] suggested that an uncharged polymer of a similar MW and radius of gyration (R_g) to the polymers used in this study (PEG 200 kDa with $R_g \sim 22\ nm$) is mostly excluded from mucus—the ratio of polymers inside mucus to the polymers in the external solution was at most ~0.3 and approached 0 as the polymer concentration increased. The HEC and CMC used in this study are slightly larger than PEG 200 kDa; the measured hydrodynamic radius (R_h) of HEC and CMC from our gel permeation chromatography (GPC) measurements (see Table 4.S1, Figure 4.S3) is $R_h \sim 20\ nm$, which we can use in conjunction with the Kirkwood–Risemann relation[44] to estimate $R_g \sim 30\ nm$. In addition, the charged polymers should experience electrostatic repulsions with the mucin strands (which also have some negative

charge). We would therefore expect that HEC and CMC should be even more excluded from mucus than PEG 200 kDa. If we then take as a second simplifying assumption that the polymer is completely excluded from mucus, we can write down ΔΠ (in units of *Pa*) as:[17]

$$\Delta\Pi = \Delta\Pi_{ion} + \Pi_{pol}$$

(4.4)

where $\Delta\Pi_{ion}$ is due to Donnan partitioning of the small ions between the external polyelectrolyte solution and the mucus network and can be written as (see Supporting Information for derivation):

$$\frac{\Delta\Pi_{ion}}{RT} = 2c_0 + p - 2\sqrt{c_0(c_0 + p)}$$

(4.5)

where R is the gas constant, T is the temperature (in kelvin), and p is the molar concentration of charges from the charged polymer (which we know because the number of charges per monomer is given by the manufacturer and we determined the polymer MW by GPC, Table 4.S1, Figure 4.S3). The polymer osmotic pressure (Π_{pol}) for an uncharged polymer can be written as:[45]

$$\frac{\Pi_{pol}}{RT} = \frac{c_p}{MW}\left(1 + \left(\frac{c_p}{c_p^*}\right)^{1.3}\right)$$

(4.6)

where c_p is the polymer concentration (in kg/m^3), *MW* is the polymer molecular weight (in *Da*), and c_p^* is the polymer overlap concentration (in kg/m^3), which can be estimated as:[45]

$$c_p^* = \frac{MW}{\frac{4\pi}{3} N_{avo} R_g^3}$$

(4.7)

where N_{avo} is the Avogadro number, and R_g is the polymer radius of gyration (in *m*). The polymer MW, based on our GPC measurements, is ~150 kDa (Table 4.S1, Figure 4.S3). We can use this along with the polymer R_g and eq. 4.7 to calculate $c_p^* \approx 1.9\ kg/m^3$. This justifies the use of eq 4.6 for the polymer osmotic pressure instead of the osmotic pressure for a dilute polymer solution (which would simply be the first term of eq 4.6) because the polymer concentrations we test in this study all exceed the polymer overlap concentration, meriting the inclusion of the second term in eq 4.6 which accounts for the behavior above overlap concentration. Using eq 4.4-7, we estimated ΔΠ for both the neutral and charged polymers used in Figure 4.2C. For the charged polymers, the ionic contribution to the osmotic pressure (eq 4.5) is substantially greater than that of the polymer contribution (eq 4.6) at all polymer concentrations, suggesting the Donnan mechanism contributes more to ΔΠ (see Figure 4.S4). We plotted the extent of mucus compression against ΔΠ in Figure 4.3B. We found that the extent of compression generally increases with ΔΠ. Furthermore, the relationship between mucus compression and ΔΠ has a similar functional form to the classical stress—elongation relation for uniaxial deformations from the affine network model, which has been used previously to describe the compression of hydrogels composed of biopolymers[46,47] and synthetic polymers,[48,49] and can be written as:[45]

$$\sigma_{eng} = -G(\lambda - \frac{1}{\lambda^2})$$

(4.8)

where σ_{eng} is the engineering stress or the applied stress on the network (which in this case is ΔΠ), *G* is the modulus of rigidity (or shear modulus) of the network (in *Pa*), and λ is the deformation factor, which is related to *% mucus compression* through: $\lambda = 1 -$

$\frac{\%\ mucus\ compression}{100}$. The negative sign is included because the stress is compressive. A fit to eq 4.8 is plotted as the dashed line in Figure 4.3B. We take G as the one free parameter in this fit, which yields $G \sim 750\ Pa$. We are not aware of directly measured values for G for colonic mucus. However, this fitted value is of the same order of magnitude as that estimated using available literature data (see Supporting Information for details). Ultimately, it is both the collapse of the mucus compression data largely onto a single curve in Figure 4.3B and the functional form of this curve which suggest that the mucus hydrogel is undergoing a form of uniaxial deformation induced by ΔΠ.

Overall, this analysis suggests that it is the difference in osmotic pressure between the external polyelectrolyte solution phase and the solution phase within the mucus hydrogel which drives the compression of mucus by CMC. It further suggests that the difference in osmotic pressure and the concomitant compression is increased for polyelectrolytes via a Donnan mechanism.

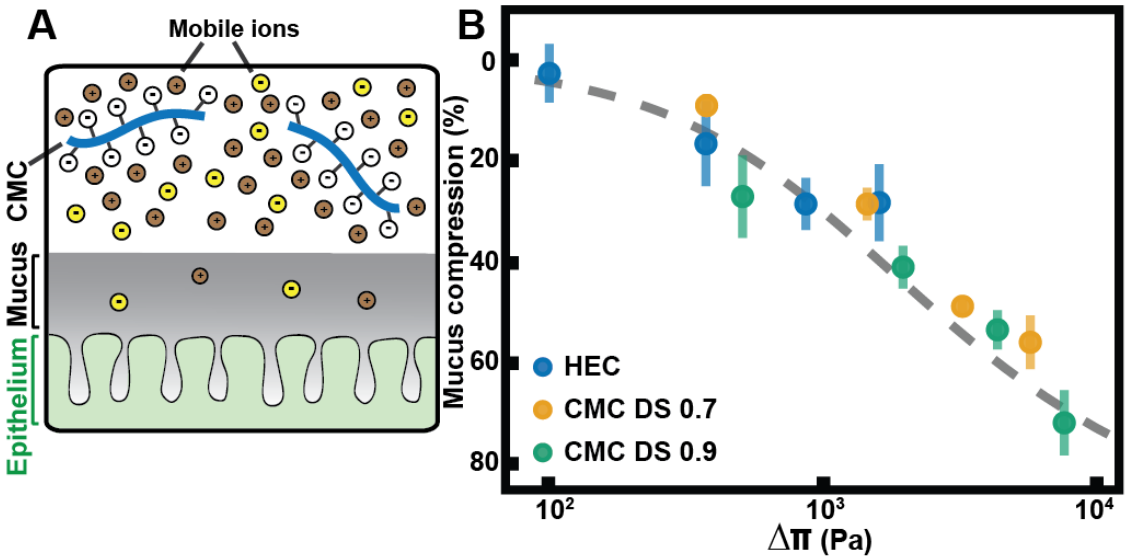

Figure 4.4: The extent of mucus compression plotted against the difference in osmotic pressure ($\Delta\Pi$) due to the added polymer. (A) Cartoon depicting the theoretical picture of Donnan partitioning by charged polymers (labeled "CMC"). Mobile ions are preferentially partitioned outside of mucus by the charged polymers. (B) Extent of mucus compression plotted against the theoretical calculation of $\Delta\Pi$. Compression values are the same experimental data as Fig. 2*C*. Dashed line is a fit to the classical stress-elongation relation, where $\Delta\Pi = G(\lambda - \frac{1}{\lambda^2})$, and $\lambda = 1 - \frac{\%\ mucus\ compression}{100}$. G (the modulus of rigidity) was

used as a free parameter and in the fit is G = 749 Pa. HEC = Hydroxyethyl cellulose, CMC DS 0.7 = carboxymethyl cellulose with a degree of substitution of 7 charged monomers per 10 monomers, CMC DS 0.9 = carboxymethyl cellulose with a degree of substitution of 9 charged monomers per 10 monomers.

Increasing ionic strength decreases mucus compression by polyelectrolytes. Because our data in Figure 4.3B suggested that the increase in the amount of compression we see for polyelectrolytes is due to a Donnan mechanism, we devised a simple set of experiments to test this hypothesis further. It is known that the amount of Donnan partitioning decreases with increasing salt concentration (this can be seen by inspection of eq 4.3 and 4.5). We therefore formulated two hypotheses: (i) Polyelectrolyte-induced compression will be reduced by high ionic strength because $\Delta\Pi_{ion}$ is reduced (see Figure 4.4A,B). (ii) For uncharged polymers, the amount of compression will remain the same when the ionic strength is increased because there is no contribution from $\Delta\Pi_{ion}$ at any ionic strength.

We expect the most significant increase in compression due to Donnan partitioning to occur in the 1% w/v CMC DS 0.9 solution, which has the highest molar concentration of charges. By solving eq 4.5, we find that for 1% CMC DS 0.9 in a 1x PBS solution ($c_0 \sim 0.137\ M$), $\Pi_{ion} \sim 6000\ Pa$. If we increase the ionic strength ten-fold to $c_0 \sim 1.37\ M$ by using a 10x PBS solution, this decreases to $\Pi_{ion} \sim 700\ Pa$. We would therefore anticipate that such an increase in the ionic strength would reduce the compression caused by 1% CMC DS 0.9.

We then tested our hypothesis experimentally by comparing the measured compression for 1% CMC DS 0.9 in 1x PBS to that of 1% CMC DS 0.9 in 10x PBS and found, consistent with our first hypothesis, that there was more compression in the 1X PBS solution (Figure 4.4C). We then tested if the high ionic strength treatment (10X PBS) affected the amount of compression for 1% HEC (an uncharged polymer) and found, consistent with our second hypothesis, that compression was the same for the 1X and 10X PBS treatments (Figure 4.4C). As a control, to ensure that the high ionic strength was not disrupting the integrity of the mucus hydrogel and eliminating its compressibility, we tested for compression on

colonic explants with 10X PBS at a high concentration of HEC (5% w/v). We found the mucus compressed to equal amounts in both the 1X and 10X PBS treatments (Figure 4.4C), suggesting that high ionic strength does not disrupt the integrity of the colonic mucus hydrogel.

Overall, these data suggest that the increase in mucus compression observed in response to polyelectrolytes, compared with uncharged polymers, is due to the preferential partitioning of mobile ions into the external solution (i.e., a Donnan mechanism). The concomitant increase in the osmotic pressure difference between the solution and mucus hydrogel results in this increase in compression.

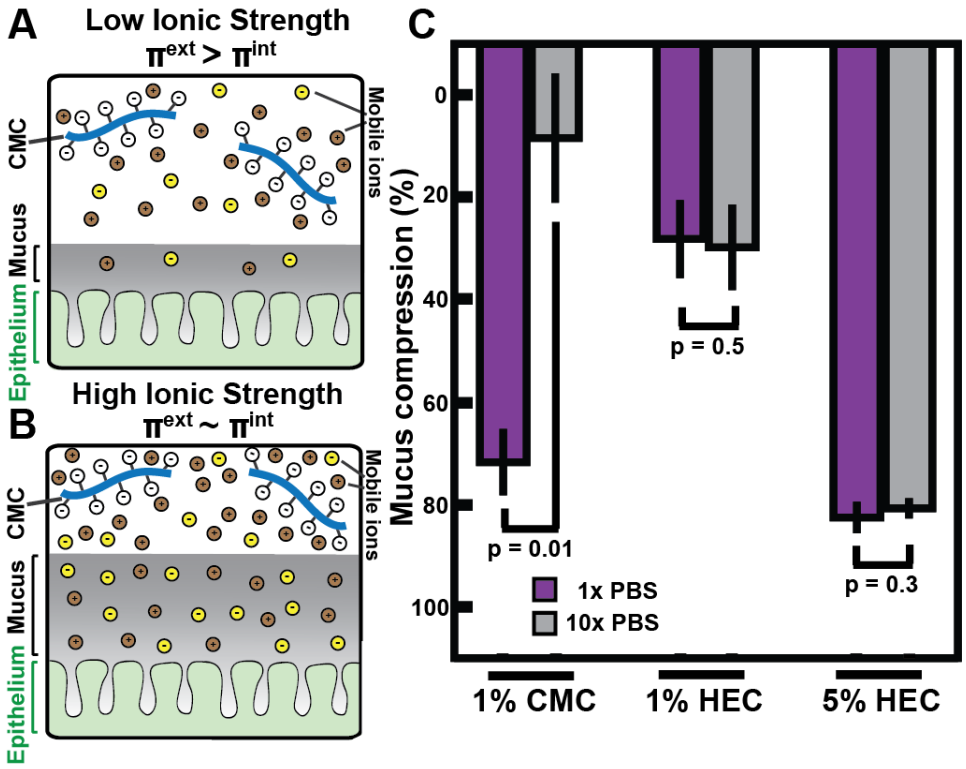

Figure 4.5: Increasing the ionic strength decreases the extent of polyelectrolyte-induced mucus compression, consistent with a Donnan mechanism. (A-B) Schematic depicting the decrease in polyelectrolyte-induced mucus compression in buffer solutions with high ionic strength. (A) When ionic strength is low, there is a greater difference in the concentrations of mobile ions in the external phase (the polymer solution) and internal phase (the mucus gel). Subsequently, there is a greater difference in the external osmotic pressure (Π^{ext}) compared to the internal osmotic pressure (Π^{int}). (B) When ionic strength is high,

polyelectrolytes still partition mobile ions, but there is a smaller difference in the concentrations of mobile ions between the polymer solution and the mucus hydrogel. Therefore, there is a smaller difference in Π^{ext} compared to Π^{int}. (C) Extent of mucus compression as determined via the microparticle imaging approach. Each bar represents the mean of compression measurements from three biological replicates (each replicate is a colonic explant from a mouse). The compression value from each individual replicate is the average of compression measurements acquired at 5 different lateral positions on that explant. Error bars are SEM with n = 3. P-values were computed using the Welch's t-test; 1% CMC = 1% w/v carboxymethyl cellulose with DS 0.9, 1% HEC = 1% w/v hydroxyethyl cellulose, 5% HEC = 5% w/v hydroxyethyl cellulose, 10x PBS = phosphate buffered saline at 10-fold its normal concentration, 1x PBS = phosphate buffered saline at its normal concentration.

Conclusions

There is considerable interest in understanding how diet impacts the composition and spatial structure of the gut microbiota and any concomitant effects that may impact the physical structure of the gut (e.g. mucus) and its physiology.[4,14,15] However, few studies have focused on understanding the underlying physics behind how the polymeric additives in food *directly* interact with gut structure and physiology.[6] Food science has traditionally focused more narrowly on aspects of food design such as the packaging, preservation, processing, and safety of food.[9,50] Yet research is showing that, at least in animal models, even in approved concentrations, some GRAS food additives are correlated with markers of disease (such as inflammation and obesity[14,15]). Thus, it is important to improve our quantitative understanding of how these food additives interact with the host and modify gut physiology. In particular, there is a need to understand how food additives interact with mucus, the critical barrier in the colon that mediates host-microbe interactions and protects the host against physical damage.[1] Changes to the thickness and mesh size of the colonic mucus barrier have been associated with dramatic changes in host health.[7,8,14]

In this work, we found that a polyelectrolyte, CMC, compresses mucus reversibly *in vivo*, in contrast to an emulsifier (Tween), which appeared to irreversibly disrupt mucus. We

found that the amount of mucus compression induced by CMC increased as a function of the degree of polymer charge, which is a characteristic that has not been considered in the design of food products. Furthermore, we found that the increase in the amount of compression due to polymer charge is consistent with a Donnan mechanism. A simple, one-parameter model was found to be sufficient to quantitatively capture the observed behavior. We have offered a potential explanation for the phenomenon observed in this work using the theoretical framework of Donnan partitioning; however, more comprehensive theoretical models need to be developed and tested to completely understand this mechanism and explicitly account for the possible penetration of polyelectrolytes into the mucus hydrogel.

Our work so far has not considered how fluid flow, possible rheological effects such as viscous relaxation of mucus on longer timescales,[42,51] and possible anisotropy in the structure of the colonic mucus hydrogel[2] affect polymer-induced compression. Additionally, another factor *in vivo* is the regulation of isotonicity between the gut lumen and epithelium by the active transport of water and salts.[52] It is unclear how much this last factor would impact the observed phenomenon for two reasons: (i) small changes in the flux of water and salts will affect the base osmotic pressure (i.e., the osmotic pressure both inside the hydrogel and in the lumen) but not the difference in osmotic pressure inside and outside the hydrogel, and (ii) our experiments and calculations suggest that the described Donnan effects disappear at ten-fold physiological ionic strength which is unlikely to occur *in vivo*. However, all of these effects will be important areas to investigate in future work to understand how different polymers compress mucus *in vivo.*

The system we have considered in this work is an example of a class of systems consisting of a polyelectrolyte solution directly interacting with a biological, polyelectrolyte network. Such systems can be found throughout nature; other examples include biofilms in contact with extracellular DNA,[53] medical hydrogels in contact with gut polymers,[54] ECM in contact with interstitial fluid,[55] and hyaluronic acid-lubricin networks (which lubricate our joints) in contact with synovial fluid.[56] Our work begins to unravel this physics in the

context of polyelectrolyte-induced mucus compression, which could lead to new, safer design of food products that do not alter the structure of colonic mucus.

Corresponding Author

*To whom correspondence should be addressed.

Tel: +1 626 395 2333; Fax: +1 626 568 8743; Email: rustem.admin@caltech.edu

Author Contributions

APS and RFI designed the research; APS performed the research; APS analyzed the data. ZGW guided the theoretical analysis. All authors wrote the paper.

Funding Sources

Army Research Office (ARO) Multidisciplinary University Research Initiative (MURI) contract #W911NF-17-1-0402

Jacobs Institute for Molecular Engineering for Medicine

Center for Environmental Microbial Interactions (CEMI)

NSF Graduate Research Fellowship DGE-144469

Caldwell CEMI Graduate Fellowship

Notes

The technology described in this publication is the subject of a patent application filed by Caltech.

Acknowledgements

This work was supported in part by Army Research Office (ARO) Multidisciplinary University Research Initiative (MURI) contract #W911NF-17-1-0402, the Jacobs Institute for Molecular Engineering for Medicine, the Center for Environmental Microbial Interactions (CEMI), an NSF Graduate Research Fellowship DGE-144469 (to APS), and a Caldwell CEMI Graduate Fellowship (to APS). We acknowledge Michael Porter for useful discussions and providing feedback on the manuscript; Andres Collazo and Caltech's Beckman Institute Biological Imaging Facility, the Caltech Office of Laboratory Animal Resources, and the Caltech veterinary technicians for technical support; Justin Rolando for providing microparticles; and Natasha Shelby for contributions to writing and editing this manuscript.

References

(1) Johansson, M. E. V; Larsson, J. M. H.; Hansson, G. C. The Two Mucus Layers of Colon Are Organized by the MUC2 Mucin, Whereas the Outer Layer Is a Legislator of Host-Microbial Interactions. *Proc. Natl. Acad. Sci. U. S. A.* **2011**, *108*, 4659–4665. https://doi.org/10.1073/pnas.1006451107.

(2) Ambort, D.; Johansson, M. E. V.; Gustafsson, J. K.; Nilsson, H. E.; Ermund, a.; Johansson, B. R.; Koeck, P. J. B.; Hebert, H.; Hansson, G. C. Calcium and PH-Dependent Packing and Release of the Gel-Forming MUC2 Mucin. *Proc. Natl. Acad. Sci.* **2012**, *109* (15), 5645–5650. https://doi.org/10.1073/pnas.1120269109.

(3) Verdugo, P. Supramolecular Dynamics of Mucus. *Cold Spring Harb. Perspect. Med.* **2012**, *2* (11). https://doi.org/10.1101/cshperspect.a009597.

(4) Desai, M. S.; Seekatz, A. M.; Koropatkin, N. M.; Kamada, N.; Hickey, C. A.; Wolter, M.; Pudlo, N. A.; Kitamoto, S.; Terrapon, N.; Muller, A.; et al. A Dietary Fiber-Deprived Gut Microbiota Degrades the Colonic Mucus Barrier and Enhances Pathogen

Susceptibility. *Cell* **2016**, *167* (5), 1339–1353.e21. https://doi.org/10.1016/j.cell.2016.10.043.

(5) Johansson, M. E. V.; Jakobsson, H. E.; Holmén-Larsson, J.; Schütte, A.; Ermund, A.; Rodríguez-Piñeiro, A. M.; Arike, L.; Wising, C.; Svensson, F.; Bäckhed, F.; et al. Normalization of Host Intestinal Mucus Layers Requires Long-Term Microbial Colonization. *Cell Host Microbe* **2015**, 1–11. https://doi.org/10.1016/j.chom.2015.10.007.

(6) Datta, S. S.; Preska Steinberg, A.; Ismagilov, R. F. Polymers in the Gut Compress the Colonic Mucus Hydrogel. *Proc. Natl. Acad. Sci. U. S. A.* **2016**, *113* (26), 7041–7046. https://doi.org/10.1073/pnas.1602789113.

(7) Johansson, M. E. V; Gustafsson, J. K.; Holmen-Larsson, J.; Jabbar, K. S.; Xia, L.; Xu, H.; Ghishan, F. K.; Carvalho, F. A.; Gewirtz, A. T.; Sjovall, H.; et al. Bacteria Penetrate the Normally Impenetrable Inner Colon Mucus Layer in Both Murine Colitis Models and Patients with Ulcerative Colitis. *Gut* **2014**, *63* (2), 281–291. https://doi.org/10.1136/gutjnl-2012-303207.

(8) Bergstrom, K. S. B.; Kissoon-Singh, V.; Gibson, D. L.; Ma, C.; Montero, M.; Sham, H. P.; Ryz, N.; Huang, T.; Velcich, A.; Finlay, B. B.; et al. Muc2 Protects against Lethal Infectious Colitis by Disassociating Pathogenic and Commensal Bacteria from the Colonic Mucosa. *PLoS Pathog.* **2010**, *6* (5). https://doi.org/10.1371/journal.ppat.1000902.

(9) Goff, H. D.; Hartel, R. W. *Ice Cream*; SpringerLink : Bücher; Springer US, 2013.

(10) Saha, D.; Bhattacharya, S. Hydrocolloids as Thickening and Gelling Agents in Food: A Critical Review. *J. Food Sci. Technol.* **2010**, *47* (6), 587–597. https://doi.org/10.1007/s13197-010-0162-6.

(11) FDA. *CFR - Code of Federal Regulations Title 21*; 2018.

(12) Hollabaugh, C. B.; Burt, L. H.; Walsh, A. P. Carboxymethylcellulose. Uses and Applications. *Ind. Eng. Chem.* **1945**, *37* (10), 943–947. https://doi.org/10.1021/ie50430a015.

(13) Leskauskaite, D.; Jasutiene, I.; Kersiene, M.; Malinauskyte, E.; Matusevicius, P. The Effect of Carboxymethyl Cellulose on the Stability of Emulsions Stabilized by Whey Proteins under Digestion in Vitro and in Vivo. *Int. J. Agric. Biosyst. Sci. Eng.* **2013**, *7* (7), 51–56.

(14) Chassaing, B.; Koren, O.; Goodrich, J. K.; Poole, A. C.; Srinivasan, S.; Ley, R. E.; Gewirtz, A. T. Dietary Emulsifiers Impact the Mouse Gut Microbiota Promoting Colitis and Metabolic Syndrome. *Nature* **2015**, *519* (7541), 92–96. https://doi.org/10.1038/nature14232.

(15) Chassaing, B.; Van De Wiele, T.; De Bodt, J.; Marzorati, M.; Gewirtz, A. T. Dietary Emulsifiers Directly Alter Human Microbiota Composition and Gene Expression Ex Vivo Potentiating Intestinal Inflammation. *Gut* **2017**, *66* (8), 1414–1427. https://doi.org/10.1136/gutjnl-2016-313099.

(16) Lock, J. Y.; Carlson, T. L.; Wang, C.-M.; Chen, A.; Carrier, R. L. Acute Exposure to Commonly Ingested Emulsifiers Alters Intestinal Mucus Structure and Transport Properties. *Sci. Rep.* **2018**, *8* (1), 10008. https://doi.org/10.1038/s41598-018-27957-2.

(17) Dobrynin, A. V.; Rubinstein, M. Theory of Polyelectrolytes in Solutions and at Surfaces. *Prog. Polym. Sci.* **2005**, *30* (11), 1049–1118. https://doi.org/10.1016/j.progpolymsci.2005.07.006.

(18) Rubinstein, M.; Papoian, G. a. Polyelectrolytes in Biology and Soft Matter. *Soft Matter* **2012**, *8* (36), 9265. https://doi.org/10.1039/c2sm90104h.

(19) Flory, P. J. *Principles of Polymer Chemistry*; Cornell University Press: Ithaca, New York, 1953.

(20) Kudaibergenov, S. E.; Nuraje, N.; Khutoryanskiy, V. V. Amphoteric Nano-, Micro-, and Macrogels, Membranes, and Thin Films. *Soft Matter* **2012**, *8* (36), 9302–9321. https://doi.org/10.1039/c2sm25766a.

(21) Priftis, D.; Tirrell, M. Phase Behaviour and Complex Coacervation of Aqueous Polypeptide Solutions. *Soft Matter* **2012**, *8* (36), 9396–9405. https://doi.org/10.1039/c2sm25604e.

(22) De Kruif, C. G.; Weinbreck, F.; De Vries, R. Complex Coacervation of Proteins and Anionic Polysaccharides. *Curr. Opin. Colloid Interface Sci.* **2004**, *9* (5), 340–349. https://doi.org/10.1016/j.cocis.2004.09.006.

(23) Schiessel, H.; Correa-Rodríguez, M. D.; Rudiuk, S.; Baigl, D.; Yoshikawa, K. Theory of DNA-Cationic Micelle Complexation. *Soft Matter* **2012**, *8* (36), 9406–9411. https://doi.org/10.1039/c2sm25603g.

(24) Sennato, S.; Truzzolillo, D.; Bordi, F. Aggregation and Stability of Polyelectrolyte-Decorated Liposome Complexes in Water-Salt Media. *Soft Matter* **2012**, *8* (36), 9384–9395. https://doi.org/10.1039/c2sm25576f.

(25) Kiefer, J.; Naser, M.; Kamel, A.; Carnali, J. Osmotic Deswelling of Microgels by Linear Polyelectrolytes. *Colloid Polym. Sci.* **1993**, *271* (3), 253–261.

(26) Elderman, M.; Sovran, B.; Hugenholtz, F.; Graversen, K.; Huijskes, M.; Houtsma, E.; Belzer, C.; Boekschoten, M.; De Vos, P.; Dekker, J.; et al. The Effect of Age on the Intestinal Mucus Thickness, Microbiota Composition and Immunity in Relation to Sex in Mice. *PLoS One* **2017**, *12* (9), 1–22. https://doi.org/10.1371/journal.pone.0184274.

(27) Sovran, B.; Hugenholtz, F.; Elderman, M.; Van Beek, A. A.; Graversen, K.; Huijskes, M.; Boekschoten, M. V.; Savelkoul, H. F. J.; De Vos, P.; Dekker, J.; et al. Age-Associated Impairment of the Mucus Barrier Function Is Associated with Profound

Changes in Microbiota and Immunity. *Sci. Rep.* **2019**, *9* (1), 1–13. https://doi.org/10.1038/s41598-018-35228-3.

(28) Leary, S.; Underwood, W.; Anthony, R.; Cartner, S. AVMA Guidelines for the Euthanasia of Animals: 2013 Edition https://www.avma.org/kb/policies/documents/euthanasia.pdf (accessed Jun 11, 2018). https://doi.org/10.1016/B978-012088449-0.50009-1.

(29) Preska Steinberg, A.; Datta, S. S.; Naragon, T.; Rolando, J.; Bogatyrev, S.; Ismagilov, R. F. High-Molecular-Weight Polymers from Dietary Fiber Drive Aggregation of Particulates in the Murine Small Intestine. *Elife* **2019**, *8*, e40387. https://doi.org/10.1101/490920.

(30) Hoogendam, C. W.; De Keizer, A.; Cohen Stuart, M. A.; Bijsterbosch, B. H.; Smit, J. A. M.; Van Dijk, J. A. P. P.; Van Der Horst, P. M.; Batelaan, J. G. Persistence Length of Carboxymethyl Cellulose as Evaluated from Size Exclusion Chromatography and Potentiometric Titrations. *Macromolecules* **1998**, *31* (18), 6297–6309. https://doi.org/10.1021/ma971032i.

(31) Sjöholm, E. Size Exclusion Chromatography of Cellulose and Cellulose Derivatives. *Handb. size exclusion Chromatogr.* **2004**, 331–352.

(32) Gustafsson, J. K.; Ermund, A.; Johansson, M. E. V; Schütte, A.; Hansson, G. C.; Sjövall, H. An Ex Vivo Method for Studying Mucus Formation, Properties, and Thickness in Human Colonic Biopsies and Mouse Small and Large Intestinal Explants. *Am. J. Physiol. Gastrointest. Liver Physiol.* **2012**, *302* (4), G430-8. https://doi.org/10.1152/ajpgi.00405.2011.

(33) Wang, Y.-Y.; Lai, S. K.; Suk, J. S.; Pace, A.; Cone, R.; Hanes, J. Addressing the PEG Mucoadhesivity Paradox to Engineer Nanoparticles That “Slip” through the Human Mucus Barrier. *Angew. Chemie-International Ed.* **2008**, *47* (50), 9726–9729. https://doi.org/10.1002/anie.200803526.

(34) Viennois, E.; Merlin, D.; Gewirtz, A. T.; Chassaing, B. Dietary Emulsifier-Induced Low-Grade Inflammation Promotes Colon Carcinogenesis. *Cancer Res.* **2017**, *77* (1), 27–40. https://doi.org/10.1158/0008-5472.CAN-16-1359.

(35) Button, B.; Cai, L.-H.; Ehre, C.; Kesimer, M.; Hill, D. B.; Sheehan, J. K.; Boucher, R. C.; Rubinstein, M. A Periciliary Brush Promotes the Lung Health by Separating the Mucus Layer from Airway Epithelia. *Science* **2012**, *337* (6097), 937–941. https://doi.org/10.1126/science.1223012.

(36) Sierra-Martin, B.; Lietor-Santos, J. J.; Fernandez-Barbero, A.; Nguyen, T. T.; Fernandez-Nieves, A. Swelling Thermodynamics of Microgel Particles. In *Microgel Suspensions*; Fernandez-Nieves, A., Wyss, H. M., Mattsson, J., Weitz, D. A., Eds.; Wiley-VCH: Weinheim, 2011; pp 71–116.

(37) Carrillo, J. M. Y.; Dobrynin, A. V. Salt Effect on Osmotic Pressure of Polyelectrolyte Solutions: Simulation Study. *Polymers* **2014**, *6* (7), 1897–1913. https://doi.org/10.3390/polym6071897.

(38) Peppas, N. A.; Khare, A. R. Preparation , Structure and Diffusional Behavior of Hydrogels in Controlled Release. *Adv. Drug Deliv. Rev.* **1993**, *11*, 1–35.

(39) Overbeek, J. T. G. The Donnan Equilibrium. *Prog. Biophys. Biophys. Chem.* **1956**, *6*, 58–64.

(40) Li, L.; Lieleg, O.; Jang, S.; Ribbeck, K.; Han, J. A Microfluidic in Vitro System for the Quantitative Study of the Stomach Mucus Barrier Function. *Lab Chip* **2012**, *12* (20), 4071. https://doi.org/10.1039/c2lc40161d.

(41) Perez-Vilar, J. Mucin Granule Intraluminal Organization. *Am. J. Respir. Cell Mol. Biol.* **2007**, *36* (2), 183–190. https://doi.org/10.1165/rcmb.2006-0291TR.

(42) Lai, S. K.; Wang, Y.-Y.; Wirtz, D.; Hanes, J. Micro- and Macrorheology of Mucus. *Adv. Drug Deliv. Rev.* **2009**, *61* (2), 86–100. https://doi.org/10.1016/j.addr.2008.09.012.

(43) Georgiades, P.; Pudney, P. D.; Thornton, D. J.; Waigh, T. A. Particle Tracking Microrheology of Purified Gastrointestinal Mucins. *Biopolymers* **2014**, *101* (4), 366–377. https://doi.org/10.1002/bip.22372.

(44) Tanford, C. *Physical Chemistry of Macromolecules*; Wiley: New York, 1961.

(45) Rubinstein, M.; Colby, R. H. *Polymer Physics*; OUP Oxford: New York, 2003.

(46) Kong, H. J.; Lee, K. Y.; Mooney, D. J. Decoupling the Dependence of Rheological/Mechanical Properties of Hydrogels from Solids Concentration. *Polymer* **2002**, *43* (23), 6239–6246. https://doi.org/10.1016/S0032-3861(02)00559-1.

(47) Boral, S.; Saxena, A.; Bohidar, H. B. Syneresis in Agar Hydrogels. *Int. J. Biol. Macromol.* **2010**, *46* (2), 232–236. https://doi.org/10.1016/j.ijbiomac.2009.12.008.

(48) Skouri, R.; Schosseler, F.; Munch, J. P.; Candau, S. J. Swelling and Elastic Properties of Polyelectrolyte Gels. *Macromolecules* **1995**, *28* (1), 197–210. https://doi.org/10.1021/ma00105a026.

(49) Muniz, E. C.; Geuskens, G. Compressive Elastic Modulus of Polyacrylamide Hydrogels and Semi-IPNs with Poly(N-Isopropylacrylamide). *Macromolecules* **2001**, *34* (13), 4480–4484. https://doi.org/10.1021/ma001192l.

(50) Potter, N.; Hotchkiss, J. *Food Science*, 5th ed.; Springer Science & Business Media: New York, 1998.

(51) Sellers, L. a.; Allen, A.; Morris, E. R.; Ross-Murphy, S. B. The Rheology of Pig Small Intestinal and Colonic Mucus: Weakening of Gel Structure by Non-Mucin Components. *BBA - Gen. Subj.* **1991**, *1115* (2), 174–179. https://doi.org/10.1016/0304-4165(91)90027-E.

(52) Keely, S. J.; Montrose, M. H.; Barrett, K. E. *Electrolyte Secretion and Absorption: Small Intestine and Colon*; 2009; Vol. 1. https://doi.org/10.1002/9781444303254.ch14.

(53) Flemming, H.-C.; Wingender, J. The Biofilm Matrix. *Nat. Rev. Microbiol.* **2010**, *8* (9), 623–633. https://doi.org/10.1080/0892701031000072190.

(54) Sharpe, L. A.; Daily, A. M.; Horava, S. D.; Peppas, N. A. Therapeutic Applications of Hydrogels in Oral Drug Delivery. *Expert Opin. Drug Deliv.* **2014**, *11* (6), 901–915. https://doi.org/10.1517/17425247.2014.902047.

(55) Wiig, H.; Swartz, M. A. Interstitial Fluid and Lymph Formation and Transport: Physiological Regulation and Roles in Inflammation and Cancer. *Physiol. Rev.* **2012**, *92* (3), 1005–1060. https://doi.org/10.1152/physrev.00037.2011.

(56) Greene, G. W.; Banquy, X.; Lee, D. W.; Lowrey, D. D.; Yu, J.; Israelachvili, J. N. Adaptive Mechanically Controlled Lubrication Mechanism Found in Articular Joints. *Proc. Natl. Acad. Sci. U. S. A.* **2011**, *108* (13), 5255–5259. https://doi.org/10.1073/pnas.1101002108.

(57) Axelsson, M. A. B.; Asker, N.; Hansson, G. C. O-Glycosylated MUC2 Monomer and Dimer from LS 174T Cells Are Water- Soluble, Whereas Larger MUC2 Species Formed Early during Biosynthesis Are Insoluble and Contain Nonreducible Intermolecular Bonds. *J. Biol. Chem.* **1998**, *273* (30), 18864–18870. https://doi.org/10.1074/jbc.273.30.18864.

Supporting Information

Derivation of the ionic contribution to osmotic pressure due to Donnan partitioning. We imagine a negatively charged polyelectrolyte solution with added salt to be in contact with the mucus layer. We take the volume of the polyelectrolyte solution (V_P) to be much larger than that of the mucus layer (V_M), which is true in our *ex vivo* set-up. In our *ex vivo* experiments, the polyelectrolyte solution volume is $V_P \sim 200\ \mu L$, and we can estimate V_M using the average thickness of colonic mucus measured in ref. 6 ($t \sim 70\ \mu m$) and the *xy* dimensions of the explants (~1 by 1 *cm*), which gives $V_M \sim 7\ \mu L$. Therefore, $\frac{V_P}{V_M} \sim 30$, and we can assume that the salt and polyelectrolyte concentrations in the polyelectrolyte solution are unaffected by any partitioning of ions into the mucus layer.

The total concentration of salt cations in the polyelectrolyte solution from the condition of electroneutrality is simply (assuming the counterion of the polyelectrolyte is the same as the cation from salt, which is the case in our system):

$$c_+^p = c_0 + p$$

(4.S1)

where c_+^p is the total concentration of salt cations in the polyelectrolyte solution phase, c_0 is the salt concentration, and p is the charge concentration from the polyelectrolyte backbones. The concentration of the salt anions (c_-^p) is just:

$$c_-^p = c_0$$

(4.S2)

This gives an osmotic pressure due to the small ions in the polyelectrolyte solution phase as:

$$\Pi_{ion}^P = RT(2c_0 + p)$$

(4.S3)

where $R = N_{avo}k$ is the gas constant.

Now consider the small ion concentrations in the mucus layer. The mucus network contributes a fixed polyelectrolyte charge density of m. Electroneutrality then dictates:

$$c_+^m = c_-^m + m$$

(4.S4)

where c_+^m and c_-^m are the small cation and small anion concentrations, respectively. Let ψ be the potential difference between the mucus layer and the polyelectrolyte solution, then equality of electrochemical potential for the small ions entails:[39]

$$e\psi + RTlnc_+^m = RTlnc_+^p$$

(4.S5)

$$-e\psi + RTlnc_-^m = RTlnc_-^p$$

(4.S6)

Eq 4.S5 and 4.S6 can be combined to give:

$$c_+^m c_-^m = c_+^p c_-^p$$

(4.S7)

Combining eq 4.S1, 4.S2, 4.S4, and 4.S7 then gives:

$$c_+^m = \frac{1}{2}\left[\sqrt{m^2 + 4c_0(c_0 + p)} + m\right]$$

(4.S8)

and:

$$c_{-}^{m} = \frac{1}{2}\left[\sqrt{m^2 + 4c_0(c_0 + p)} - m\right]$$

(4.S9)

The osmotic pressure from the small ions in the mucus layer is thus:

$$\Pi_{ion}^{m} = RT\sqrt{m^2 + 4c_0(c_0 + p)}$$

(4.S10)

The osmotic pressure difference between the polyelectrolyte solution and the mucus layer due to ions ($\Delta\Pi_{ion}$) is obtained by subtracting eq 4.S10 from eq 4.S3:

$$\Delta\Pi_{ion} = RT\left[2c_0 + p - \sqrt{m^2 + 4c_0(c_0 + p)}\right]$$

(4.S11)

In the limit of $m \ll c_0$, the expression simplifies to:

$$\Delta\Pi_{ion} = RT\left[2c_0 + p - 2\sqrt{c_0(c_0 + p)}\right]$$

(4.S12)

Estimation of modulus of rigidity for the colonic mucus hydrogel. The simplest model for uniaxial deformations of a polymer network can be derived from the "affine network model", which assumes affine deformation of the polymer network. The driving physics behind deformations in this model is the entropic elasticity of the chains.[45] This model gives the classical stress-elongation relation as (also eq 4.9 in main text):

$$\sigma_{eng} = -G(\lambda - \frac{1}{\lambda^2})$$

(4.S13)

where σ_{eng} is the engineering stress or the applied stress on the network (which in this case we took to be ΔΠ), *G* is the modulus of rigidity (or shear modulus) of the network (in *Pa*), and λ is the deformation factor. The negative sign in front of *G* is due to the fact that we are applying a compressive stress. In this model, *G* can be written as:

$$G = \frac{\rho RT}{M_s}$$

(4.S14)

where ρ is the mass concentration of network strands (kg/m^3) and M_s is the MW of a network strand (in kDa). If we take the MW of a MUC2 network strand to be the MW of the polymer between network cross-links (often referred to as a "MUC2 monomer" in the biology literature), we can estimate $M_s \sim 400 - 600\ kDa$.[2,57] There are not existing literature values for the mass concentration of the murine colonic mucus hydrogel, but for porcine gastrointestinal mucus it is: $\rho \sim 19 - 30\ mg/mL$.[43,51] Taking the arithmetic mean of these values and inserting them into eq S14 yields $G \sim 120\ Pa$. We speculate that eq 4.S14 may be lower than the value for *G* obtained by the curve fitting done in Figure 4.3 because eq 4.S14 assumes that the network strands are non-interacting.

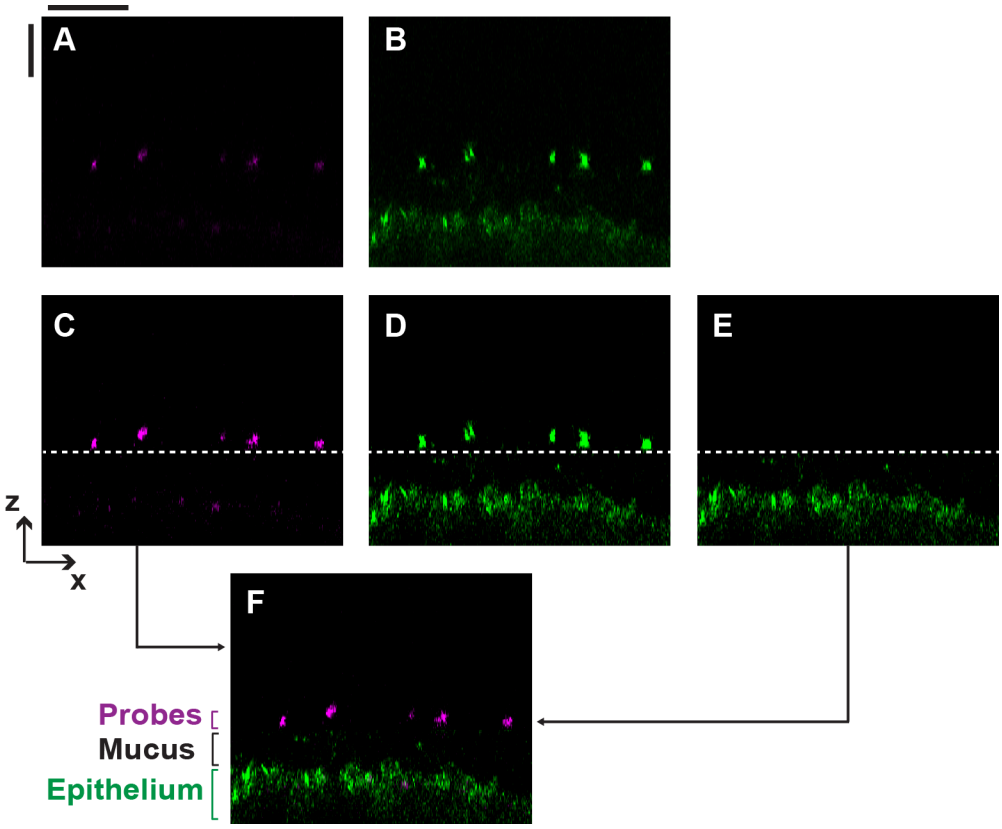

Figure 4.S1: Description of image processing for side-views presented in Figure 2. (A-B) False-colored confocal fluorescence (*A*) and confocal reflectance (*B*) xz side-views presented in Figure 2B. Brightness and contrast was not enhanced from the original images in either panel. (C) The confocal fluorescence image in *A* but with enhanced brightness and contrast. (D) The confocal reflectance image in (*B*) but with enhanced brightness and contrast. (E) The confocal reflectance image from *D* but with the top part of the image, above the dashed line, removed. Because the particles also scatter light, we split the image below the position of the particles, which were located in the fluorescence image (shown in *C*) for clarity. The dashed line in *C, D,* and *E* are at the exact same z-position (right below the particles). (F) Combination of *C* and *E* presented in Figure 4.2B. Scale bars are 30 μm.

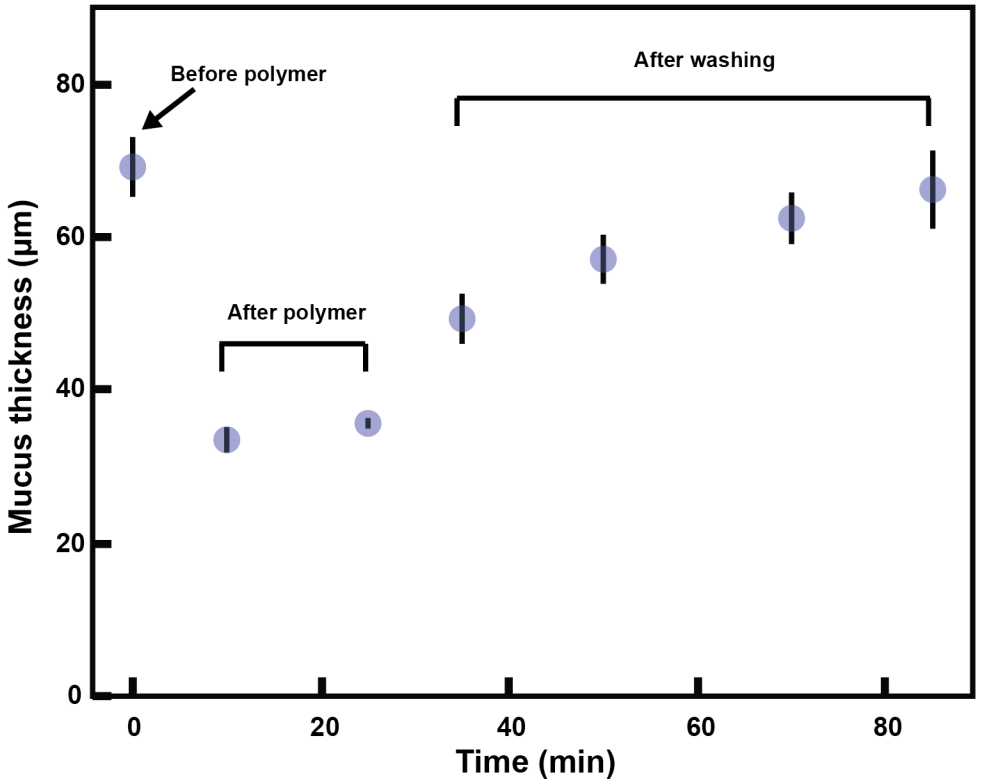

Figure 4.S2: Compression with carboxymethyl cellulose (CMC) is reversible. Plot of mucus thickness over time before and after adding CMC with a degree of substitution of 0.7 to a murine colonic explant. The following time-points were taken: Before adding CMC (time = 0 min), 10 and 25 min after adding CMC (time = 10 and 25 min), and then 10 min to an hour after washing the explant three times with 1 mL of ice-cold 1x PBS to remove the CMC from the explant (time = 35 to 85 min). Mucus thickness was measured using the "microparticle method" (see *Materials and Methods)* and each data point represents the average thickness measured at 5 points on the explant. Error bars are SEM with n = 5.

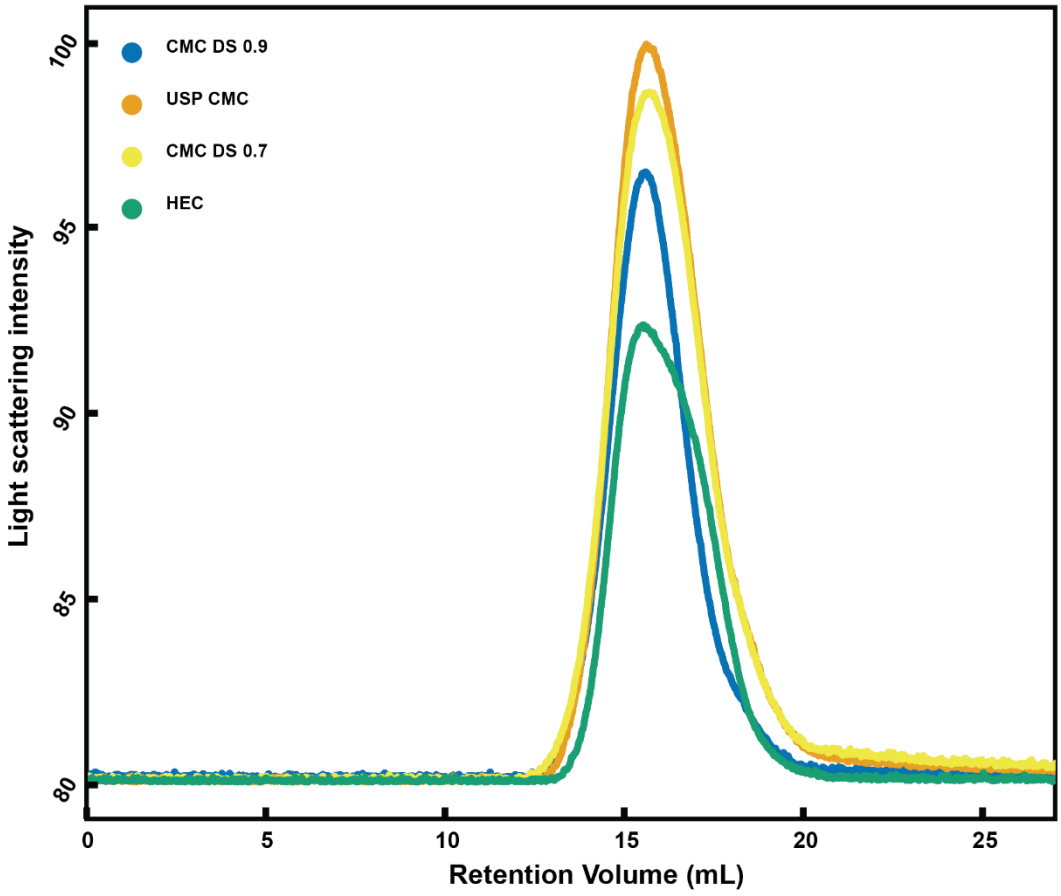

Figure 4.S3: Gel permeation chromatography (GPC) measurements of charged and uncharged polymers. Chromatograms of polymers used in the study. Method of detection is right-angle light scattering which is plotted on the vertical axis (unitless). CMC DS 0.9 = carboxymethyl cellulose with a degree of substitution of 0.9, USP CMC = U.S.P. grade carboxymethyl cellulose fed to mice in Figure 1, CMC DS 0.7 = carboxymethyl cellulose with a degree of substitution of 0.7, HEC = hydroxyethyl cellulose.

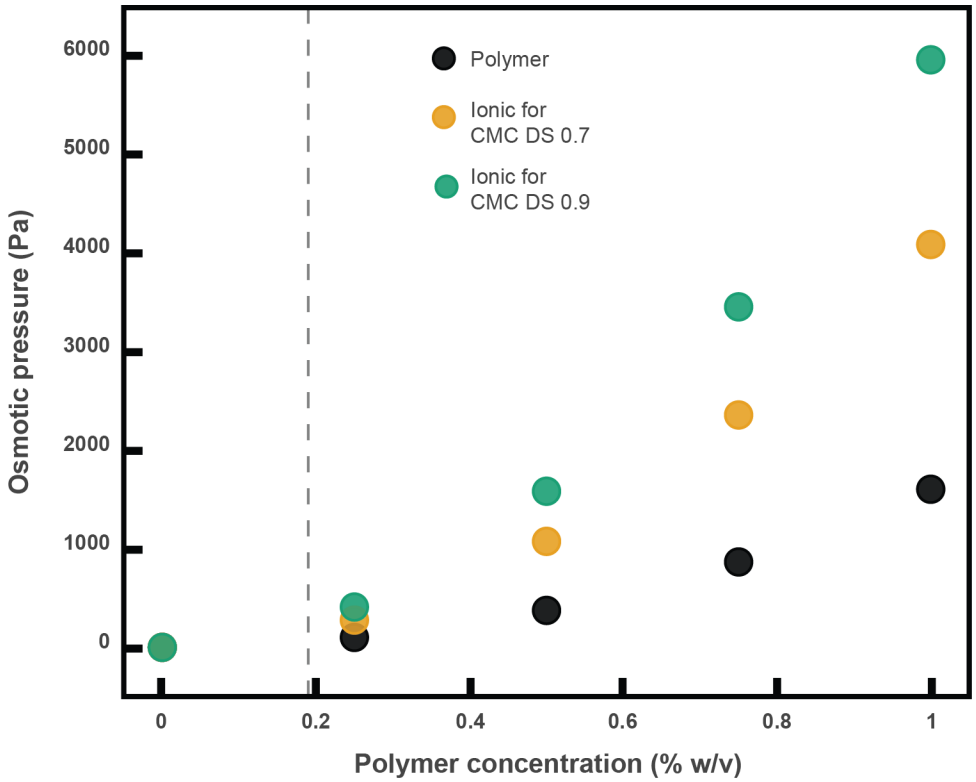

Figure 4.S4: Polymer contribution and ionic contribution to the osmotic pressure. The contributions to the osmotic pressure (eq 4.4**)** from ionic effects (i.e., Donnan partitioning) which is given by eq 4.5 and from the polymer osmotic pressure which is given by eq 4.6. The polymer osmotic pressure (black) is equal for all polymers (both carboxymethyl cellulose [CMC] derivatives and hydroxyethyl cellulose [HEC]). There is no ionic contribution for HEC as it is uncharged. Dashed line indicates the polymer overlap concentration (c^*), where $c^* = 0.19\ \%w/v$. "Ionic for CMC DS 0.7" is the ionic contribution to the osmotic pressure for carboxymethyl cellulose with a degree of substitution of 0.7. "Ionic for CMC DS 0.9" is the ionic contribution to the osmotic pressure for CMC with a degree of substitution of 0.9.

Table 4.S1: Gel permeation chromatography of polymers in phosphate-buffered saline.

Sample	HEC	USP CMC	CMC DS 0.9	CMC DS 0.7
M_w (kDa)	152	148	150	146
M_w/M_n	3.17	2.19	2.25	2.10
R_h (nm)	18.8	20.6	22.2	19.9

Carboxymethyl cellulose derivatives were analyzed using a refractive index increment (dn/dc) of $\frac{dn}{dc} = 0.163$.[30] Hydroxyethyl cellulose was analyzed using $\frac{dn}{dc} = 0.150$.[31] HEC = hydroxyethyl cellulose, USP CMC = U.S.P. grade carboxymethyl cellulose (fed to mice in Fig. 1), CMC DS 0.9 = carboxymethyl cellulose with a degree of substitution of 0.9, CMC DS 0.7 = carboxymethyl cellulose with a degree of substitution of 0.7. M_w = weight-average molecular weight; M_w/M_n = the dispersity; R_h = hydrodynamic radius.